Development Of A Human iPSC-Derived Cortical Neuron Model Of Adaptor-Protein-Complex-4-Deficiency

Entwicklung eines humanen iPSC-abgeleiteten kortikalen Neuronenmodells der Adaptor-Protein-Komplex-4-Defizienz

Doctoral thesis for a medical doctoral degree
at the Graduate School of Life Sciences,
Julius-Maximilians-Universität Würzburg,
Section Neuroscience

In collaboration with the Sahin Lab
F.M. Kirby Neurobiology Center
Boston Children's Hospital, Department of Neurology, Harvard Medical School

submitted by
Robert Stefan Friedrich Behne
from
Bielefeld
Würzburg 2021

Submitted on: 01.02.2022

Members of the Thesis Committee:

Chairperson: Prof. Dr. Alma Zernecke-Madsen

Primary Supervisor: Prof. Dr. med. Jens Volkmann

Supervisor (Second): Prof. Dr. med. Helge Hebestreit

Supervisor (Third): Prof. Dr. Philip Tovote

Collaborators at the F.M. Kirby Neurobiology Center:

Director: Clifford Woolf, MB, BCh, PhD, Professor Neurobiology and Neurology

Principal Investigator: Mustafa Sahin, MD, PhD, Professor in Neurology

Mentor: Darius Ebrahimi-Fakhari, MD, PhD

Date of Public Defence: 22.11.2023

Date of Receipt of Certificates: 22.11.2023

TABLE OF CONTENTS

Abbreviations

AD	Autosomal-dominant
ALS	Amyotrophic lateral sclerosis
AMP	Adenosine monophosphate
AMPAR	Alpha-amino-3-hydroxy-5-methyl-4-isoxazolepropiomic acid receptor
AMPK	AMP-activated protein kinase
AP-4	Adaptor protein complex 4
AP4B1	Adaptor protein complex 4 beta subunit
AP4E1	Adaptor protein complex 4 epsilon subunit
AP4M1	Adaptor protein complex 4 mu subunit
AP4S1	Adaptor protein complex 4 sigma subunit
APP	Amyloid precursor protein
AR	Autosomal-recessive
ARF1	ADP-ribosylation factor 1
ATG	Autophagy-related protein
ATG9A	Autophagy-related protein 9 A
ATP	Adenosine triphosphate
CNS	Central nervous system
DIV	Days in vitro
DMSO	Dimethyl sulfoxide
EM	Electron microscopy
EMCCD	Electron multiplying charge-coupled device
ER	Endoplasmatic reticulum
GRID2/ GluRδ2	Glutamate receptor, ionotropic, delta 2
HAP1 cells	Leukemia-derived haploid cells
HBSS	Hanks balanced salt salution
HEK293	Human embryonic kidney cells
HepG2 cells	Human liver cancer cells
HI	High intensity

HSP	Hereditary spastic paraplegia
IM	Isolation membrane
IP	Immunoprecipitation
iPSC	Induced pluripotent stem cells
IXM	ImageXpress Micro confocal high-content imaging system
kDA	Kilo Dalton
KO	Knockout
LC3	Microtubule-associated protein light chain 3
LDLR	Low-density lipoprotein receptor
LoF	Loss of function
MEF	Mouse embryonic fibroblasts
Mm	Millimeter
µm	Micrometer
MOI	Multiplicity of infection
ms	Milliseconds
MTDR	MitoTracker Deep Red
mTORC	Mammalian target of rapamycin complex
NA	Numerical aperture
nm	Nanometer
PAS	Pre-autophagosomal structure
PCR	Polymerase chain reaction
PE	Phosphatidylethanolamine
PI-3 kinase complex	Phosphatidylinositol 3-kinase complex
PGK	Phosphoglycerate kinase
pS6	Phosphorylated ribosomal protein S6
RT-PCR	Real time polymerase chain reaction
SERINC1/3	Serin incorporator 1/3
RUN and SH3 domain-containing protein 1 and 2	RUSC1 and RUSC2
SH-SY5Y cells	Neuroblastoma-derived cells

SMA	Spinal muscular atrophy
SPG	Spastic paraplegia
STR	Short tandem repeats
SQSTM1/p62	Sequestosome 1/ubiquitin-binding protein 62
TARP	Transmembrane AMPA receptor regulatory protein
Tetra-epsin	TEPSIN
TGN	Trans-Golgi network
TMRE	Tetramethylrhodamine, ethyl ester
ULK1	Unc-51 like autophagy activating kinase
V-ATPase	Vacuolar-type ATPases
WES	Whole exome sequencing
WGS	Whole genome sequencing
WT	Wildtype

List Of Tables

List Of Figures

1 Introduction

1.1 The Hereditary Spastic Paraplegias – A Brief Overview

The hereditary spastic paraplegias (HSP) are a clinically and genetically heterogenous group of neurodegenerative diseases that share common clinical features while spanning a wide range of pathogenetic themes.

In the 19th century, the German physician Ernst Adolf Gustav Gottfried von Strümpell provided the first description of a form of likely autosomal-dominant HSP. In his case series, Strümpell described two 50-year-old brothers with adult-onset spastic gait and hyperreflexia and a father who was "a little paralyzed" according to his sons (Strümpell, 1880). In a *post-mortem* study of one of the brothers, Strümpell found a degeneration of the distal corticospinal tracts identifying the primarily affected area of the central nervous system (CNS) in HSP (Strümpell, 1886). Strümpell and his French colleague Maurice Lorrain continued to describe similar cases in the following years (Lorrain, 1898; Strümpell, 1893).

Since then, HSP has evolved into a large and heterogenous group of diseases, whose classification remains a challenge to this day. Lower limb spasticity and weakness in combination with a positive family history, as described by Strümpell are still considered cardinal features of HSPs (Blackstone, 2018; Fink, 2013; Tesson, Koht, & Stevanin, 2015), but additional symptoms and a wide range of onset-ages add to the complexity and diagnostic difficulty. HSPs have been historically divided into "pure" and "complicated" forms (Harding, 1983). "Pure" forms are defined by spasticity and paresis in the lower limbs and potentially distal sensory impairment and bladder dysfunction, whereas "complicated" forms present with additional symptoms including motor developmental delay, intellectual disability, microcephaly and seizures, among others. Hereditary spastic paraplegias have been named using the abbreviation "SPG" for "spastic gait gene" and a subsequent number in order of the discovery of the gene or genetic locus (e.g. SPG1 for the first discovered gene causing HSP).

While the clinical phenotype of HSP varies greatly, the pathogenetic findings point towards converging pathways and disturbances affecting primarily the axons of the long corticospinal tracts (Blackstone, 2012). The axonal compartment of these post-mitotic neurons often reaches lengths of up to one meter and a highly vulnerable system of ante-

and retrograde transport of proteins, vesicles and organelles is necessary to maintain axonal function. This might also explain, why small animal models, who possess much shorter corticospinal tracts, show less severe phenotypes (De Pace et al., 2018). Growing research suggests that affected gene products in HSP play important roles in the formation and organization of the smooth endoplasmatic reticulum (ER) (Park, Zhu, Parker, & Blackstone, 2010), lipid droplet turnover (Eastman, Yassaee, & Bieniasz, 2009), axonal autophagosome (Davor Ivankovic et al., 2020) and endosome function (Hirst et al., 2011) and mitochondrial function (Ferreirinha et al., 2004) with disturbances in the ER machinery being the most common (Blackstone, 2012). For example, SPG4, a type of autosomal-dominant HSP, is caused by mutations in the *SPAST* gene, which is an important regulator of microtubules and ER organization (Claudiani, Riano, Errico, Andolfi, & Rugarli, 2005).

The estimated prevalence of HSPs ranges from 1 to 9 per 100.000 (Erichsen, Koht, Stray-Pedersen, Abdelnoor, & Tallaksen, 2009; Ruano, Melo, Silva, & Coutinho, 2014) depending on the population. The majority of HSPs follow an autosomal-dominant (AD) inheritance pattern and 50-60% of autosomal-dominant forms present as "pure" (Schüle et al., 2016), adult-onset HSPs without a significant decrease in lifespan. Autosomal-recessive (AR) forms on the other hand are often "complicated" with onset of symptoms in early childhood and a higher prevalence in populations with high rates of consanguinity (Lo Giudice, Lombardi, Santorelli, Kawarai, & Orlacchio, 2014; Ruano et al., 2014). Besides these two inheritance patterns, a few X-linked forms (Jouet et al., 1994) and HSP associated with mitochondrial DNA mutations (Verny et al., 2011) exist.

Diagnosing HSP remains a challenge considering the significant phenotypic overlap with other neurological diseases. Predominant symptoms include lower limb spasticity and weakness, lower limb hyperreflexia and extensor plantar response also known as the Babinski sign (Hedera, 1993). The diagnosis can be confirmed by genetic testing and is made after the exclusion of other causes such as inherited metabolic disease, motor neuron disease such as amyotrophic lateral sclerosis (ALS), neuroimmunological and infectious diseases, brain malformations or cerebral palsy to name a few (Ebrahimi-Fakhari, Saffari, & Pearl, 2021; Tesson et al., 2015). Cerebral palsy is suspected to be a common misdiagnosis in children with early-onset complicated HSP (Ebrahimi-Fakhari, Cheng, Dies, Diplock, Pier, Ryan, Lanpher, Hirst, Chung, Sahin, Rosser, Darras, &

Bennett, 2018), especially if genetic testing is not readily available. Radiology and laboratory findings can rule out differential diagnoses, but genetic testing, mostly whole exome sequencing (WES), is needed for a definitive diagnosis. Treatment is limited to symptomatic and consists of physiotherapy, occupational therapy and treatment of spasticity exemplified by oral or intrathecal baclofen or botulinum injections (Hedera, 1993). In complicated forms, clinicians are challenged with the treatment of a wider range of symptoms such as seizures or developmental delay.

1.2 Adaptor Protein Complex 4-associated Hereditary Spastic Paraplegias

This study focuses on the development of a model of SPG47, a childhood-onset form of autosomal-recessive, AP-4-associated, complicated HSP. SPG47 belongs to a group of complicated HSPs associated with bi-allelic loss-of-function variants in one of the four subunits of the adaptor-protein-complex-4 (AP-4), a heterotetrameric protein complex that is involved in protein sorting and whose function will be discussed further below. Loss-of-function variants in the AP-4-subunits result in four conditions, SPG47 (*AP4B1*, OMIM #614066), SPG50 (*AP4M1*, OMIM #612936), SPG51 (*AP4E1*, OMIM #613744) and SPG52 (*AP4S1*, OMIM #614067), respectively (Abou Jamra et al., 2011; Ebrahimi-Fakhari et al., 2020; Moreno-De-Luca et al., 2011).

1.2.1 Genetical, Clinical And Imaging Features

AP-4-associated HSP is a rare disease and the largest report to date includes 156 patients (Ebrahimi-Fakhari et al., 2020). With genetic testing becoming more readily available and affordable, an increase in cases, often previously misdiagnosed as cerebral palsy, is expected. In the largest cohort studied yet (Ebrahimi-Fakhari et al., 2020), 82% of cases were caused by homozygous mutations and 18% are caused by compound heterozygous mutations. Consanguinity was reported in two-thirds of families in this cohort. Most variants are frameshift or nonsense mutations resulting in a truncated AP-4-subunit which prevents the formation of a stable AP-4-complex (Borner et al., 2012; Hirst, Irving, & Borner, 2013). For yet unknown reasons the larger AP4E1-subunit (1137 amino acids), but also AP4S1 (144 amino acids) are less commonly affected than AP4B1 (739 amino acids) and AP4M1 (453 amino acids) (Ebrahimi-Fakhari et al., 2020).

Clinically, the four AP-4-associated HSPs are indistinguishable and comparison of 156 patients has not revealed any clinical phenotypes to differentiate between the affected AP-4-subunit (Table 1). Children with AP-4-HSP are usually born at term and often present with mild hypotonia at birth and the majority of patients show mild to moderate microcephaly (Abdollahpour et al., 2015; Ebrahimi-Fakhari, Cheng, Dies, Diplock, Pier, Ryan, Lanpher, Hirst, Chung, Sahin, Rosser, Darras, Bennett, et al., 2018; Moreno-De-Luca et al., 2011; Tüysüz et al., 2014). Peri- or postnatal complications that require care in a neonatal intensive are uncommon. Onset of symptoms is typically around 8 months and most families are referred to a clinician because of motor developmental delay, i.e. delayed or no achievement of motor milestones, around 9 months (Ebrahimi-Fakhari et al., 2020). All patients show a delay in achieving motor milestones with only 43% ever achieving unassisted walking. Over time, most patients exhibit a loss of skills including the ability to walk (Ebrahimi-Fakhari et al., 2020). Additionally, developmental delay and later intellectual disability are present in all patients which typically includes speech development with half of the patients remaining nonverbal (Abdollahpour et al., 2015; Abou Jamra et al., 2011; Ebrahimi-Fakhari et al., 2020; Moreno-De-Luca et al., 2011; Tüysüz et al., 2014; Verkerk et al., 2009).

Motor symptoms include postnatal hypotonia, which progresses to spasticity of the lower limbs in the first life decade. When patients reach adolescence or adulthood there is a progression to tetraplegia in a subset (Abdollahpour et al., 2015; Abou Jamra et al., 2011; Moreno-De-Luca et al., 2011; Tüysüz et al., 2014; Verkerk et al., 2009). Almost all patients exhibit hyperreflexia and a positive Babinski sign. Foot deformities and contractures due to lower limb spasticity are often seen and patients might require surgery (Abdollahpour et al., 2015; Abou Jamra et al., 2011; Ebrahimi-Fakhari, Cheng, Dies, Diplock, Pier, Ryan, Lanpher, Hirst, Chung, Sahin, Rosser, Darras, & Bennett, 2018; Tüysüz et al., 2014; Verkerk et al., 2009). Although dysmorphic facial features such as a flat nasal bridge, prominent nose and wide mouth and an everted upper vermillion are present in many patients, they are not distinctive enough to define a characteristic *facies* of AP-4-associated HSP (Abdollahpour et al., 2015; Abou Jamra et al., 2011; Ebrahimi-Fakhari, Cheng, Dies, Diplock, Pier, Ryan, Lanpher, Hirst, Chung, Sahin, Rosser, Darras, & Bennett, 2018). A short statue is another common finding (Abou Jamra et al., 2011;

Ebrahimi-Fakhari, Cheng, Dies, Diplock, Pier, Ryan, Lanpher, Hirst, Chung, Sahin, Rosser, Darras, Bennett, et al., 2018; Kong et al., 2013; Vill et al., 2017).

In a cohort of 156 patients, febrile or unprovoked seizures are seen in 67% with 66% fulfilling the criteria for epilepsy (Ebrahimi-Fakhari et al., 2020). Most patients can be treated successfully with standard antiepileptic drugs and only 27% exhibit refractory seizures or need multiple antiepileptic agents. No clear tendency towards generalized or focal seizures has been delineated (Abdollahpour et al., 2015; Ebrahimi-Fakhari, Cheng, Dies, Diplock, Pier, Ryan, Lanpher, Hirst, Chung, Sahin, Rosser, Darras, Bennett, et al., 2018; Moreno-De-Luca et al., 2011; Tüysüz et al., 2014). Ebrahimi-Fakhari et al. were able to show that epilepsy is associated with higher spasticity scores and might be indicative of worse outcome (Ebrahimi-Fakhari et al., 2020).

Stereotypic unprovoked laughter, possibly due to a pseudobulbar affect has been described in a subset of patients and might help with differentiating AP-4-HSP from other early-onset forms of HSP (Abou Jamra et al., 2011; Bettencourt et al., 2017; Kong et al., 2013; Langouët et al., 2015; Tüysüz et al., 2014; Verkerk et al., 2009; Vill et al., 2017). Two studies further describe a shy character, although this does not seem to be a unifying feature across patients (Abdollahpour et al., 2015; Abou Jamra et al., 2011).

Neuroimaging findings include a thinning of the corpus callosum, which is seen in nearly all patients (Abdollahpour et al., 2015; Bettencourt et al., 2017; Ebrahimi-Fakhari, Alecu, et al., 2021; Ebrahimi-Fakhari, Cheng, Dies, Diplock, Pier, Ryan, Lanpher, Hirst, Chung, Sahin, Rosser, Darras, Bennett, et al., 2018; Hardies et al., 2015; Langouët et al., 2015; Moreno-De-Luca et al., 2011; Tessa et al., 2016; Tüysüz et al., 2014; Vill et al., 2017) but also in other HSP such as SPG11, for instance (Lossos et al., 2006). Around two-thirds of patients show ventriculomegaly in particular of the posterior ventricles also known as colpocephaly (Accogli et al., 2018; Bettencourt et al., 2017; Ebrahimi-Fakhari, Cheng, Dies, Diplock, Pier, Ryan, Lanpher, Hirst, Chung, Sahin, Rosser, Darras, Bennett, et al., 2018; Hardies et al., 2015; Langouët et al., 2015; Tessa et al., 2016; Tüysüz et al., 2014; Vill et al., 2017). Unspecific white matter lesions or loss of white matter are another common finding and a subset of patients might show cerebellar or cerebral atrophy (Accogli et al., 2018; Kong et al., 2013; Moreno-De-Luca et al., 2011; Verkerk et al., 2009). One study describes a family with several adult patients with AP-4-associated HSP and brain iron accumulation on MRI (Roubertie et al., 2018). Iron accumulation has

neither been reported in other patients, nor has testing patient-derived fibroblasts revealed elevated iron levels (Behne et al., 2020) suggesting a mechanism unrelated to AP-4-deficiency or a phenotype only seen in older patients. Descriptions of human pathology are scarce, but a *post-mortem* study of a 17-month-old patient with mutations in the AP4M1-subunit, who died of pneumonia, found a thin corpus callosum, cerebral white matter loss and ventriculomegaly (Verkerk et al., 2009) in keeping with above mentioned imaging findings. White matter loss was accompanied by axonal swellings and gliosis and the group further described a pronounced loss of neurons in the dentate nucleus of the cerebellum. Although these findings might not be representative, they suggest that AP-4 is ubiquitously needed for axonal health, but some neuron types are more vulnerable to its deficiency than others.

In summary, diagnosis of AP-4-associated HSP can only be confirmed by molecular testing. A clinical suspicion should be raised, if children with a history of postnatal hypotonia and without any other complications fail to achieve motor milestones. When anamnesis, neurological examination and brain imaging reveal a positive family history, progressive spasticity, global developmental delay, seizures and the mentioned MRI findings, the clinician should consider HSP as a differential diagnosis and offer genetic counseling. Further basic research as well as the continuation of natural history and clinical studies is needed to search for diagnostic markers as well as therapeutic targets to provide earlier and better treatment for patients with AP-4-associated HSP.

Table 1 Clinical and radiographic features of AP-4-associated HSP

Clinical features	**Frequency**
Neonatal or infantile hypotonia	89%
Developmental delay/intellectual disability	100%
Spasticity	97%
Postnatal microcephaly	83%
Febrile Seizures	62%
Epilepsy	66%
Stereotypic laughter	56%
Radiographic features	**Frequency**
Thinning of corpus callosum	90%

Ventriculomegaly	65%
White matter changes	68%

Modified after Ebrahimi-Fakhari et al. (2020)

1.3 Adaptor-Protein-Complex 4

All cells depend on the correct distribution of membranes and transmembrane proteins to ensure functional cell-cell-interactions on the outside and spatial organization on the inside. Post-mitotic neurons with their high-speed signal transduction require a polarized cell architecture and highly specialized compartments, namely axon, soma and dendrites, to function properly. Another example are epithelial cells, which depend on the correct distribution of transmembrane proteins to the apical and basolateral membrane. These demanding tasks are in part performed by adaptor protein complexes (AP), a group of highly conserved heterotetrameric proteins, that are responsible for coating transport vesicles and sorting transmembrane cargo (Bonifacino, 2014).

1.3.1 Form And Function

In brief, AP-complexes will recognize sorting-motifs of their respective cargo and incorporate them into vesicles formed out of a donor membrane (Traub & Bonifacino, 2013). Vesicles are sphere-shaped membranous structures, which possess one or more phospholipid bilayers on the outside and contain cytoplasm on the inside, serving a myriad of cellular functions including protein transport. AP-coated vesicles are distributed throughout the cell and fuse with the membrane of their acceptor compartment. Post-Golgi trafficking of proteins relies heavily on AP-complexes (Sanger, Hirst, Davies, & Robinson, 2019).

Currently, there are five known adaptor protein complexes of which AP-1, AP-2 and AP-3 are found at high mRNA and protein levels in HeLa cells, while AP-4 and AP-5 are less abundantly expressed (Hirst et al., 2013). Differences between cell types need further studies. Additionally, while AP-1, AP-2 and AP-3 are found in all species, AP-4 and AP-5 are lost in some model organisms such as *Saccharomyces cerevisiae* and *Caenorhabditis elegans* (Boehm & Bonifacino, 2001; Hirst, Bright, Rous, & Robinson, 1999; Hirst et al., 2013). This raises the question of functional redundancy and implies species-dependent differences, that have yet to be elucidated. The importance of

functional protein sorting is underscored by the fact, that knockout of AP-1 or AP-2 are embryonically lethal in mice (Mitsunari et al., 2005; Zizioli et al., 1999).

When looking at the diverse tasks of AP-complexes, it is not surprising, that deficiencies of different isoforms and subunits of AP-complexes span a wide range of diseases affecting multiple organ systems (Sanger et al., 2019). These disorders have been termed "coatopathies" (Esteban C. Dell'Angelica & Bonifacino, 2019) and provide insides into the complex roles of AP-complexes. Here, we focus on AP-4 deficiency, which leads to a form of early-onset complicated HSP.

Similar to other AP-complexes, AP-4 consists of four subunits; the larger ε (AP4E1, 127kDa) and β4 (AP4B1, 83kDa), the medium sized μ4 (AP4M1, 50kDa) and the smallest subunit σ4 (AP4S1, 17kDa), respectively (E. C. Dell'Angelica, Mullins, & Bonifacino, 1999; Hirst et al., 1999) (Figure 1). Knockout or deficiency of one subunit leads to an unstable, dysfunctional AP-4-complex and to decreased levels of the other subunits (Borner et al., 2012; Hirst et al., 2013). This is further corroborated by the fact, that in worms, yeast and flies all subunits are concomitantly lost suggesting that the single subunits alone are unable to serve a function (Boehm & Bonifacino, 2001; Hirst et al., 1999).

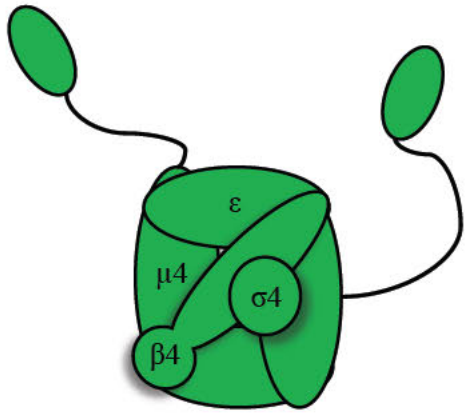

Figure 1 Structure of the adaptor protein complex 4

AP-4 forms an obligate complex consisting of the two larger subunits ε and β4, which possess an ear-like appendage, and the smaller μ4 and σ4. Modified after E. C. Dell'Angelica et al. (1999)

Looking at mRNA and protein expression, AP-4 is found at low levels in all human tissues, but cell type-specific differences remain to be addressed in detail (E. C. Dell'Angelica et al., 1999; Hirst et al., 1999).

AP-complexes localize to subcellular compartments, that represent their respective donor membrane site and give insights into their distinct roles. In immunofluorescence microscopy of HeLa cells, mouse hippocampal neurons and patient-derived fibroblasts, AP-4 localizes to fine puncta in the juxtanuclear region and shows a strong overlapping signal with trans-Golgi network (TGN) markers, which is the cell's sorting hub for proteins (Borner et al., 2012; E. C. Dell'Angelica et al., 1999; Hirst et al., 1999; D. Ivankovic et al., 2020; Mattera, Park, De Pace, Guardia, & Bonifacino, 2017). These puncta are thought to be AP-4-coated vesicles which is further corroborated by immuno-electron microscopy (EM) findings (Hirst et al., 1999). Despite these findings, the understanding of AP-4 function is still lacking. However, an image of AP-4 mediating cargo sorting and transport from the TGN emerges.

This sorting and transporting process consists of different phases (Figure 2). First, to initiate cargo selection and vesicle budding, AP-4 must bind to a donor membrane. This is mediated by ADP-ribosylation factor 1 (ARF1), a small GTP-binding protein. ARF1 recruits AP-4 to the TGN as shown by treatment with brefeldin A, which prevents AP-4 from binding to the TGN by modulating ARF1 activity and leads to re-distribution of AP-4 throughout the cytosol (E. C. Dell'Angelica et al., 1999; Hirst et al., 1999). In keeping with these findings, ARF1 directly interacts with the AP4M1- and AP4E1-subunit (Boehm, Aguilar, & Bonifacino, 2001). This implicates, that AP-4 switches between cytosolic and membrane-bound states in a GTP-dependent manner. It also shows that the AP-4-subunits seem to serve different complementary functions, all of which are needed for a functioning complex.

In a second step, membrane-bound AP-4 recognizes sorting-motifs in the cytoplasmatic tail of its respective cargoes (Sanger et al., 2019). One way to test the AP-4-dependency of different cargoes is to investigate changes in their subcellular localization upon AP-4-depletion. While some cargo proteins are recognized by the μ-subunit of AP-2, AP-3 and AP-4, respectively, and have unaltered subcellular localization in AP-4-deficient cells (Aguilar et al., 2001; Hirst et al., 1999; Janvier & Bonifacino, 2005; Stephens & Banting, 1998), others rely on correct sorting mediated solely by AP-4. Focusing on these cargoes

holds the promise of revealing the disrupted sorting pathways responsible for AP-4-associated HSP. The following formation and transport of vesicles is a delicate process with multiple regulatory elements ensuring correct cargo delivery and will not be discussed in detail here. In brief, after AP-4 is recruited to the donor membrane (e.g. the TGN), it will interact with transmembrane cargo while simultaneously assembling a vesicle coat on the "outside", i.e. the cytosolic side. AP-1 and AP-2 recruit a clathrin-coat, which acts as a membrane shaper and also facilitates cargo recognition. However, no coat components of AP-4-vesicles have yet been identified and it is unclear whether AP-4 alone is able to shape vesicles. After this, a process called "scission" separates the budding vesicle from its donor membrane and after the coat is shed, the vesicles are transported to their respective acceptor site *via* the cytoskeleton. Here, they are recognized by a process called "tethering" and then fuse with the donor membrane to deliver their cargo. Unsurprisingly, polarized cells such as neurons are highly vulnerable to missorting of their compartment-defining cargo proteins. Accessory proteins and cargoes of AP-4, whose missorting leads to AP-4-associated HSP are detailed below.

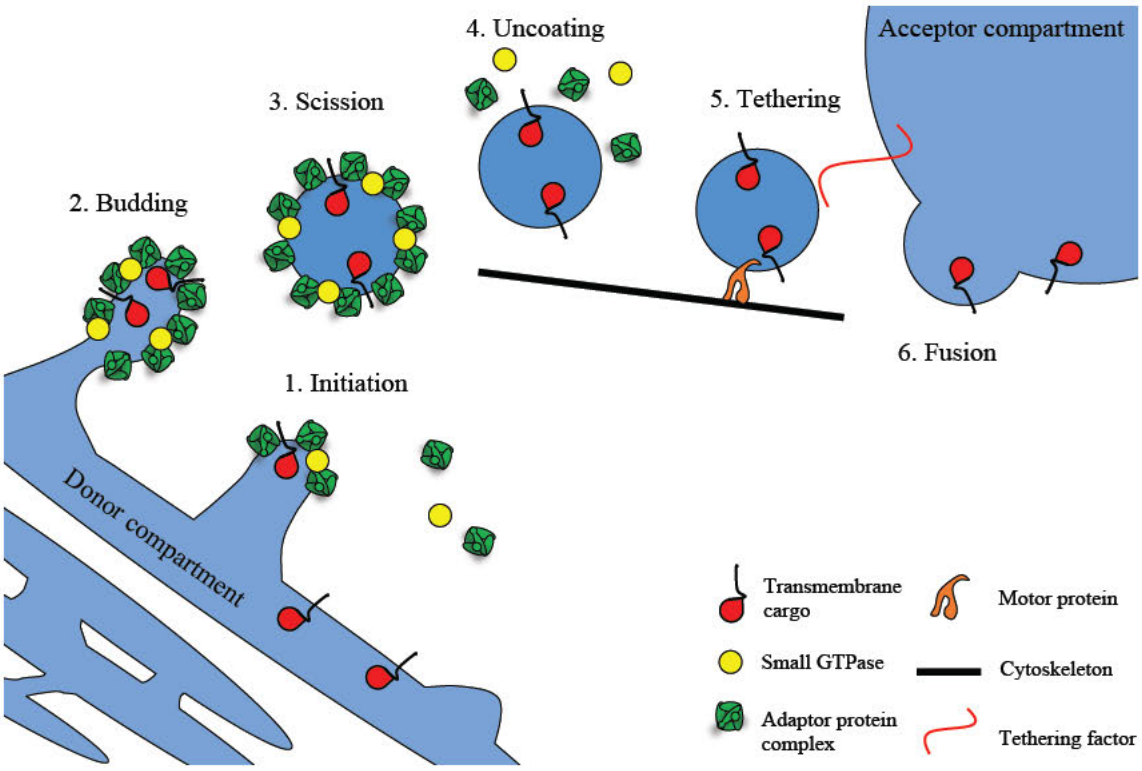

Figure 2 Schematic of AP-mediated transport

In AP-mediated transport, **(1.)** sorting-motifs of transmembrane cargoes are recognized and AP-complexes are recruited to the donor compartment by a small GTPase to initiate vesicle formation. **(2.)** A vesicle-coat is formed and mediates budding of the membrane. **(3.)** The completed vesicle is then released in a process called "scission". **(4.)** The vesicle coat is shed to enable transport *via* the cytoskeleton. **(5.)** The donor compartment recognizes the cargo *via* tethering factors. **(6.)** Finally, the transmembrane cargo is released into the acceptor compartment. Modified after Bonifacino (2014); Sanger et al. (2019).

1.3.2 Accessory Proteins And Cargoes

Cargo recognition and binding is not only dependent on sorting-motifs but is also facilitated by accessory proteins of AP-4. Besides cargo recognition, accessory proteins of AP-complexes have additional functions such as interaction with the cytoskeleton (C. M. Guardia et al., 2021). These accessory proteins can be identified by comparing vesicle profiles using mass spectrometry. With this approach developed by the Hirst lab (Davies et al., 2018), the loss of proteins from vesicle fractions upon AP-4-depletion reveals accessory and cargo proteins, that are not recruited to the vesicle without AP-4. Tetra-epsin (TEPSIN) was the first identified AP-4 accessory protein and binds to the C-terminal "ear-appendages" of the AP4E1- and AP4B1-subunit (Borner et al., 2012). Like

AP-4, it has been concomitantly lost from yeast, worms and flies suggesting a functional relationship. The function of TEPSIN is unknown, but Mattera et al. speculate that TEPSIN aids in vesicle coat formation by enabling interaction of multiple AP-4-complexes (Mattera, Guardia, Sidhu, & Bonifacino, 2015).

Simmen et al. identified cargoes including low-density lipoprotein receptor (LDLR), which is missorted to the apical compartment of AP4M1-depleted Madin-Darby Canine Kidney cells (MCDK) (Simmen, Höning, Icking, Tikkanen, & Hunziker, 2002). This shows that AP-4 is indeed crucial for maintaining cell polarity at least in epithelial cells. However, hypercholesterolemia caused by insufficient LDL uptake is not reported in any cases of AP4-associated HSP. LDLR was later found to be missorted to axons of Purkinje cells of *Ap4b1*-knockout mice implicating again, that AP-4 is responsible for basolateral or somatodendritic sorting of LDLR (S. Matsuda et al., 2008). However, the significance for AP-4-associated HSP remains unknown.

Another cargo protein is the amyloid precursor protein (APP), which is widely known for its implications in Alzheimer's disease (Schenk et al., 1999). In AP-4-deficient HeLa and H4 neuroglioma cells, transport of APP from the TGN to the endosomes is disrupted and amyloidogenic processing is increased (Burgos et al., 2010). Similar to LDLR, the significance for Alzheimer's disease as well as AP-4-associated HSP remains unknown.

An exciting prospect was the discovery of Yap et al. that the ionotropic delta 2 subtype of the glutamate receptor (GRID2, also known as GluRδ2) interacts with the AP4M1-subunit (Yap et al., 2003). Moreover, GRID2 together with LDLR and Alpha-amino-3-hydroxy-5-methyl-4-isoxazolepropiomic acid receptor (AMPAR) is missorted to Purkinje cell axons of *Ap4b1*-knockout mice (S. Matsuda et al., 2008) and *Ap4e1*-knockout mice (De Pace et al., 2018). In keeping with this, the *post mortem* study of a patient with an affected AP4M1-subunit showed a GRID2 staining pattern suggestive of missorting (Verkerk et al., 2009). GRID2 is only expressed in cerebellar Purkinje cells (Takayama, Nakagawa, Watanabe, Mishina, & Inoue, 1995, 1996) and is crucial for synapse integrity (K. Matsuda et al., 2010). Interestingly, GRID2 deficiency in humans causes spastic paraplegia and cerebellar ataxia (Maier et al., 2014; Utine et al., 2013). AMPAR is implicated in a variety of neurodevelopmental disorders as well (Salpietro et al., 2019). These findings suggest that AP-4 is involved in cell type-specific cargo sorting from the TGN to the somatodendritic compartment of neurons (so far, only cerebellar and

hippocampal neurons have been examined). Strikingly, missorted AMPARs localize to accumulating autophagosomes, that cause axonal swellings in mouse Purkinje cells. This links AP-4-deficiency to the autophagy pathway and a recently identified cargo protein further supports this notion.

The Hirst and Bonifacino lab independently identified autophagy-related protein 9A (ATG9A), the mammalian isoform of ATG9, as a cargo of AP-4 (Davies et al., 2018; Mattera et al., 2017). ATG9 was first identified in yeast (Tsukada & Ohsumi, 1993) and growing research suggests its role in membrane recruitment for functional autophagy (Matoba et al., 2020; Papinski et al., 2014) , a "recycling process" of the cell, discussed in the following section. Additionally, two cargo proteins called Serin incorporator 1 and 3 (SERINC1 and 3) of unknown function were identified by the Hirst and Borner lab (Davies et al., 2018).

In the same study, two accessory proteins named RUN and SH3 domain-containing protein 1 and 2 (RUSC1 and RUSC2) were identified by the Hirst lab (Davies et al., 2018). They show, that RUSC2 colocalizes with vesicles containing ATG9A, SERINC1 and 3 and that AP-4 is necessary for the interaction of RUSC2 and ATG9A. RUSC1 and 2 have been implicated in vesicle transport (Bayer et al., 2005; MacDonald et al., 2012) and in keeping with these findings, disruption of microtubules by nocodazole treatment leads to an impaired distribution of RUSC2- and ATG9A-containing vesicles. A recent study confirmed that RUSC2 couples ATG9A-containing vesicles to kinesin-1, a motor protein involved intracellular transport (C. M. Guardia et al., 2021). Davies et al. propose that AP-4, RUSCs and ATG9A come together transiently at the TGN to form a coated vesicle. AP-4 is then lost from the vesicle fraction as has been described for other AP-complexes (Robinson, 2015) and RUSCs mediate microtubule transport to the cell periphery. In addition, knockdown of RUSC2 or knockdown of both RUSCs leads to impaired autophagy in HeLa cells further strengthening the link between correct ATG9A distribution and functional autophagy. Along the same lines, RUSC2 deficiency causes intellectual disability and a thin corpus callosum in humans, reminiscent of clinical and imaging findings in patients with AP-4-associated HSP (Alwadei et al., 2016).

Taken together, these findings showcase three striking features of AP-4-deficient cells. First, the disruption of compartment-specific sorting of transmembrane cargo. For instance, AMPARs are responsible for recognizing fast excitatory synaptic signals and

are sorted to the somatodendritic domain in wildtype neurons. Second, the cell-specificity of AP-4-mediated protein sorting. Since only neurons rely on polarized sorting of synaptic receptors, they exhibit a cell type-specific vulnerability to AP-4-deficiency mirrored by the fact, that AP4-associated HSP manifests itself in the nervous system. Third, the impaired autophagic function, which seems to be cell type-specific as well and will be discussed further below.

1.3.3 AP-4, Autophagy And ATG9A – An Important Cargo

ATG9A is distributed throughout the cell in an AP-4-dependent manner raising the question whether spatial control of autophagy is impaired in AP-4-associated HSP.

Autophagy (from Greek αὐτόφαγος, „self-devouring") is a highly conserved cellular function, that describes the membrane engulfment and lysis of intracellular proteins, whole organelles and other cellular "waste". Autophagy results into macromolecules such as proteins, lipid droplets and so forth, being reused by the cell to build new organelles or to serve as energy resources. While autophagic flux is constantly active to some degree, it can be up- or downregulated, depending on whether the cell finds itself in a nutrient-rich environment or under starvation conditions. There are currently three known types of autophagy. Chaperone-mediated autophagy, microautophagy and macroautophagy. The latter is the most studied and relevant for this work. The term "autophagy" will hereafter be used to refer to macroautophagy. The autophagic machinery has been revealed by the groundbreaking research of Yoshinori Ohsumi and colleagues, who studied the self-devouring process of the cell in yeast (Tsukada & Ohsumi, 1993). They showed that cells – upon starvation – form double-membraned vesicles, called autophagosomes, which engulf cargo. In mammalian cells autophagosomes then fuse with acidic lysosomes to form autolysosomes, where the cargo is degraded. This process can be divided into six steps: initiation, nucleation, elongation, maturation, fusion and degradation, respectively (Figure 3).

Briefly summarized, two kinases lie at the heart of autophagy regulation. First, the mammalian target of rapamycin complex 1 (mTORC1), which functions as a nutrient sensing complex regulating growth, metabolism and autophagy (Lipton & Sahin, 2014; Wullschleger, Loewith, & Hall, 2006). MTORC1 inhibits autophagy in nutrient-rich conditions, but cellular stress such as starvation, conversely leads to mTORC1 inhibition

and autophagy activation (Ganley et al., 2009; Wong, Puente, Ganley, & Jiang, 2013). Second, AMP-activated protein kinase (AMPK) induces autophagy when adenosine monophosphate (AMP) to adenosine triphosphate (ATP) ratio is high, indicating low cellular energy levels. These two counteracting enzymes enable the cell to fine-tune its metabolism to the current energy needs by changing the phosphorylation status of the Unc-51 like autophagy activating kinase (ULK1) complex (Kim, Kundu, Viollet, & Guan, 2011). The ULK1-complex is recruited to the endoplasmatic reticulum (ER) and initiates autophagosome formation by activating yet another protein complex, the phosphatidylinositol 3-kinase III complex (PI-3 kinase III complex) or Beclin1 complex. In the next steps, multiple groups of autophagy-related proteins (ATGs) promote the budding of an isolation membrane or phagophore, which begins to elongate. Importantly this elongation is facilitated by microtubule-associated protein light chain 3 (LC3, mammalian homologue of ATG8). The cytosolic form, called LC3-I, undergoes phosphatidylethanolamine-conjugation (PE-conjugation) upon recruitment to the autophagosome and is then called LC3-II (Ichimura et al., 2000). Of note, LC3-II is present in the internal and external membrane of the mature autophagosome and is widely used to quantify autophagic flux (Klionsky et al., 2016). During autophagosome formation, cargoes are engulfed, which can either happen unselectively or selectively, targeting only mitochondria for example (mitophagy) (Ashrafi & Schwarz, 2013). One way to label cargo for autophagy is post-translational ubiquitination, which is recognized by the sequestosome 1/ubiquitin-binding protein 62 (SQSTM1/p62) (Liu et al., 2016). SQSTM1/p62 not only acts as an adaptor between LC3-II and autophagic cargo but is also degraded within the autolysosome making it another useful marker for impaired autophagy (Bjørkøy et al., 2009). After the autophagosome has matured to a fully closed, double-membraned vesicle, it fuses with the lysosome to form the autolysosome. The latter possesses vacuolar-type ATPases (V-ATPases), a proton pump which produces an acidic milieu inside the autolysosome necessary for cargo degradation (Mauvezin & Neufeld, 2015). After degradation by lysosomal hydrolases, the autophagic yield is ready to be re-metabolized.

What role does ATG9A play in this process? Connected to this is the question, how the autophagosome obtains the membranes necessary for its *de novo* formation. Previous studies suggest that autophagosomes can recruit membranes from the ER (Hayashi-

Nishino et al., 2009), plasma membrane (Ravikumar, Moreau, Jahreiss, Puri, & Rubinsztein, 2010) and the Golgi apparatus (Geng, Nair, Yasumura-Yorimitsu, & Klionsky, 2010). ATG9 takes up a special place in the group of ATGs because it is the only multi-spanning transmembrane protein in the autophagy machinery (Noda et al., 2000; Young et al., 2006). It is required as a membrane source and for the expansion of the isolation membrane or phagophore, but interestingly is not incorporated into the autophagosome (Orsi et al., 2012; Papinski et al., 2014). Rather than being a structural component of autophagosomes, ATG9 transiently interacts with the expanding isolation membrane suggesting that it might function as a "phospholipid supplier". Indeed, "ATG9 reservoirs", i.e. conglomerates of ATG9-positive vesicles and tubular structures, locate to assembling autophagosomes in yeast (Mari et al., 2010) upon starvation and cycle between cellular compartments including the TGN, late endosomes (Young et al., 2006) and the plasma membrane (Claude-Taupin et al., 2021). Human embryonic kidney cells (HEK293 cells) show a similar pattern (Orsi et al., 2012) and in mouse Purkinje neurons, ATG9 is found to cycle between lysosomes and the TGN, but also localizes to the ER and axon terminals (Tamura, Shibata, Koike, Sasaki, & Uchiyama, 2010). Structural analysis supports the notion that ATG9 additionally facilitates elongation of the isolation membrane. Recent studies from Matoba et al. and Maeda et al. reveal that mammalian ATG9A forms a homotrimer and functions as a lipid scramblase at the isolation membrane (Maeda et al., 2020; Matoba et al., 2020). ATG2 transfers phospholipids from the donor compartment to the outer leaflet of the isolation membrane and some of these phospholipids are then transferred to the inner leaflet by ATG9A, which is crucial for elongation (Figure 3). While its function remains poorly defined, growing research exemplifies ATG9A's crucial role in autophagosome formation due to its ability to supply phospholipids to the inner leaflet of the isolation membrane.

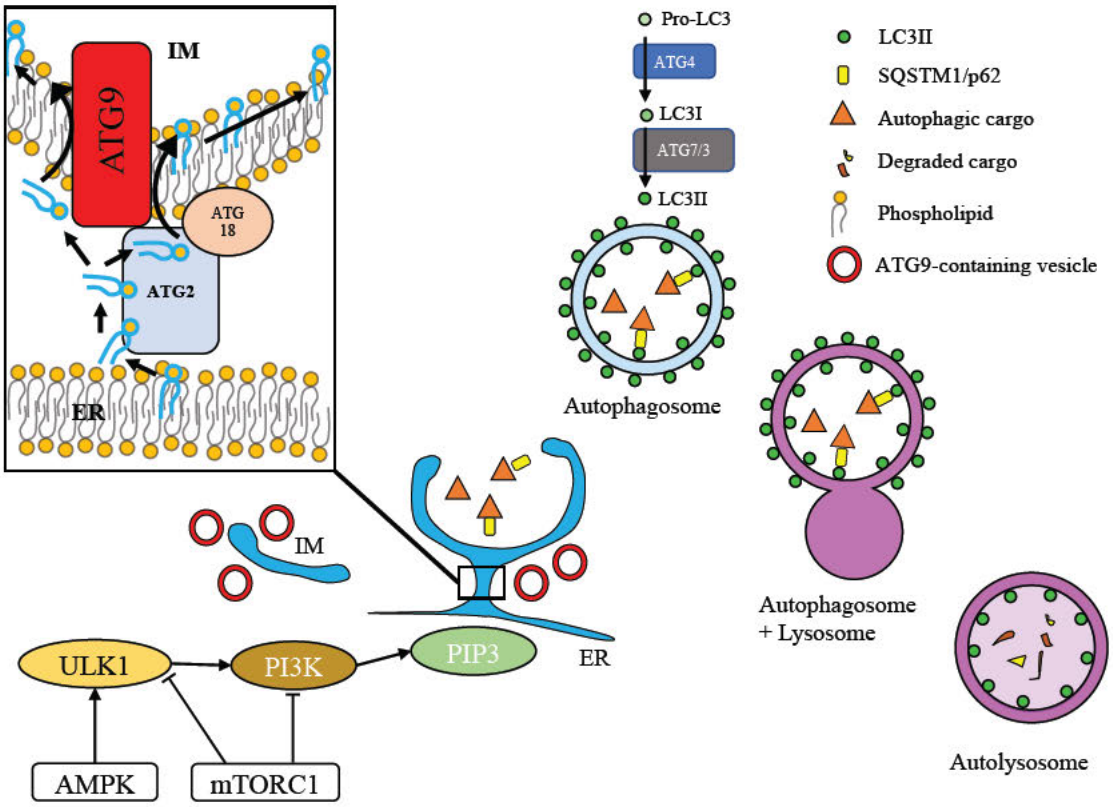

Figure 3 The role of ATG9 in the autophagy pathway.

During the initiation/nucleation steps (1./2.), ATG9-containing vesicles function as a membrane source for the isolation membrane (IM). ATG9 is then relocated to the expanding ends of the forming autophagosome during the elongation step (3.). Here, ATG9 functions as a scramblase to move phospholipids from the outer to the inner leaflet of the IM. ATG2 and ATG18 supply ATG9 with phospholipids from the endoplasmatic reticulum (ER). After the elongation step, the mature autophagosome (4.) fuses with a lysosome (5.) to form the autolysosome (6.), where the cargo is degraded. Not all functional groups involved in autophagy are depicted for the sake of simplification. Modified after Matoba et al. (2020) and Teinert, Behne, Wimmer, and Ebrahimi-Fakhari (2019)

The highly polarized architecture of neurons likely accounts for differences in the autophagic machinery (Lüningschrör & Sendtner, 2018) compared to other cell types. While skeletal muscle cells, for instance, activate autophagy mainly under starvation conditions, neuronal cells exhibit a continuous formation of autophagosomes in the distal

axon (Maday & Holzbaur, 2014; Maday, Wallace, & Holzbaur, 2012). This is necessary to maintain homeostasis in the axonal compartment, which is constantly challenged by accumulating synaptic proteins and mitochondria. Autophagosomes are built in the distal axon and are then retrogradely transported towards the soma to fuse with lysosomes. This means that an efficient supply of proteins needed for autophagosome formation must be ensured at all times and renders neurons particularly vulnerable against disturbances in protein sorting and transport. The emerging group of congenital disorders of autophagy are unified by the affection of the CNS, an indicator of the special role of autophagy in neuronal cells (Ebrahimi-Fakhari, Behne, Davies, & Hirst, 1993; Ebrahimi-Fakhari, Saffari, Wahlster, Lu, et al., 2016).

1.4 AP-4-Deficiency – Disrupting Neuronal Protein Trafficking And Autophagy?

How are the clinical phenotype and pathological findings of AP-4-associated HSP connected with AP-4's role of AP-4 in cargo sorting and ATG9A trafficking?

AP-4-associated HSP is predominantly a CNS disorder and other organ systems are mostly spared. Brain MR imaging shows a thinning of the corpus callosum, ventriculomegaly and cerebral or cerebellar atrophy in some cases. Progressive lower limb weakness and spasticity can be attributed to the degeneration of the long corticospinal tracts similar to other HSPs. Since this phenotype is caused by AP-4-deficiency, AP-4 – or more precisely its cargo – must play a vital role in the development and homeostasis of neurons, but to a lesser extent in other cell types. Highly polarized, post-mitotic neurons depend on the correct antegrade distribution of newly synthesized receptors and organelles from the soma to the axon and dendrites over long distances (Carlos M. Guardia, De Pace, Mattera, & Bonifacino, 2018). On the other hand, engulfment, retrograde transport and autophagic degradation of dysfunctional organelles such as old mitochondria are necessary to maintain homeostasis as neurons are not able to "dilute" their cellular content by cell division. Due to its cargoes, some of which are only expressed in neurons and explicitly depend on AP-4 for correct sorting, AP-4 is indispensable for neuronal health.

Indeed, AP-4-knockout HeLa cells, neuroblastoma-derived cells (SH-SY5Y), mouse embryonic fibroblasts (MEFs), leukemia-derived HAP1 cells and patient-derived

fibroblasts (Davies et al., 2018; Mattera et al., 2017) as well as Purkinje and hippocampal neurons from *Ap4e1*-knockout mice (De Pace et al., 2018; D. Ivankovic et al., 2020) all show missorting of ATG9A to the juxtanuclear region colocalizing with TGN markers. Furthermore, these studies found increased protein levels of ATG9A potentially compensating for the AP-4-dependent loss of ATG9A from the peripheral tubulovesicular structures or "ATG9A reservoir". Interestingly, Ivankovic et al. found increased levels of ATG9A in the soma of *Ap4e1*-knockout mice but decreased levels in the axonal compartment further supporting the notion, that transport of ATG9A is impaired (D. Ivankovic et al., 2020). Although the function of ATG9A remains poorly defined, it is implicated in early autophagosome formation and not surprisingly AP-4-deficient cells show signs of impaired autophagy. Reduced LC3 lipidation, i.e. conversion from the cytosolic form LC3I to the autophagosome-bound LC3II, and at the same time elevated total levels of LC3 are seen in AP-4-deficient MEFs (Mattera et al., 2017), HeLa cells (Davies et al., 2018) and neurons of *Ap4e1*-knockout mice (De Pace et al., 2018; Davor Ivankovic et al., 2020) and could point towards impaired autophagosome formation. Of note, knockdown of RUSC2, an AP-4 accessory protein that is thought to link ATG9A-vesicles to the microtubule system, causes similar disturbances of autophagic markers (Davies et al., 2018). This is corroborated by the finding that hippocampal and Purkinje neurons of *Ap4e1*- and *Ap4b1*-knockout mice exhibit axonal swellings, which represent accumulating autophagosomes (De Pace et al., 2018; D. Ivankovic et al., 2020; S. Matsuda et al., 2008). Moreover, these autophagosomes show unimpaired antegrade but decreased retrograde mobility, the ladder of which is critical for fusion with lysosome, which are located in the soma.

The question arises why AP-4-deficient neurons are still able to form autophagosomes despite the missorting of ATG9A? The decreased retrograde transport, the increased total levels of ATG9A and LC3 and the altered size and shape of LC3-positive vesicles suggest that AP-4-deficient cells are partially compensating the missorting of ATG9A by increasing ATG9A levels but at the same time, immature or deformed autophagosomes are built in the distal axon, which cannot be effectively transported to the soma leading to axonal swellings. Missorted AMPARs and GRID2 receptors might further contribute to the axonal overload with cargo that AP-4-deficient neurons fail to eliminate. Although variants in the GluA2 subunit of the AMPAR cause a disease characterized by

neurodevelopmental delay, seizures and brain atrophy (Salpietro et al., 2019) and partial deletion of the GRID2 gene causes spastic paraplegia and ataxia but no cognitive dysfunction (Maier et al., 2014), the role of receptor missorting in AP-4-associated HSP, which has some phenotypic overlap with both conditions, remains poorly defined and needs further study. Of note, AP-4-associated HSP has recently been added to the constantly growing group of congenital disorders of autophagy, all of which show prominent neurological manifestations (Teinert, Behne, Wimmer, & Ebrahimi-Fakhari, 2020). Interestingly, some of these disorders present as multisystem diseases such as the Vici syndrome (Byrne et al., 2016), whereas others only show CNS manifestations underscoring the specialized tasks of autophagy in different organs.

Do the *Ap4e-1* and *Ap4b1*-knockout mice exhibit a phenotype that could be explained by an axonopathy? The animals show motor impairments including reduced strength and coordination as well as behavioral changes such as increased startle response and ambulation (De Pace et al., 2018; S. Matsuda et al., 2008). The authors did not detect any learning or memory deficits using maze tests but could demonstrate that neuroimaging findings are highly reminiscent of those seen in patients with AP-4-associated HSP (De Pace et al., 2018; D. Ivankovic et al., 2020). In summary, AP-4-deficient mice show a milder phenotype presumably due to shorter axon length or a different role of AP-4-dependent transport in human cells. A recent study in *Ap4s1*-deficient zebrafish confirmed and expanded these findings by showing that besides motor impairments, reduced axonal outgrowth and length and neuronal hyperexcitability are present in a model of AP-4-associated HSP (D'Amore et al., 2020).

Another striking resemblance of the symptoms and imaging findings of AP-4-associated HSP is seen in CNS-specific knockout of *Atg9A* in mice (Yamaguchi et al., 2018). These mice exhibit prominent motor impairments and show additional growth retardation, convulsions and a shorter lifespan. Importantly, complete knockout of *Atg9A* is embryonically lethal proving that *Atg9A* is obligatory in early development and demonstrating that *Atg9A* function must be preserved to some degree in AP-4-deficiency despite its missorting. Concerning ATG9A's role in autophagy, primary cortical neurons of *Atg9A* conditional knockout mice showed signs of impaired autophagic flux after 2 weeks of age, which resolved at 4 weeks of age for unknown reasons. Yamaguchi et al. further demonstrated that *Atg9A* is needed for neurite outgrowth independent of its

function in autophagy. This implicates functions of *Atg9A* besides autophagy and adds to the previously described roles in the innate immune response (Saitoh et al., 2009) and ferritin metabolism (Goodwin et al., 2017).

To summarize, AP-4-deficiency causes missorting of several proteins in both *in vivo* and *in vitro* models and primarily affects the development and homeostasis of highly polarized neurons. Although it remains to be determined to what extent AP-4-dependent cargoes contribute to the disease, a working model can be proposed (Figure 4).

Loss of one of the four AP-4-subunits leads to instability of the whole complex leaving AP-4 without function. ATG9A is subsequently lost from the axonal compartment causing defects in autophagosome formation and axonal outgrowth. Immature autophagosomes accumulate in the axon and are responsible for axonal swellings. This is further aggravated by missorted somatodendritic receptors and other cargo proteins. Axonal homeostasis is impaired leading to a progressive axonopathy. This model is mirrored by the course of the disease of patients with AP-4-associated HSP, who are born with mild motor symptoms and neuroanatomical abnormalities and later show global developmental delay accompanied by progressive motor impairments.

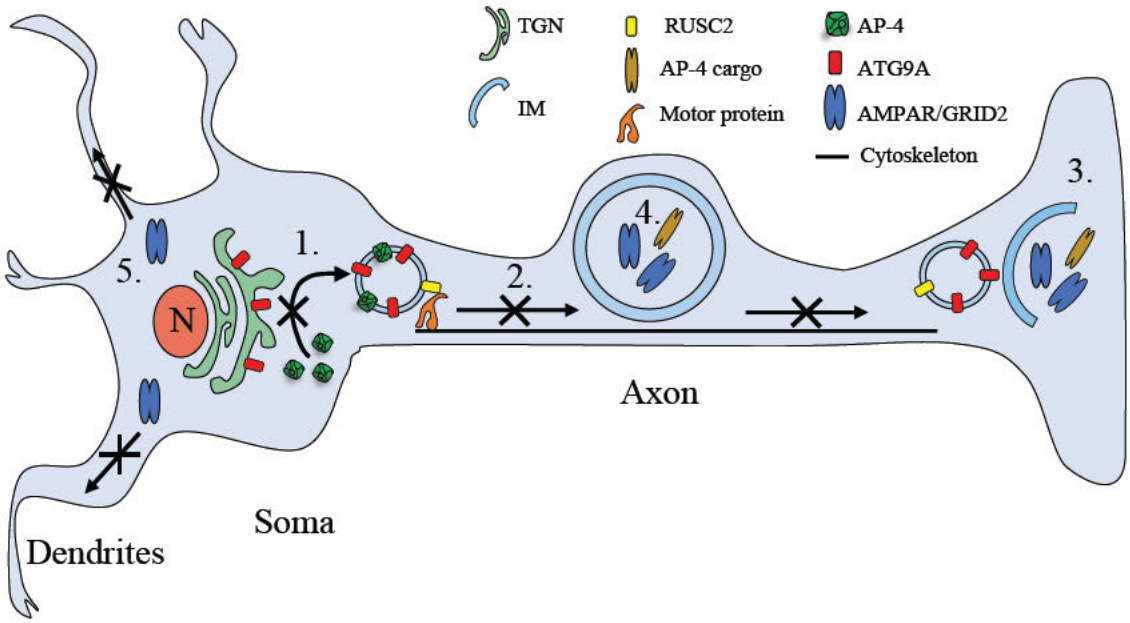

Figure 4 Proposed model of AP-4-deficiency in the neuron

Deficiency of one of the AP4-subunits leads to an instable complex and the inability to sort ATG9A and RUSC2 into transport vesicles **(1.)**. In healthy cells, RUSC2 facilitates

vesicle transport *via* the cytoskeleton **(2.)**. The lack of ATG9A-containing vesicles in the distal axonal compartment leads to disturbed autophagosome formation **(3.)**. These immature autophagosomes containing missorted AMPAR, GRID2 and other AP-4-cargoes accumulate in the axons and cause swellings **(4.)**. The dendritic compartment lacks receptors such as AMPAR, which are sorted in an AP-4-dependent manner **(5.)**. N, nucleus; IM, isolation membrane. Modified after (Davies et al., 2018).

1.5 iPSC-Derived Disease Models And High-Content Screenings

The described cellular and animal models give first insights into the pathomechanism underlying AP-4-associated HSP but insecurity remains whether they are able to replicate the pathology in human neurons. Concerning the fact that AP-4 is not present in all organisms and has specialized functions in the respective cell type (and organism), a disease model using patient-derived neurons could confirm the previous findings. The breakthrough discovery of Takahashi and Yamanaka that differentiated cells can be reprogrammed to the state of pluripotent stem cells (iPSCs) has opened up new possibilities for studying CNS disease *in vitro* (Takahashi & Yamanaka, 2006). Human fibroblasts can be taken from patients with CNS disease, reprogrammed into iPSCs and then differentiated into neurons. This has enabled the study of CNS disease on an individual level and is now a widely used and successful method in neuroscience (C. Y. Chang et al., 2015; Chen et al., 2014; Kondo et al., 2013; Seibler et al., 2018). This method does not only hold the promise of revealing human- and even patient-specific phenotypes but also has wide implications in the field of drug discovery. Advances in automated imaging and data analysis make screening of thousands of cells in a short period of time feasible. These so-called high-content screenings are set up by defining disease-associated phenotypic markers such as subcellular protein localization or neurite outgrowth. Cells are imaged after treatment with compound libraries, collections of bioactive small molecules. Automated imaging and image analysis assays are set up to detect “hits”, i.e. compounds that rescue the disease-associated phenotype in the cell. For instance, a missorted protein could serve as a marker in an assay that is set up to detect its re-distribution. Thus, it is crucial to identify phenotypic markers, which are robustly associated with disease and can be reliably detected. This type of investigation is useful, when the pathway that causes the disease is not clearly defined but phenotypic changes are detectable in cell. Combining iPSC-derived cellular models of CNS disease with high-throughput screenings is now a widely used tool to reveal such disease-causing pathways

and new therapeutic targets in neurological disease (C.-Y. Chang et al., 2020; Elkouzi, Vedam-Mai, Eisinger, & Okun, 2019; Fang et al., 2019; Rehbach et al., 2019).

1.6 Aims Of This Study

The aim of this study is the development of an iPSC-derived cortical neuron model of SPG47 using cells derived from patients with bi-allelic variants in the AP4B1-subunit. These iPSC-derived cortical neurons will be characterized in respect to AP-4-related phenotypes to identify robust phenotypic markers applicable in a high-content screen.

AP-4-deficiency leads to a poorly understood form of early-onset complicated HSP characterized by global developmental delay, intellectual disability and progressive spasticity of the lower limbs with treatment being limited to symptomatic. However, the recent discovery of ATG9A as a cargo of AP-4 (Davies et al., 2018; Mattera et al., 2017) has provided new insights into the mechanism underlying the disease. Moreover, the striking similarities of behavioral, motor, imaging and cellular phenotypes of CNS-specific *Atg9A*-knockout mice with those of AP-4-associated HSP strongly suggest that ATG9A sorting plays a crucial role (Yamaguchi et al., 2018). Its implications in autophagy are corroborated by the findings of altered autophagy in AP-4-deficient cells (De Pace et al., 2018; D. Ivankovic et al., 2020; Mattera et al., 2017) and the significant phenotypic overlap of AP-4-associated HSP with other congenital disorders of autophagy (Ebrahimi-Fakhari, Saffari, Wahlster, Lu, et al., 2016; Teinert, Behne, Wimmer, et al., 2019). Still, evidence from human neurons is lacking and the question arises whether the phenotypes seen in *in vitro* and *in vivo* models replicate the human pathology.

To test this, *in vitro* biochemical and imaging assays including automated high-content imaging and analysis were applied. First, patient-derived fibroblasts were characterized with respect to AP-4-related phenotypes with a focus on ATG9A and autophagic flux. Sex-matched heterozygous parental and wildtype fibroblasts were used as controls. These proof-of-concept experiments provided the basis for studies in human iPSC-derived cortical neurons. Skin cells of the same patient and control lines were used to generate iPSCs and differentiate them into iPSC-derived excitatory cortical neurons providing the first platform to study AP-4-associated HSP in human neurons. The iPSC-derived cortical neurons were then characterized with a focus on phenotypic markers identified in the

patient-derived fibroblasts. The range of phenotypic markers was further expanded by investigating neurite outgrowth and branching.

Under the hypotheses that AP-4-deficient iPSC-derived cortical neurons:

1. exhibit accumulation of ATG9A in the TGN
2. show elevated ATG9A protein levels
3. show impaired autophagy
4. exhibit impaired neurite outgrowth and branching

The objectives of this study are:

1. To characterize primary human fibroblasts from patients with SPG47 regarding the following AP-4-related phenotypes:
    a. Subcellular ATG9A localization
    b. ATG9A protein levels
    c. Autophagy markers
2. To develop an iPSC-derived cortical neuron model derived from patients with SPG47 and investigate the AP-4-related phenotypic markers applicable in a high-content screening:
    a. Subcellular ATG9A localization
    b. ATG9A protein levels
    c. Autophagy markers
    d. Neurite outgrowth and branching

Development of a human iPSC-derived cortical neuron model of SPG47 will provide first insights into the cellular pathology that is present in AP-4-deficient human neurons. It holds the promise of confirming recent findings of *in vitro* and *in vivo* models, expanding the range of AP-4-related phenotypic markers and providing a powerful tool to study AP-4-associated HSP and a platform to uncover novel therapeutic targets in a high-content screen.

2 Materials And Methods

2.1 Materials

Reagent	Obtained from	Catalogue number
0.25% Trypsin EDTA	Thermo Fisher Scientific	25200-056
20% SDS	Thermo Fisher Scientific	BP13111
24 Well Plate Thermo Scientific BioLite Multidishes and Microwell Plate	Thermo Fisher Scientific	930186
488 donkey anti-sheep IgG (H+L) Alexa Fluor®	Thermo Fisher Scientific	A11015
488 goat anti-mouse IgG (H+L) antibody Alexa Fluor®	Thermo Fisher Scientific	A11001
488 goat anti-rabbit IgG (H+L) antibody Alexa Fluor®	Life Technologies	A11008
594 donkey anti-sheep IgG (H+L) Alexa Fluor®	Thermo Fisher Scientific	A11016
594 goat anti-rabbit IgG (H+L) Alexa Fluor®	Thermo Fisher Scientific	A-11037
6 Well Tissue Culture Plate with lid, Individual, Sterile	CELLTREAT	CT2210
647 goat anti-chicken IgY (H+L) antibody Alexa Fluor®	Thermo Fisher Scientific	A21449
647 goat anti-guinea-pig IgG (H+L) Alexa Fluor®	Thermo Fisher Scientific	A-21450
647 goat anti-mouse IgG (H+L) Alexa Fluor®	Thermo Fisher Scientific	A-21236
647 goat anti-mouse IgG (H+L) antibody Alexa Fluor®	Thermo Fisher Scientific	A21235
Advanced DMEM/F12	Thermo Fisher Scientific	12634010
Anti-Adaptin ε antibody, Clone 32/Adaptin ε (RUO), mouse anti-human	BD Biosciences	612019
Anti-AP4B1 antibody (1B2) mouse anti-human	Novus Biologicals	H00010717-M03
Anti-AP4B1 antibody mouse anti-human	Thermo Fisher Scientific	PA5-48836
Anti-AP4B1 antibody rabbit anti-human	Abcam	ab130589
Anti-ATG9A antibody rabbit anti-human	Abcam	ab108338
Anti-beta-III tubulin antibody mouse anti-human	Novus Biologicals	NB100-1612-0.05ml
Anti-ENTHD2 polyclonal antibody rabbit anti-human	Thermo Fisher Scientific	PA566581
Anti-GM130/GOLGA2 antibody sheep anti-human	R&D Systems	AF8199-SP
Anti-LC3 antibody (5H3) mouse anti-human	Enzo Life Sciences	ALX-803-082-C100
Anti-LC3B antibody (D11) XP® rabbit anti-human	Cell Signaling Technology	3868S
Anti-LC3B antibody rabbit anti-human	Novus Biologicals	100-2220

Anti-MAP 2 antibody guinea pig anti-human	Synaptic Systems	MAP 2 - 188 004
Anti-MAP2 antibody rabbit anti-human	Abcam	ab32454
Anti-p62/SQSTM1 antibody rabbit anti-human	Sigma-Aldrich	P0067-200UL
Anti-phospho-S6 ribosomal protein (Ser235/236) antibody rabbit anti-human	Cell Signaling Technology	2211S
Anti-RUSC1 antibody rabbit anti-human	Thermo Fisher Scientific	PA556299
Anti-RUSC2 antibody rabbit anti-human	Abcam	ab156280
Anti-SQSTM1 / p62 antibody mouse anti-human	Abcam	ab56416
Anti-TGN46 antibody sheep anti-human	Biorad	AHP500G
Anti-α-tubulin antibody mouse anti-human	Sigma-Aldrich	T9026-.2ML
Anti-β-Tubulin III antibody mouse anti-human	Sigma-Aldrich	T8660-.2ML
Bafilomycin A1, >98%	LC Laboratories	B-1080
BCA Protein Assay Reagent	Thermo Fisher Scientific	23225
BioLite Cell-Culture Treated 10mm Dish	Thermo Fisher Scientific	130182
Bovine Serum Albumin	American Bioanalytical	AB004400-0100
Color Prestained Protein Standard, Broad Range (11–245 kDa)	New England Biolabs	P7712S
cOmplete™, Mini Protease Inhibitor Cocktail	Sigma-Aldrich	04693124001
Corning® 96-well Clear Flat Bottom Polystyrene TC-treated Microplate, Individually Wrapped, with Low Evaporation Lid, Sterile	Corning	3595
Coverslips (12mm thickness) for 24 Well Plates	Warner Instruments	64-0702 (CS-12R)
Cryogenic Vials 2mL	Corning	430488
CYTO-ID® Autophagy detection kit 2.0	Enzo Life Sciences	ENZ-KIT175-0050
Dimethyl Sulfoxide, DMSO	American Bioanalytical	AB03091-00100
DPBS, no calcium, no magnesium	Thermo Fisher Scientific	14190-250
Dulbecco's modified eagle's medium - HIG	Sigma-Aldrich	D5796-6X500ML
Ethyl Alcohol, Ethanol	American Bioanalytical	AB00138-04000
Falcon™ 50mL Conical Centrifuge Tube	Thermo Fisher Scientific	14-432-22
Fetal Bovine Serum (FBS), Heat Inactivated	Thermo Fisher Scientific	10438026
Fisherbrand™ Superfrost™ Plus Microscope Slides, Superfrost Plus	Thermo Fisher Scientific	22-037-246
Formaldehyde, 10%, methanol free, Ultra Pure	Polysciences	04018-1
Formaldehyde, 10%, methanol free, Ultra Pure	Polysciences Inc.	4018-1

Geltrex™ LDEV-Free, hESC-Qualified, Reduced Growth Factor Basement Membrane Matrix	Thermo Fisher Scientific	A1413301
Gentle Cell Dissociation Reagent	STEMCELL Technologies	07174
Glycine	Thermo Fisher Scientific	BP381-1
Greiner CELLSTAR® 96 well plates	Greiner Bio-One	655090
HBSS, calcium, magnesium, no phenol red	Thermo Fisher Scientific	14025-092
HIBERNATE E LOW FLUORESCENCE	BrainBits LLC	HELF
Hibernate E Low Fluorescence	BrainBits	HE-Lf
High Glucose DMEM	Thermo Fisher Scientific	11960-069
High Glucose DMEM	Thermo Fisher Scientific	11960-069
High Pure RNA Isolation Kit	Roche	11828665001
Hoechst 33258, Pentahydrate	Biotium	40045
Invitrogen Molecular Probes CellMask Deep Red Plasma Membrane Stain	Thermo Fisher Scientific	C10046
Invitrogen Novex NuPAGE 4 12% Bis Tris Protein Gels, 1.0mm, 15 well	Thermo Fisher Scientific	NP0323BOX
Invitrogen Novex NuPAGE MES SDS Running Buffer (20X)	Thermo Fisher Scientific	NP0002
IRDye® 680LT donkey anti-rabbit IgG antibody (H+L)	Licor	926-68023
IRDye® 680LT donkey anti-mouse IgG antibody (H + L)	Licor	926-68022
IRDye® 800CW donkey anti-mouse IgG antibody (H+L)	Licor	926-32212
IRDye® 800CW donkey anti-rabbit IgG antibody (H+L)	Licor	926-32213
Iron Assay Kit	Sigma-Aldrich	MAK025-1KT
JC-1 Dye (Mitochondrial Membrane Potential Probe)	Thermo Fisher Scientific	T-3168
Methanol	Thermo Fisher Scientific	A412P-4
MitoTracker® Deep Red FM - Special Packaging	Thermo Fisher Scientific	M22426
Ncyte Astrocyte Kit	Ncardia	Nc-K-HA-2M
NucBlue® Live ReadyProbes® Reagent	Thermo Fisher Scientific	R37605
Nunc™ Cell-Culture Treated 12 Well Plate	Thermo Fisher Scientific	150628
Nunc™ Glass Bottom Dish, 27mm	Thermo Fisher Scientific	150682
NuPAGE® Antioxidant	Thermo Fisher Scientific	NP0005
NuPAGE® MOPS SDS Running Buffer (20X)	Thermo Fisher Scientific	NP0001

NuPAGE® Novex® 4-12% Bis-Tris Protein Gels, 1.0 mm, 12 well	Thermo Fisher Scientific	NP0322BOX
NuPAGE™ LDS Sample Buffer (4X)	Thermo Fisher Scientific	NP0008
NuPAGE™ Sample Reducing Agent (10X)	Thermo Fisher Scientific	NP0009
Odyssey® Blocking Buffer (PBS)	Licor	927-40000
P35G-1.5-14-C Case Glass Bottom Dishes	MatTek Corporation	P35G-1.5-14-C Case
Parafilm M	Sigma-Aldrich	P6543
PBS Tablets	Millipore Sigma	524650-1EA
Penicillin-Streptomycin (10,000 U/mL)	Thermo Fisher Scientific	15140122
Pierce™ AEBSF Protease Inhibitor	Thermo Fisher Scientific	78431
Pierce™ BCA Protein Assay Kit	Thermo Fisher Scientific	23225
PowerUp™ SYBR™ Green Master Mix	Thermo Fisher Scientific	A25741
ProLong™ Diamond Antifade Mountant	Thermo Fisher Scientific	P36965
Protein A Sepharose®	Abcam	Ab193256
PVDF Transfer Membrane, 0.45 µm	Thermo Fisher Scientific	88518
Red Blood Cell Lysis Buffer	Sigma-Aldrich	11814389001
RIPA Lysis and Extraction Buffer	Thermo Fisher Scientific	89900
Saponin	Sigma-Aldrich	47036-50G-F
StemFlex Medium	Thermo Fisher Scientific	A3349401
Superfrost Plus Miscroscope Slides	Thermo Fisher Scientific	12-550-15
Tetramethylrhodamine, Ethyl Ester, Perchlorate (TMRE)	Thermo Fisher Scientific	T-669
Torin 1 Cat. No. 4247	Tocris Bioscience	4247
Transcriptor First Strand cDNA Synthesis Kit	Roche	04379012001
Tween 20	Sigma-Aldrich	P9416
V5 Tag Monoclonal Antibody	Thermo Fisher Scientific	R960-25

2.2 Cell Culture

The Institutional Review Board at Boston Children's Hospital approved all work involving human fibroblasts and iPSCs (IRB#: P00016119).

2.2.1 Primary Human Fibroblasts

Skin punch biopsies (2-3mm) were taken from three patients with AP-4-associated HSP carrying bi-allelic variants in the AP4B1-subunit and from same-sex parents (heterozygous carriers, clinically unaffected) (Table 2). Three skin punch biopsies from

healthy individuals were taken as additional controls. Skin samples were processed by the Human Neuron Core as described previously (Drouin-Ouellet et al., 2017) to isolate fibroblasts. Written informed consent was obtained for all donations of skin fibroblasts.

Table 2 Primary human fibroblast lines

Line ID	Abbreviation in figures	Source	Sex	Age	Ethnicity	Allele 1	Allele 2
0052-01	#01 AP4B1 LoF/LoF	Patient	M	2	Caucasian	c.1345A>T (p.Arg449*)	c.1160_1161delCA (p.Thr387Argfs*30)
0052-03	#01 AP4B1 WT/LoF	Parent	M	38	Caucasian	c.1160_1161delCA (p.Thr387Argfs*30)	WT
0054-01	#02 AP4B1 LoF/LoF	Patient	F	3	Caucasian	c.530_531insA (p.Asn178Glufs*20)	c.114-2A>C
0054-02	#02 AP4B1 WT/LoF	Parent	F	33	Caucasian	c.114-2A>C	WT
0058-01	#03 AP4B1 LoF/LoF	Patient	F	3y9m	Caucasian	c.1216C>T (p.Arg406*)	c.1328T>C (p.Leu443Pro)
0058-02	#03 AP4B1 WT/LoF	Parent	F	39y6m	Caucasian	c.1328T>C (p.Leu443Pro)	WT
UN-01	#01 AP4B1 WT/WT	Healthy donor	F	-	Caucasian	WT	WT
UN-02	#02 AP4B1 WT/WT	Healthy donor	F	-	Caucasian	WT	WT
UN-03	#03 AP4B1 WT/WT	Healthy donor	F	-	Caucasian	WT	WT

Primary human fibroblasts were cultured in DMEM (Dulbecco's Modified Eagle Medium, without L-Glutamine and Pyruvate, 4.5g/l D-Glucose) with 20% FBS (Fetal Bovine Serum) and 1% Penicillin/Streptomycin (10,000 U/ml) on a 96 well plate (Greiner CELLSTAR, black polystyrene), a 24 well plate (Corning, non-treated polystyrene) with 12mm coverslips (Warner Instruments), a 12 well plate (Thermo Fisher Scientific, cell culture treated), a 6 well plate (Celltreat, cell culture treated polystyrene) or a 100mm dish (Thermo Fisher Scientific, cell culture treated) depending on the experiment (Table 3). Fibroblasts were plated at a density of $1.5x10^4$ on 12mm coverslips.

Table 3 Cell culture dish and plate specifications

Dish/Plate	Surface area (cm^2)	Seeding density	Cells at confluency	Trypsin (ml)	Medium (ml)
100mm	78.5	2.2×10^6	8.8×10^6	2	10-15
6-well	9	0.3×10^6	1.2×10^6	1	2
12-well	4	0.1×10^6	0.4×10^6	0.5	1
24-well	2	0.05×10^6	0.2×10^6	-	0.5
96-well	0.34	0.2×10^5	-	-	0.1-0.2

Human Fibroblasts were cultured under growth conditions (37°C, 5% CO2). Fibroblast media was changed entirely 24h after plating and then every other day. Cells were passaged after 7 days. Before passaging, cells were washed once with prewarmed DPBS (Dulbecco's Phosphate Buffered Saline without calcium or magnesium), incubated with 0.25% Trypsin EDTA for 5min with cell detachment being confirmed by brightfield microscopy, centrifuged for 5min at 1500 rpm in a 50ml conical tube and subsequently resuspended in fresh, prewarmed media for plating. For long-term storage, 1 ml of fibroblasts in resuspension media was added to 1 ml of 20% FBS in DMSO in a cryogenic vial (Corning) and stored at -80°C.

2.2.2 iPSC-Derived Cortical Neurons

iPSC-derived cortical neurons cultured for protein and RNA collection were maintained in human astrocyte conditioned medium (Astro.4 U, Ncardia) after a differentiation period of 6 days. Neurons were grown on laminin coated 12 well plates at a plating density of $8x10^5$ and collected on day 14. Neurons for high-content confocal imaging using the ImageXpress Micro Confocal High-Content Imaging System (Molecular Devices) were plated in 96 well plates (Greiner Bio-One) at $2x10^4$ per well, co-cultured with human $3x10^3$ iPSC-derived astrocytes (Astro.4U, Ncardia) and fixed in 4% PFA for immunocytochemistry after 14 days. For assessing neurite outgrowth using the IncuCyte S3 Live Cell Analysis System (Essen BioScience), neurons were plated at $1x10^4$ in 96 well plates (Greiner Bio-One) and fixed in 4% PFA after 24h in the IncuCyte. The outer wells of all 96 well-plates were filled with DPBS to prevent media evaporation of the 60 inner wells.

2.3 Generation Of Human iPSC And Differentiation Into Cortical Neurons (*With Human Neuron Core)*

Human iPSC lines were generated at the Harvard Stem Cell Institute. In collaboration with the Human Neuron Core three fibroblast lines of patients and sex-matched parental lines (Table 4) were transduced with Sendai virus (Fusaki, Ban, Nishiyama, Saeki, & Hasegawa, 2009) to introduce reprogramming factors Oct4, Sox2, Klf4 and L-Myc. Embryoid body formation was assessed as previously described (Teinert, Behne, D'Amore, et al., 2019) and was normal. Karyotyping showed normal results across all lines and pluripotency markers showed high expression using RT-PCR and immunocytochemistry. STR profiling matched iPSC lines to their respective fibroblast lines. StemFlex medium (Thermo Fisher Scientific) was used to culture iPSCs on a Geltrex Membrane Matrix (Thermo Fisher Scientific) and lines were passaged after 7 days with Gentle Cell Dissociation Reagent (STEMCELL Technologies) (Teinert, Behne, D'Amore, et al., 2019). The Human Neuron Core differentiated the cortical neurons using previously described protocols (Zhang et al., 2013). Briefly, iPSCs were treated with Accutase (Thermo Fisher Scientific) to induce dissociation and plated on a Geltrex-coated 6-well-plate. Ngn2-containig lentivirus together with polybrene was added for 24h on day -1. On day 0 a medium change was performed adding Advanced DMEM/F12 medium

(Thermo Fisher Scientific) together with human BDNF (10 µg/l, PeproTech), human NT-3 (10 µg/l, PeproTech), mouse laminin (0.2 mg/l, Invitrogen) and Doxycycline (2 g/l, Clontech). A 24h puromycin (1 mg/l) selection was performed on day 1 and ended with a 50% medium change on day 2, that was then performed every other day for 6 days. EGFP-expressing differentiated cortical neurons were selected using the EVOS M5000 Imaging System (Thermo Fisher Scientific).

Table 4 Human iPSC lines used for cortical neuron differentiation

Line ID	Abbreviation in figures	Source	Sex	Age	Ethnicity	Allele 1	Allele 2
HNDS_0052-01-iPS-D	#01 AP4B1 LoF/LoF	Patient	M	2	Caucasian	c.1345A>T (p.Arg449*)	c.1160_1161delCA (p.Thr387Argfs*30)
HNDS_0052-03-iPS-A	#01 AP4B1 WT/LoF	Parent	M	38	Caucasian	c.1160_1161delCA (p.Thr387Argfs*30)	WT
HNDS_0054-01-iPS-B	#02 AP4B1 LoF/LoF	Patient	F	3	Caucasian	c.530_531insA (p.Asn178Glufs*20)	c.114-2A>C
HNDS_0054-02-iPS-A	#02 AP4B1 WT/LoF	Parent	F	33	Caucasian	c.114-2A>C	WT
HNDS_0058-01-iPS-B	#03 AP4B1 LoF/LoF	Patient	F	3y9m	Caucasian	c.1216C>T (p.Arg406*)	c.1328T>C (p.Leu443Pro)
HNDS_0058-02iPS-B	#03 AP4B1 WT/LoF	Parent	F	39y6m	Caucasian	c.1328T>C (p.Leu443Pro)	WT

AP4B1 transcript NM_001253852.3

2.4 Autophagy Assays

To examine differences between AP-4-deficient fibroblasts and heterozygous controls under starvation conditions, two different sets of experiments were performed using established methods of autophagy induction (Ebrahimi-Fakhari, Saffari, Wahlster, DiNardo, et al., 2016; Klionsky et al., 2016; Sahani, Itakura, & Mizushima, 2014). To create starvation conditions in human fibroblasts, HBSS (Hank's Balanced Salt Solution) without calcium, magnesium and without serum, glucose or aminoacids was used instead of media. As additional conditions, autophagy inducing (Torin 1) or inhibiting drugs (Bafilomycin A1) were added to warm medium or HBSS. Bafilomycin A1 was used at a concentration of 200nM to inhibit lysosome-autophagosome fusion as well as lysosomal degradation. Bafilomycin A1 inhibits the H^+-ATPase, a proton pump, that is responsible for acidifying the lysosome before degradation (Klionsky, 2016; Mauvezin & Neufeld, 2015) and leads to an accumulation of autophagosomes. Torin 1 blocks phosphorylation of mTORC 1 and mTORC2 depleting the cell of signals for cell growth and proliferation (Thoreen et al., 2009) and thereby simulating starvation conditions and inducing autophagy. It was used at a concentration of 250nM. LC3B and SQSTM1 were used as autophagy markers. LC3B, the mammalian homologue of ATG8, is a widely used marker for autophagy and has a non-lipidated (hereafter LC3I) and a lipidated or PE-conjugated form (hereafter LC3II). While LC3I can be found ubiquitously in the cytosol, LC3II is found primarily in completed autophagosomes (Kabeya et al., 2000). Under starvation conditions, when more autophagosomes are formed, LC3II total levels rise and LC3II/I ratio increases. Care must be taken when interpreting autophagy assay results using the LC3II/I ratio. An increase of the LC3II/I ratio can either be the result of increased autophagosome formation and a resulting shift from LC3I to its lipidated form, LC3II, or a blockage of autophagic flux with an accumulation of autophagosomes, that can also be induced by drugs such as Bafilomycin A1. The former additionally depends on the timepoint of measurement, since autophagosomes constantly get degraded, which can decrease the LC3II/I ratio (Tanida, Minematsu-Ikeguchi, Ueno, & Kominami, 2005) and LC3II levels have been reported to decrease during longer starvation periods in MEFs (Mizushima & Yoshimori, 2007). The LC3II/I ratio can be used as an indirect marker of autophagosome formation and autophagic state, but a combined approach looking at baseline levels as well as changes under autophagy induction or blockage and additionally

microscopy-based identification of LC3-positive structures should be applied. As a second marker for autophagy, the autophagy substrate SQSTM1/p62 was used. SQSTM1/p62 binds to polyubiquinated proteins and these eventually get incorporated into autophagolysosomes and degraded (Liu et al., 2016; Pankiv et al., 2007). SQSTM1/p62 levels have previously been described to increase when autophagy is blocked and to decrease when autophagy is activated in different cell types, such as MEFs (Klionsky et al., 2016; Sahani et al., 2014). As a measure of mTORC1 activity, protein levels of phosphorylated ribosomal protein S6 (pS6) were examined. PS6 is a downstream target of mTORC1 substrates and is phosphorylated to a lesser extent under starvation conditions, when mTORC1 activity is inhibited (Pende et al., 2004).

The first set of experiments was performed by starving fibroblasts for 4h with or without the addition of Bafilomycin A1 to inhibit lysosome-autophagosome fusion. After 4 hours, cells were harvested for western blotting or fixed on coverslips for immunocytochemistry (Chapter 2.9.1). For the second set of experiments, fibroblasts were starved or treated with autophagy inducing or inhibiting drugs for different durations, ranging from 1h to 8h, making a total of 6 different conditions (Figure 5). For conditions only using HBSS or medium, DMSO (dimethyl sulfoxide) was added, since it is a solvent used for both Bafilomycin A1 and Torin 1 to exclude a toxic effect of DMSO. After the set duration, fibroblasts were harvested for western blotting.

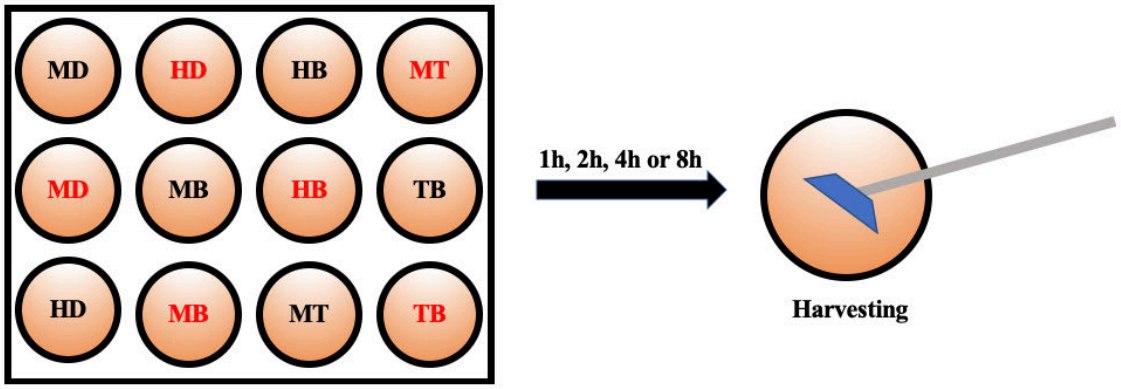

Figure 5 Autophagy assay layout

Schematic for starvation experiments showing a 12 well plate with the conditions MD: medium + DMSO, HD: HBSS + DMSO, MB: medium + Bafilomycin A1, HB: HBSS + Bafilomycin A1, MT: medium + Torin 1, TB: Torin 1 + Bafilomycin 1. Wells with *black* letters contain AP4B1 LoF/LoF fibroblasts lines and wells with *red* letters contain AP4B1 WT/LoF lines. For each set of experiments, four 12 well plates with the conditions shown above were harvested after 1h, 2h, 4h or 8h, respectively. LoF, Loss of function; WT, wildtype.

2.5 Protein Collection And Western Blotting

Cell lysis for fibroblasts cultured in a 6 well plate (Celltreat, cell culture treated polystyrene) was performed when cells reached 80-90% confluency after 3-4 days. For iPSC-derived cortical neurons cultured in a 12 well plate (Greiner Bio One) cell lysis was done 7 days after replating. Human fibroblast medium was aspirated and cells were washed with 2ml ice-cold PBS (Phosphate Buffered Saline) per well on ice. For iPSC-derived cortical neurons the washing step was skipped to avoid detachment from the plate. 100ul of Pierce™ RIPA Lysis and Extraction Buffer supplemented with cOmplete™ Protease Inhibitor Cocktail was added to each well and cells were scraped and transferred to a pre-chilled 1.5ml tube. The tubes were vortexed and put on ice, vortexed again after 15min and after another 15min centrifuged at $13.4x10^3$ rpm at 4°C for 10min. Supernatant (whole cell lysate) was aspirated without touching the pellet (cell membrane) and stored at -20°C. Pierce™ Protein Assay Kit was used to assess total protein concentration after thawing lysates on ice using the manufacturer's protocol. 5µl of BSA Standard Concentrations (2, 1.5, 1, 0.75, 0.5, 0.25, 0.125, 0.025, 0 µg/µl) were added to a clear-bottom 96 well plate (Corning) in duplicates and 5µl of samples were added subsequently. Reagent A (100µl) and B (5ml) were mixed and 200µl of the mixture was added to each

well. After an incubation period of 30min in the dark at 37°C, absorbance was read at 562nm using a Tecan Spark plate reader (Tecan). A standard curve was created using Microsoft Excel to determine protein concentrations. For western blotting, protein concentration (6µg for human fibroblasts, 15µg for cortical neurons) was adjusted depending on the gel size and deionized water was used to even volume differences of samples (Table 5). Reagent mixture was prepared in PCR tubes, vortexed and boiled for 10min at 70°C in a C1000^{TM} Thermal Cycler (Bio-Rad). Next, gels were loaded and separated for around 50min at 200V in 40ml NuPAGE 20X MOPS Running Buffer in 760ml deionized water with 500µl of NuPAGE Antioxidant in the inner chamber.

Table 5 Reagent concentrations for NuPAGE Novex 4-12% Bis-Tris Protein-Gels (1mm)

Reagent	10 wells (µl)	12 wells (µl)	15 and 17 wells (µl)
NuPage LDS Buffer 4x	6.25	5	3.75
10x NuPage Reducing Agent	2.5	2	1.5
Sample lysate	16.25	13	9.75
Total volume	25	20	15

PVDF membranes for transfer were activated in methanol for 30s, rinsed in deionized water briefly and kept in transfer buffer for 5min. Transfer buffer consisted of 30ml NuPAGE 20X Transfer Buffer, 60ml methanol and 510ml deionized water. After filling the inner chamber with transfer buffer and the outer chamber with deionized water, separated proteins were transferred on a 0.45µm PVDF membrane for 60min at 30V. After transferring PVDF membranes were put in methanol for 1min, rinsed briefly in deionized water and wet in PBS for 2min before blocking in Odyssey Blocking Buffer (PBS-based for 1h at room temperature on a shaker). The PVDF membrane was incubated in primary antibodies (Table 6) in Odyssey Blocking Buffer with 0.2% Tween 20 overnight at 4°C on a shaker. After washing 4x5min with 1X PBS with 0.1% Tween 20 the PVDF membrane was incubated with secondary antibodies in Odyssey Blocking Buffer with 0.2% Tween 20 and 0.01% SDS (Sodium Dodecyl Sulfate) for 1h at room temperature (in the dark). IRDye 800CW and 680LT antibodies were used at a 1:4000

concentration. Then 4x5min of washing in 1X PBS was performed with a final rinse in 1X PBS to remove the Tween 20 were performed. Membranes were imaged using the Licor Odyssey CLX setup and quantified with the ImageStudio Software. As a loading control, anti-α-tubulin antibody was used.

Table 6 Antibody concentrations for western blotting

Primary Antibody	**Concentration**
Anti-ATG9 Rabbit	1:500
Anti-AP4E1 Mouse	1:500
Anti-SQSTM1/p62 Rabbit	1:2000
Anti-α-Tubulin Mouse	1:1000
Phospho-S6 Ribosomal Protein (Ser235/236)	1:1000
Anti-LC3B Rabbit	1:1000
Secondary Antibody (IRDye®)	
Anti-Rabbit IgG 680LT	1:4000
Anti-Mouse IgG 680LT	1:4000
Anti-Rabbit IgG 800CW	1:4000
Anti-Mouse IgG 800CW	1:4000

2.6 Co-Immunoprecipitation *(With Angelica D'Amore)*

Co-immunoprecipitation experiments were performed by growing fibroblasts on a 100mm dish (Thermo Fisher Scientific, cell culture treated) under growth conditions as described earlier (Chapter 2.2.1). Cells were washed with ice-cold PBS and then lysed with Triton X containing Pierce AEBSF protease inhibitor (Aminoethylbenzenesulfonyl fluoride hydrochlorid, Thermo Fisher Scientific). Lysates were then vortexed, incubated on ice for 10min and centrifuged at 21000g for 20min at 4°C. Pierce™ Protein Assay Kit was used to adjust protein concentrations as described above (Chapter 2.5). Half of the lysate was used as input while the other was treated with Anti-AP4B1 antibody (Abcam) and Protein A Sepharose beads (Abcam) to isolate protein complexes containing the AP4B1-subunit. After washing the beads five times with ice-cold PBS, lysates were

boiled for 10min at 70°C in a C1000™ Thermal Cycler (Bio-Rad) and gels were loaded for western blotting as described above (Chapter 2.5).

2.7 mRNA-Collection And RT-PCR *(With Angelica D'Amore)*

The High Pure RNA Isolation Kit (Roche) was used to examine ATG9A and AP4B1 expression in AP-4-deficient fibroblasts and heterozygous controls. Fibroblasts were plated on 6 well plates at a density of 2.5 x 10^6 and harvested 3 days later following manufacturer's instructions. Reverse Transcription was performed using Transcriptor First Strand cDNA Synthesis Kit (Roche) to generate cDNA following manufacturer's instructions. Primers for quantitative real-time PCR were generated with the website rtprimerdb.org. In a 96 well plate, 5µl of PowerUp™ SYBR™ Green Master Mix (Thermo Fisher Scientific) were combined with cDNA and the primers to a total volume of 10µl following manufacturer's instructions. Real-time PCR was performed using the iCycler iQ™ Real-Time Detection System (Bio-Rad) as described previously (Ebrahimi-Fakhari et al., 2011). The PCR products were analyzed using agarose gel electrophoresis (2%).

2.8 Lentivirus Generation And Re-Expression Of AP4B1 In Human Fibroblasts (*With Angelica D'Amore)*

The V5-tagged lentiviral vector with a PGK promoter carrying human AP4B1 to re-express AP4B1 in AP4B1-deficient fibroblasts was a kind gift from Professor M. Azzouz, University of Sheffield, Department of Neuroscience, UK. For lysates, cells were plated at a density of $5x10^5$ on 6-well-plates. To achieve a multiplicity of infection (MOI) of 1:20 (virus concentration: $1.3x10^8$ vector genomes/ml), 62µl of lentivirus were added to 500ml of medium (DMEM + 20% FBS + 1% Penicillin/Streptomycin) and 2.81µg of Polybrene (5µg/ml). 24h after plating medium was removed and the medium containing AP4B1-V5-Lentivirus was added. After 24h of incubation lentivirus-containing medium was removed and fresh medium was added. Harvesting for western blotting was done three days after transduction as described above (Chapter 2.5). For immunocytochemistry, fibroblasts were plated in 96 well plates (Greiner Bio-One) at $2x10^4$ per well. Lentivirus transduction was performed as described above, but with a MOI of 1:50.

2.9 Immunocytochemistry

2.9.1 Primary Human Fibroblasts

Human Fibroblasts were fixed 24h after plating on 12mm coverslips at a density of around 30% using either 100% Methanol or 3% Formaldehyde in 1xPBS. For iPSC-derived cortical neurons cultured in 96 well plates, fixation was performed either 7 days after replating or 28h after plating (IncuCyte experiment) in 4% Formaldehyde in 1X PBS. Solutions described were filtered using a 0.45µm bottle top filter (Corning).

For methanol fixation, fibroblasts were washed with 1X PBS once and incubated with ice-cold 100% methanol on ice for 5min. Next, cells were washed three times with 1X PBS at room temperature and stored at 4°C.

For formaldehyde fixation, human fibroblasts were washed with 1X PBS once and then fixed with 3% Formaldehyde for 20min at room temperature before washing once with 1X PBS and subsequent quenching of unreacted aldehyde with 20mM glycine in 1X PBS for 5min was performed. For the final step, cells were washed three times with 1X PBS and stored at 4°C.

Methanol fixed fibroblasts on 12mm coverslips were submerged in a blocking solution of 1% BSA (Bovine Serum Albumin) in 1X PBS for 10min at room temperature. Primary antibodies were prepared in blocking solution (Table 7) and each coverslip was incubated cell side down in a 25µl drop on parafilm (Sigma-Aldrich) for 1h at room temperature in the dark. After incubation coverslips were washed three times with blocking solution and secondary antibodies were prepared in blocking solution. Hoechst 33258 was added to the solution for nuclear staining. Coverslips were incubated cell side down on a 50µl drop of secondary antibody solution on parafilm in the dark for 4min. Then coverslips were washed three times in 1X PBS and rinsed with deionized water once. All washing steps were performed using a 24 well plate with the cell side facing up. For confocal imaging coverslips were mounted on a microscopy slide (Thermo Fisher Scientific) using ProLong Diamond Antifade Reagent (Thermo Fisher Scientific). Methanol fixed coverslips were used to look at autophagy markers LC3B and SQSTM1/p62 (Table 7).

Formaldehyde fixed fibroblasts were permeabilized with 0.1% Saponin and 1% BSA in 1X PBS for 10min at room temperature. Following this, a 10min blocking step with 0.01% and 1% BSA in 1X PBS was done. All subsequent steps are similar to the protocol

described for methanol fixed coverslips except that blocking solution included 0.01% Saponin additionally. Formaldehyde fixed coverslips were used to look at ATG9A co-localization with the trans-Golgi network marker TGN46. Coverslips were imaged using the 20X objective of the UltraVIEW VoX Spinning Disk Confocal Microscope (Perkin Elmer).

2.9.2 iPSC-Derived Cortical Neurons

iPSC-derived cortical neurons were fixed by adding 100µl of 8% formaldehyde to each well that contained 100µl of medium to reach a final concentration of 4%. Washing three times with 1X PBS was only performed after fixation to avoid detachment of neurons from the plate and glycine quenching was not used. Formaldehyde fixed neurons on 96 well plates were permeabilized with 0.1% Saponin and 1% BSA in 1X PBS for 10min at room temperature followed by a 50min blocking step with 0.01% Saponin and 1% BSA in 1X PBS. Primary antibodies (Table 7) were prepared in the blocking solution and incubated for 20h in the dark at 4°C. Following three washing steps with blocking solution secondary antibodies in blocking solution were added for 1h in the dark. Hoechst 33258 was added to the solution for nuclear staining. Finally, three washes with 1X PBS were performed and neurons were imaged using a 20x Objective of the ImageXpress Micro Confocal High-Content Imaging System (Molecular Devices). ATG9A localization as well as co-localization with trans-Golgi-marker GM130 was performed in neurons, that were identified by β-Tubulin III, a protein found almost exclusively in neuronal microtubules (Mariani et al., 2015).

Table 7 Antibody Concentrations for Immunocytochemistry

Primary Antibody	Human Fibroblasts	Human iPSC-derived Cortical Neurons
Anti-ATG9 Rabbit	1:200	1:800
Anti-TGN46 Sheep	1:200	
Anti-LC3B Rabbit	1:200	
Anti-SQSTM1/p62 Mouse	1:200	
Anti-GM130/GOLGA2 Sheep		1:800
Anti-β-Tubulin III Mouse		1:800
Secondary Antibody		
Anti-Rabbit 488	1:400	1:800
Anti-Sheep 594	1:400	1:800
Anti-Mouse 647		1:800
Hoechst 33258	1:1000	1:1000

2.10 Confocal Imaging And Image Analysis

2.10.1 Primary Human Fibroblasts On Coverslips

For formaldehyde, methanol fixed coverslips and live cells, confocal imaging was performed with the UltraVIEW VoX Spinning Disk Confocal Microscope (Perkin Elmer), which is equipped with a Nikon Eclipse Ti inverted microscope and an electron multiplying charge-coupled device (EMCCD) camera (Hamamatsu C9100-50). A 20x dry objective (0.75NA), 40X oil objective (1.3NA) and 60X oil objective (1.4NA) were used. The Volocity software (Version 6.3.0) together with a motorized X-Y-stage allowed for automated imaging of large regions of interest (ROI) with images being stitched afterwards. All configurations were kept constant for the entire experiment and laser power was kept low to prevent photobleaching

2.10.2 Mitochondrial Assay – JC1-Dye And TMRE/MTDR

To investigate mitochondrial membrane potential ($\Delta\Psi_m$) and mitochondrial mass, two methods were used to stain mitochondria in living cells. JC-1 dye (tetraethylbenzimidazolylcarbocyanine iodide) is a cationic carbocyanine that accumulates in a membrane-potential dependent manner in mitochondria of different cell types including fibroblasts (Scanlon & Reynolds, 1998; Want et al., 2016). While emitting green light (529nm) in its monomeric state, JC1 aggregates in mitochondria emit red light (590nm) allowing the calculation of the green to red ratio to compare $\Delta\Psi_m$ between cell lines. This fluorescence intensity ratio is a surrogate measure for mitochondrial polarization status and a lowering of the red/green ratio translates to mitochondrial depolarization. MTDR (MitoTracker® Deep Red) is a far-red dye that accumulates in active mitochondria and was used to determine mitochondrial mass (Lugli et al., 2005) while TMRE (Tetramethylrhodamine, ethyl ester) was used to measure mitochondrial membrane potential (Condo, Ventura, Malisan, Tomassini, & Testi, 2006). TMRE is a positively charged, cell permeant dye, that accumulates in active i.e. negatively-charged mitochondria. For JC-1 staining, human fibroblasts were plated on a 27mm glass bottom dish (Thermo Fisher Scientific). The next day 1µl of JC-1 in DMSO (2.5:1000) was added to 1ml of warm media from the plate and fibroblasts were incubated for 20min under growth conditions (37°C, 5% CO2) before washing with Hibernate E medium. Live cells were kept in an environmental chamber in Hibernate E medium during imaging. TMRE and MTDR were added to warm fibroblast medium from the dish (TMRE: 20µM, MTDR: 250nM) and the protocol outlined above was repeated. Additionally, TMRE (20µM) was added to Hibernate E medium for live cell confocal imaging. In both approaches a drop of NucBlue staining was added to every dish to stain the nucleus. Cells were imaged using the UltraVIEW VoX Spinning Disk Confocal Microscope (Perkin Elmer) at a 20X magnification.

2.10.3 CellProfiler Analysis

CellProfiler is an open-source high-throughput image analysis software (Carpenter et al., 2006) and was used to identify and quantify subcellular structures such as the trans-Golgi-network, LC3-positive vesicles or ATG9A in images of human fibroblasts acquired with the UltraVIEW VoX Spinning Disk Confocal Microscope (Perkin Elmer). To investigate the distribution of ATG9A throughout the cytosol and its colocalization with the trans-Golgi-network, an unbiased CellProfiler pipeline was used to compare AP-4-deficient fibroblasts and heterozygous controls (Figure 6, Figure 7).

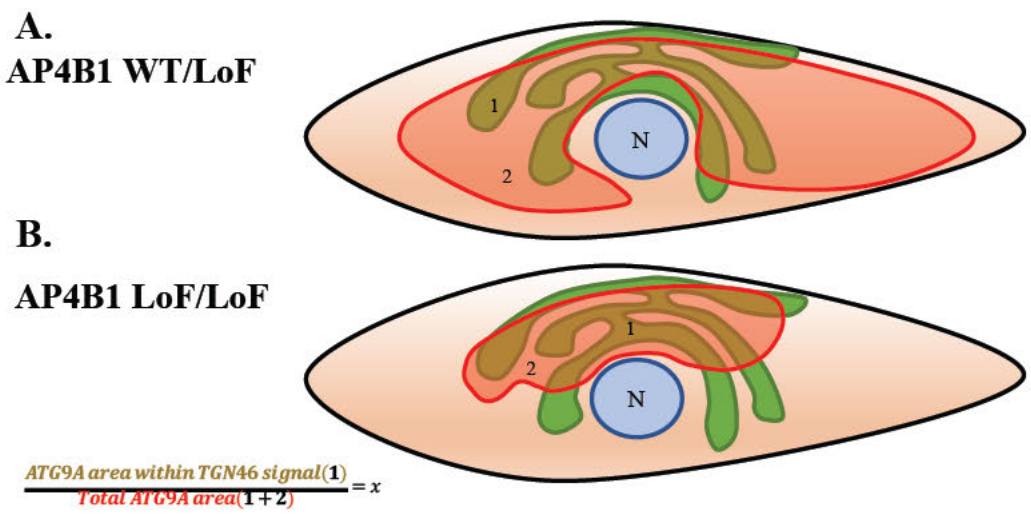

Figure 6 Principle of CellProfiler pipeline measuring ATG9A/TGN46 overlap

Schematic of heterozygous/wildtype fibroblasts **(A.)** immunofluorescence signal in comparison to AP-4-deficient fibroblasts **(B.)** and the equation used in the CellProfiler pipeline to quantify the ATG9A distribution phenotype. N, Nucleus; 1, ATG9A area overlapping with TGN46 signal (*brown*); 2, ATG9A area without TGN46 overlap (*red*); LoF, loss of function; WT, wildtype.

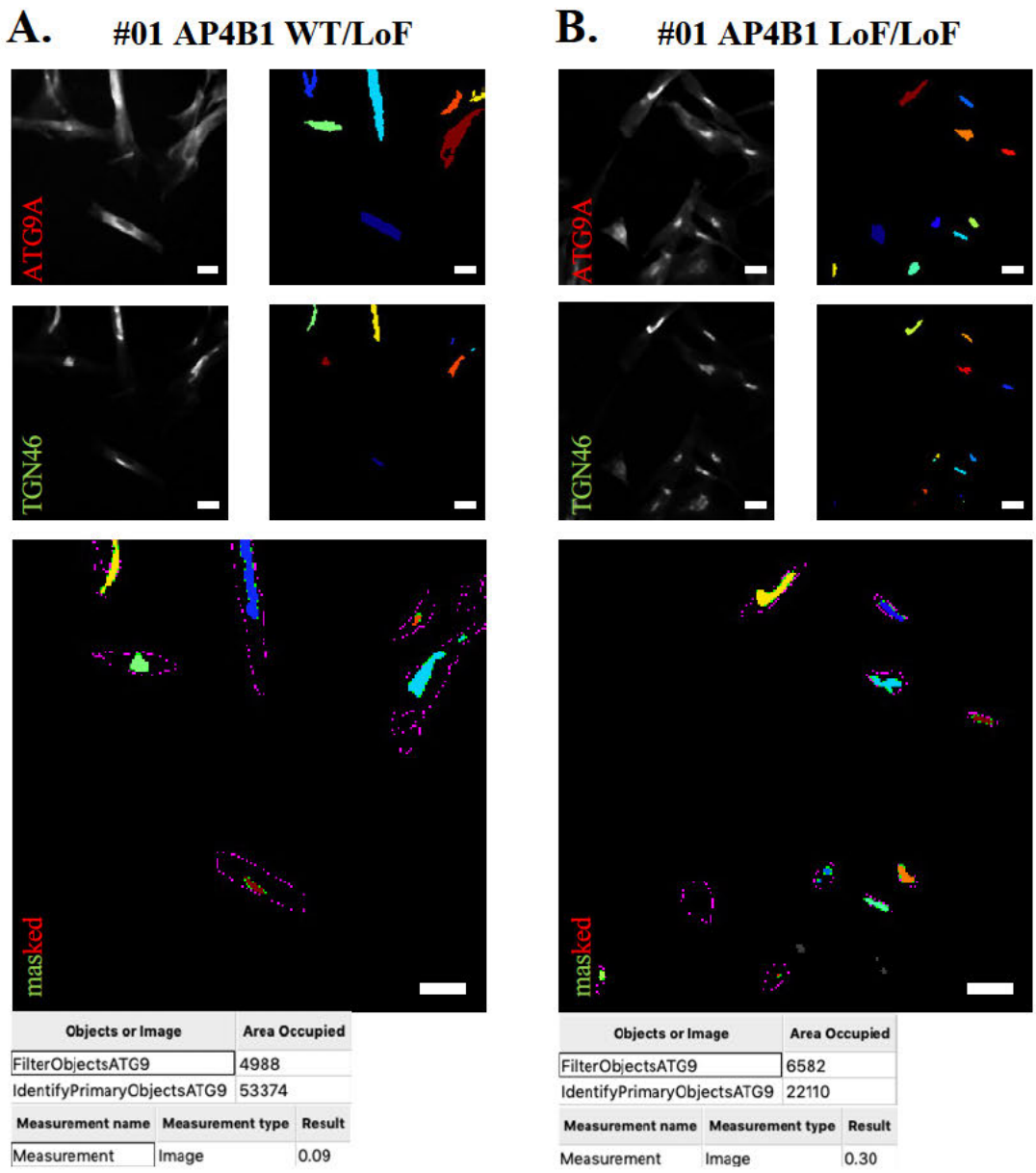

Objects or Image	Area Occupied
FilterObjectsATG9	4988
IdentifyPrimaryObjectsATG9	53374

Measurement name	Measurement type	Result
Measurement	Image	0.09

Objects or Image	Area Occupied
FilterObjectsATG9	6582
IdentifyPrimaryObjectsATG9	22110

Measurement name	Measurement type	Result
Measurement	Image	0.30

Figure 7 CellProfiler pipeline measuring ATG9A/TGN46 overlap

Sample images of the CellProfiler Pipeline used to quantify the ATG9A signal overlapping with the TGN46 signal in relation to total ATG9A signal (measured in pixels). Looking at the overlay of both signals AP4B1-deficient fibroblasts **(B.)** exhibit a closely confined ATG9A signal (purple lines) colocalizing with the TGN46 signal (colored spots) as compared to heterozygous controls **(A.)**, which show a more evenly distributed cytosolic ATG9A signal. Measurement results shown were generated using the CalculateMath function of CellProfiler with the formula (Figure 6, e.g. $\frac{ATG9A\ area\ within\ TGN46\ signal}{Total\ ATG9A\ area} = \frac{4988}{53374} = 0.09$). Scale bar 10µm; LoF, loss of function; WT, wildtype.

An unbiased CellProfiler pipeline was also used to quantify the number and average size of LC3-positive vesicles and SQSTM1/p62 puncta in AP-4-deficient fibroblasts and controls (Figure 8).

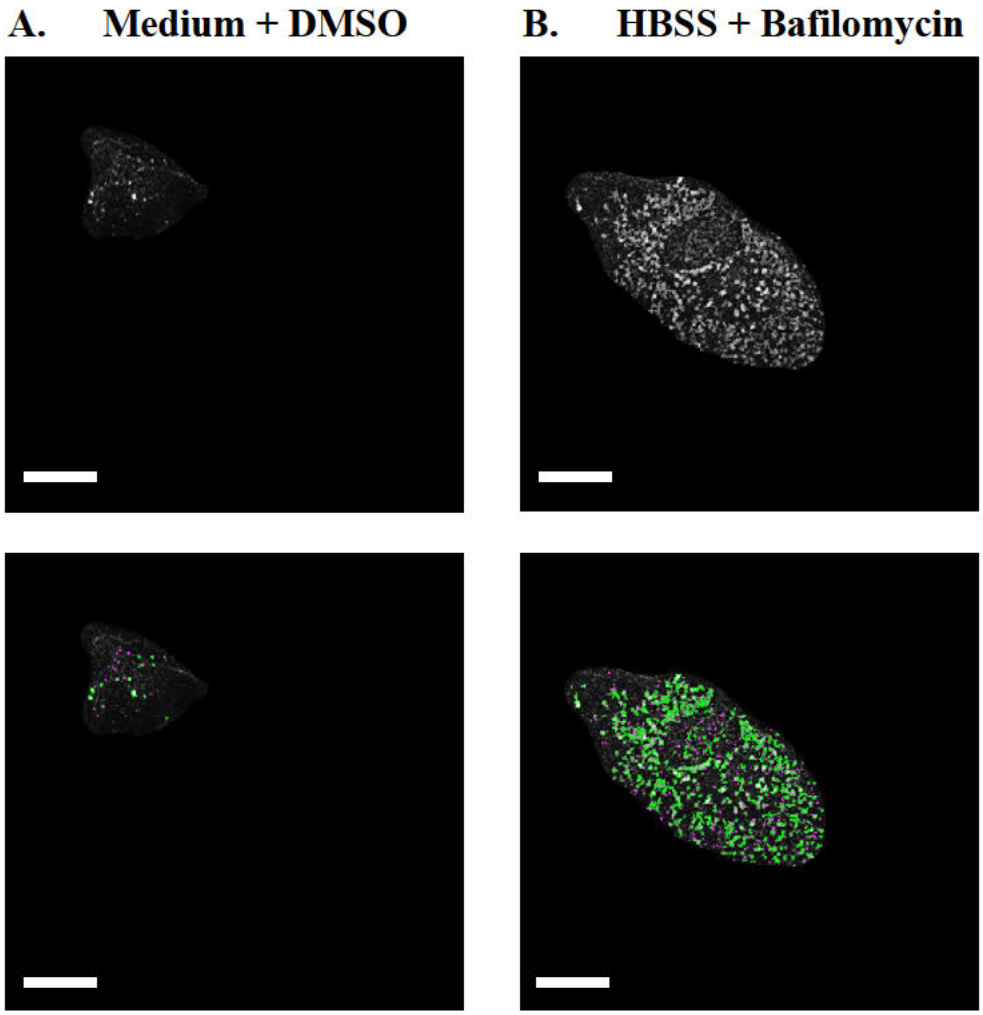

Figure 8 CellProfiler pipeline measuring LC3-vesicle size and number

Sample images of an unbiased CellProfiler pipeline identifying number and size of LC3-positive vesicles (*green*) under nutrient-rich conditions **(A.)** and starvation conditions and additional Bafilomycin treatment **(B.)**. SQSTM1/p62 puncta were imaged and quantified in a similar fashion. Scale bar 10µm; LoF, loss of function; WT, wildtype.

2.11 High-Content Imaging And Analysis

The ImageXpress Micro Confocal High-Content Imaging System (Molecular Devices) is an automated high-content imaging system allowing for fast screening of thousands of specimens. The iPSC-derived cortical neurons fixed on 96 well plates were imaged using a Nikon 20X/0.45 S Plan Fluor ELWD and a Z-series with 7 steps of 2µm step size was performed for each location. 9 sites per well were imaged using autofocus for each well. The MetaXpress image analysis software (Molecular Devices) was used to automatically detect and quantify at least 1000 neurons per well and condition. Since GM130 and TGN46 antibodies as TGN markers did not work reliably in neurons, a different approach from the one using CellProfiler was applied. AP4B1-deficient neurons showed a high intensity ATG9A signal in the nuclear and perinuclear area while heterozygous controls showed less or no high intensity signal in the perinuclear area. This difference was quantified as outlined below (Figure 9).

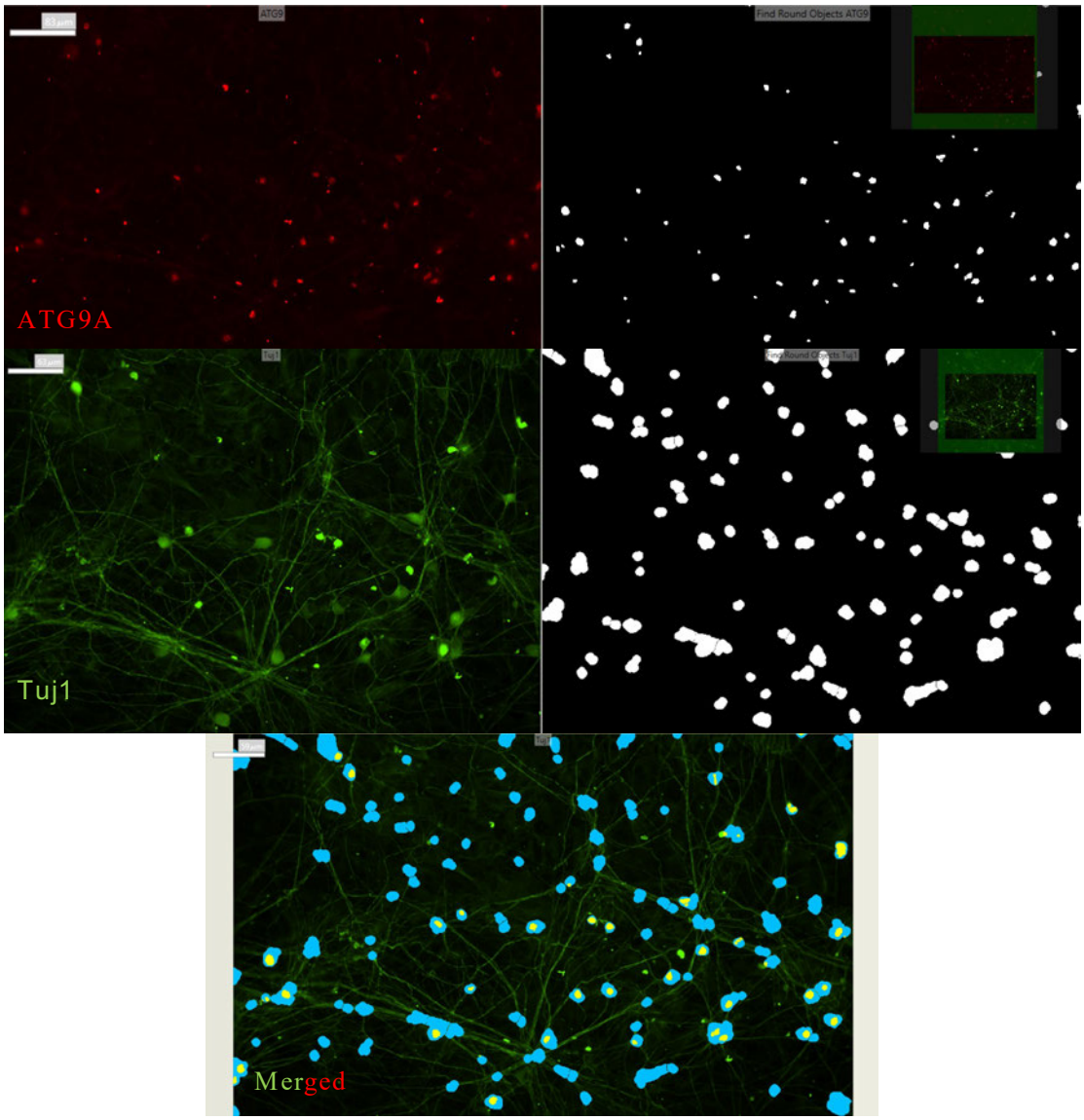

Figure 9 IXM pipeline measuring neuronal high intensity ATG9A signal

The automated IXM pipeline identified the neuronal soma using the ß-Tubulin III (Tuj1, *green*) signal and the high intensity ATG9A signal (*red*), respectively. In a second step all ATG9A signal contained in the soma was included while ATG9A signal not contained in the neuronal soma, i.e. debris, was excluded. The ratio of the area of the high intensity ATG9A signal (*yellow* on bottom image) to the soma area defined by ß-Tubulin III signal (*blue* on bottom image) was calculated on a per cell basis (over $9x10^4$ cells per condition) as well as per cell line differentiation. LoF, loss of function; WT, wildtype.

2.12 IncuCyte S3 Live-Cell Analysis System

Dendrite outgrowth and branching of human iPSC-derived cortical neurons was examined using the IncuCyte S3 Live-Cell Analysis System (Essen BioScience). The IncuCyte allows for undisturbed automated imaging and analysis of live cells inside the incubator. Cell lines #01 and #02 with their respective heterozygous controls were used. Human iPSC-derived cells were left undisturbed after plating to allow attachment for 4h and then transferred into the IncuCyte incubator under growth conditions. The cells were then imaged with a brighfield microscope at a 20x resolution every 4h for 24h and then analyzed using the integrated software (Figure 10). While the software could not differentiate between axons and dendrites, it analyzed neurite outgrowth in mm per cell body, neurite branching as a measure of branchpoints per cell body as well as soma number per mm^2 and cell body area in mm^2/mm^2.

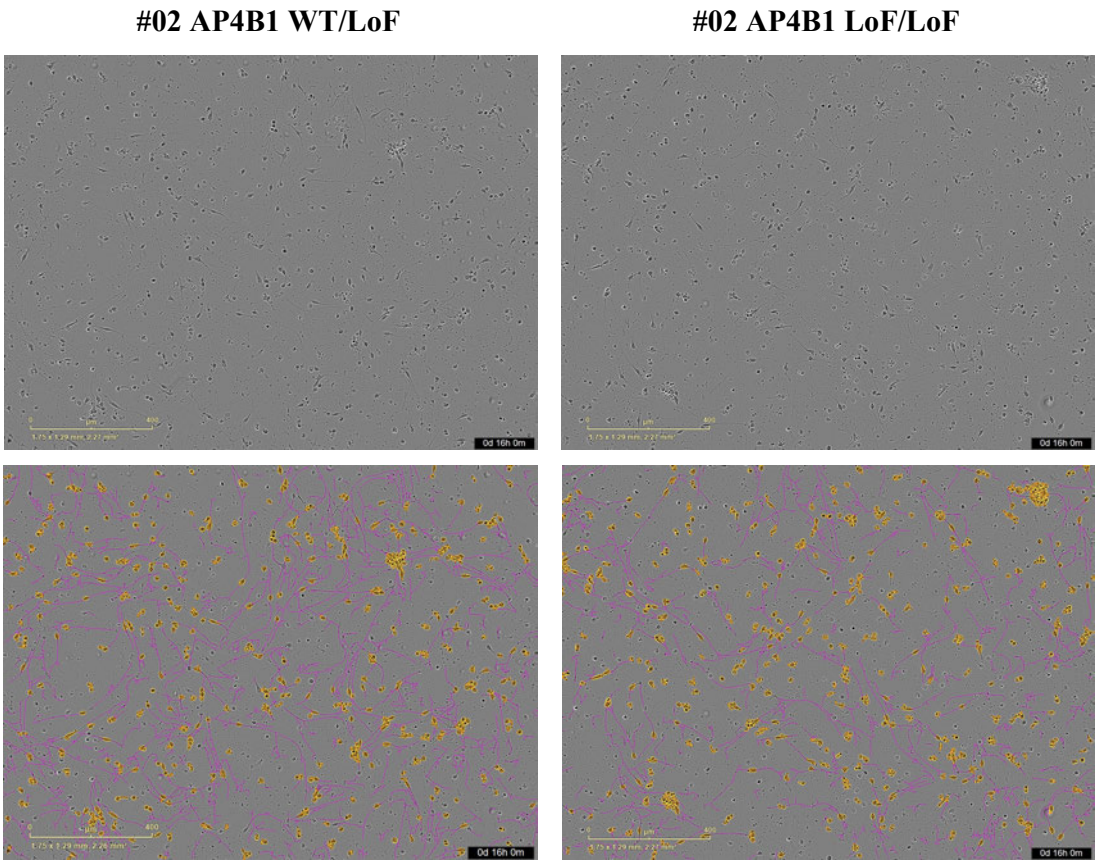

Figure 10 IncuCyte S3 Live-Cell Analysis System Pipeline

Human iPSC-derived cortical neurons after 16h in the IncuCyte incubator. The image analysis software identifies neurites (*purple* lines, no differentiation between axons and dendrites) and neuronal soma (*yellow*) and measures soma number and area, neurite length and outgrowth as well as branching points. LoF, loss of function; WT, wildtype.

2.13 Statistical Analysis

Statistical Analysis was performed using GraphPad Prism version 9.2. Data are shown as mean ± standard error of the mean (SEM). To determine significance, unpaired t-test (Figure 11B, 19, 20, 22D&E, 25), ratio paired t-test (Figure 12, 13, 15, 21, 24) and one-way ANOVA with Tukey's multiple comparisons test (14, 16, 17) were used. For figure 18, unpaired t-test was used to compare different timepoints of one cell line and paired t-test was used to compare between patient and control lines. A p-value <0.05 was considered significant and significance is indicated as follows: P <0.05 (*); P <0.01 (**); P <0.001 (***); P <0.0001 (****). All experiments were performed in triplicate except for the neurite outgrowth and branching experiment (Figure 25), where only two differentiations were analyzed.

3 Results

3.1 AP-4 Deficiency Leads To ATG9A Accumulation In The Trans-Golgi Network In Human Fibroblasts

ATG9A is an autophagy-related protein, which is responsible for lipid membrane recruitment needed for the formation of autophagosomes (Noda et al., 2000) and has been identified as a cargo protein of AP-4 using an organellar proteomics approach (Davies et al., 2018). When AP-4 levels are depleted, different cell types such as MEFs, HeLa cells, patient-derived fibroblasts and *Ap4e1*-knockout mouse hippocampal neurons show a missorting phenotype of ATG9A. While AP-4 mainly localizes to the trans-Golgi network (TGN) (E. C. Dell'Angelica et al., 1999; Hirst et al., 1999), ATG9A is found in the juxtanuclear region colocalizing with markers for the trans-Golgi network and throughout the cytosol in wildtype cells, but shows a strong accumulation in the TGN area in AP-4 deficient cells (Davies et al., 2018; D. Ivankovic et al., 2020; Mattera et al., 2017; Young et al., 2006). Furthermore, conditional CNS-specific *Atg9A*-knockout mice show an axonopathy with dysgenesis of the corpus callosum (Yamaguchi et al., 2018) strongly resembling findings in *Ap4e1*-knockout mice and patients with AP-4-associated HSP suggesting that ATG9A distribution is dependent on AP-4 and that lack of ATG9A in the axonal compartment leads to an axonopathy.

These findings make ATG9A a promising candidate for a phenotypic marker in a patient-derived cellular model of AP-4-associated HSP. Three human fibroblast lines of patients with AP-4-associated HSP and their sex-matched heterozygous parental controls as well as three wild type controls were tested using immunocytochemistry to investigate subcellular ATG9A localization in AP-4-deficient fibroblasts. All fibroblast lines were stained for ATG9A and TGN46, a marker of the trans-Golgi network (TGN). An unbiased CellProfiler pipeline (Carpenter et al., 2006) was used to identify single cells and define ATG9A and TGN46 signal after confocal imaging (Figure 11A). The ratio of ATG9A signal overlapping with the TGN46 signal and the total ATG9A signal of the cell showed a significant increase of ATG9A signal overlapping with the TGN in AP-4-deficient cells for all patient lines (Figure 11B). In comparison, heterozygous sex-matched parental lines and wildtype controls showed a significantly lower ratio. Additionally, line blots of AP-4-deficient fibroblasts showed a striking overlap of ATG9A and TGN46 signal, which was not seen in controls (Figure 11C). These findings confirmed a robust alteration of

subcellular ATG9A localization and suggested an accumulation of ATG9A in the trans-Golgi network.

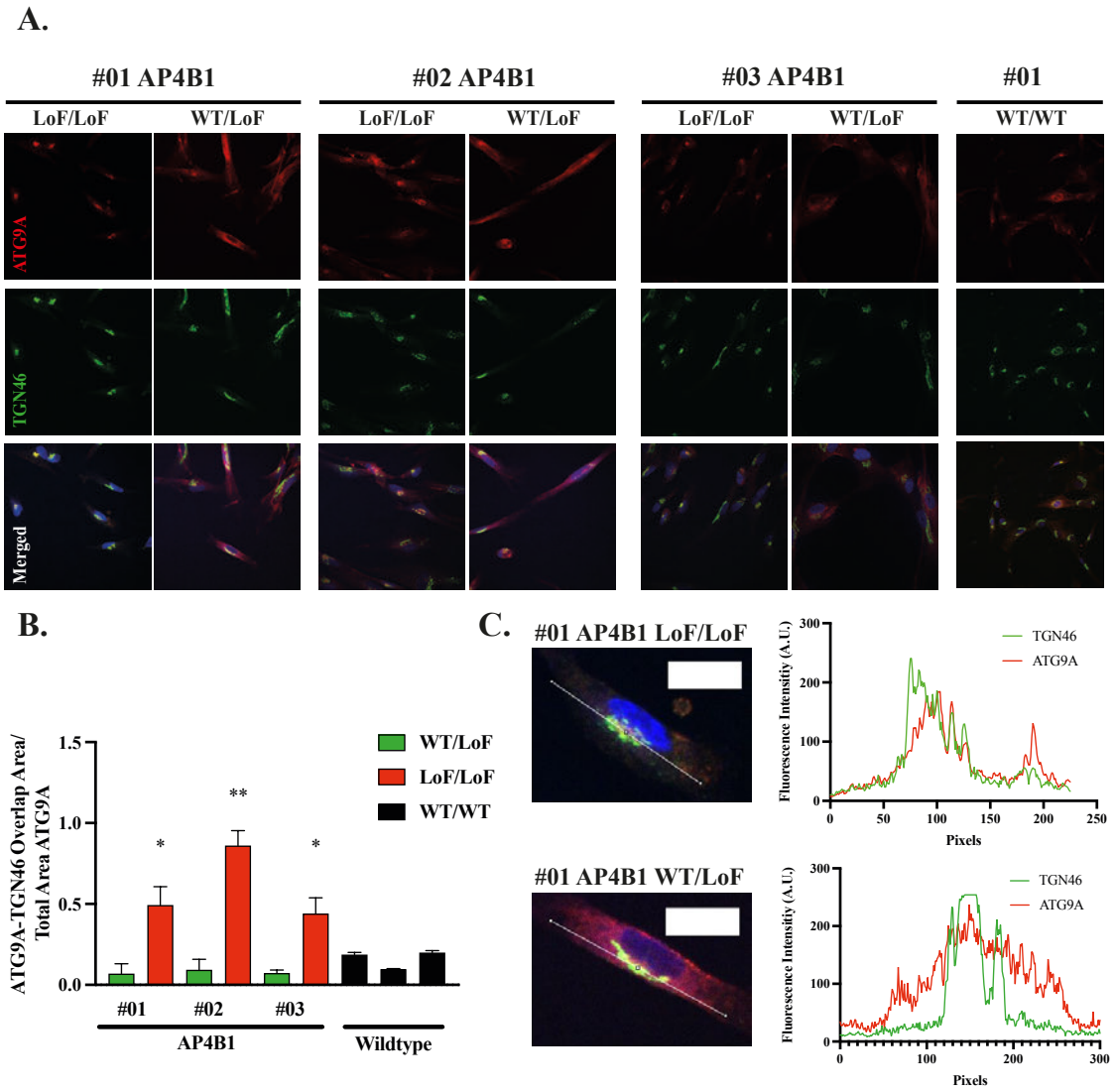

Figure 11 Accumulation of ATG9A in the trans-Golgi-network in AP-4-deficient human fibroblasts

A. Immunocytochemistry of patient-derived fibroblasts from patients with bi-allelic variants in the AB4B1-subunit, heterozygous parental controls and wildtype controls. ATG9A signal *(red)* in patient-derived fibroblasts is confined to the TGN46 area *(green)*, while heterozygous and wildtype cells show an even subcellular distribution. Nuclear marker DAPI *(blue)*; Scale bar 10µm. **B.** Quantification of ATG9A signal overlap with TGN46 signal in relation to total ATG9A area shows a significantly higher overlap in patient-derived fibroblasts. **C.** Line blot showing similar fluorescence intensity profiles of ATG9A and TGN46 of patient-derived fibroblasts in comparison to heterozygous controls. Scale bar 5µm; A.U., arbitrary units; LoF, loss of function; WT, wildtype.

3.2 AP-4-Deficient Human Fibroblasts Have Increased Levels Of ATG9A And An Instable AP-4-Complex

The forementioned results confirmed a distinct cellular phenotype with ATG9A accumulation in the trans-Golgi network. This gave rise to the question, whether ATG9A levels are altered in AP-4-deficient human fibroblasts. To assess this question, western blotting of whole cell lysates was performed for all three lines as well as their sex-matched, heterozygous parental controls and three wildtype controls. All patient-derived lines showed significantly increased levels of ATG9A compared to the controls (Figure 12A&C). No difference was seen between wildtype controls and heterozygous parental controls. Interestingly, relative ATG9A mRNA expression showed no significant differences between AP-4-deficient cells and controls suggesting a post-translational mechanism (Figure 12E). AP4E1 levels were used as a surrogate marker for the stability of the AP-4-complex. All patient-derived fibroblast lines exhibited significantly decreased AP4E1 levels, presumably due to an instable AP-4-complex (Figure 12 A&D). Co-immunoprecipitation of the AP4B1- and AP4E1-subunits was performed using whole cell lysates to confirm a disturbed AP-4-complex formation. While all heterozygous parental controls showed robust co-immunoprecipitation of the two subunits, no signal was seen in the AP4B1-deficient fibroblast lines suggesting that AP-4-complex formation is disturbed (Figure 12B). In conclusion, loss of the AP4B1-subunit in human fibroblasts leads to an instable AP-4-complex, on which ATG9A trafficking to the cell periphery depends. This lack of ATG9A in the cell periphery seems to be compensated by an increase of ATG9A accumulating in the TGN.

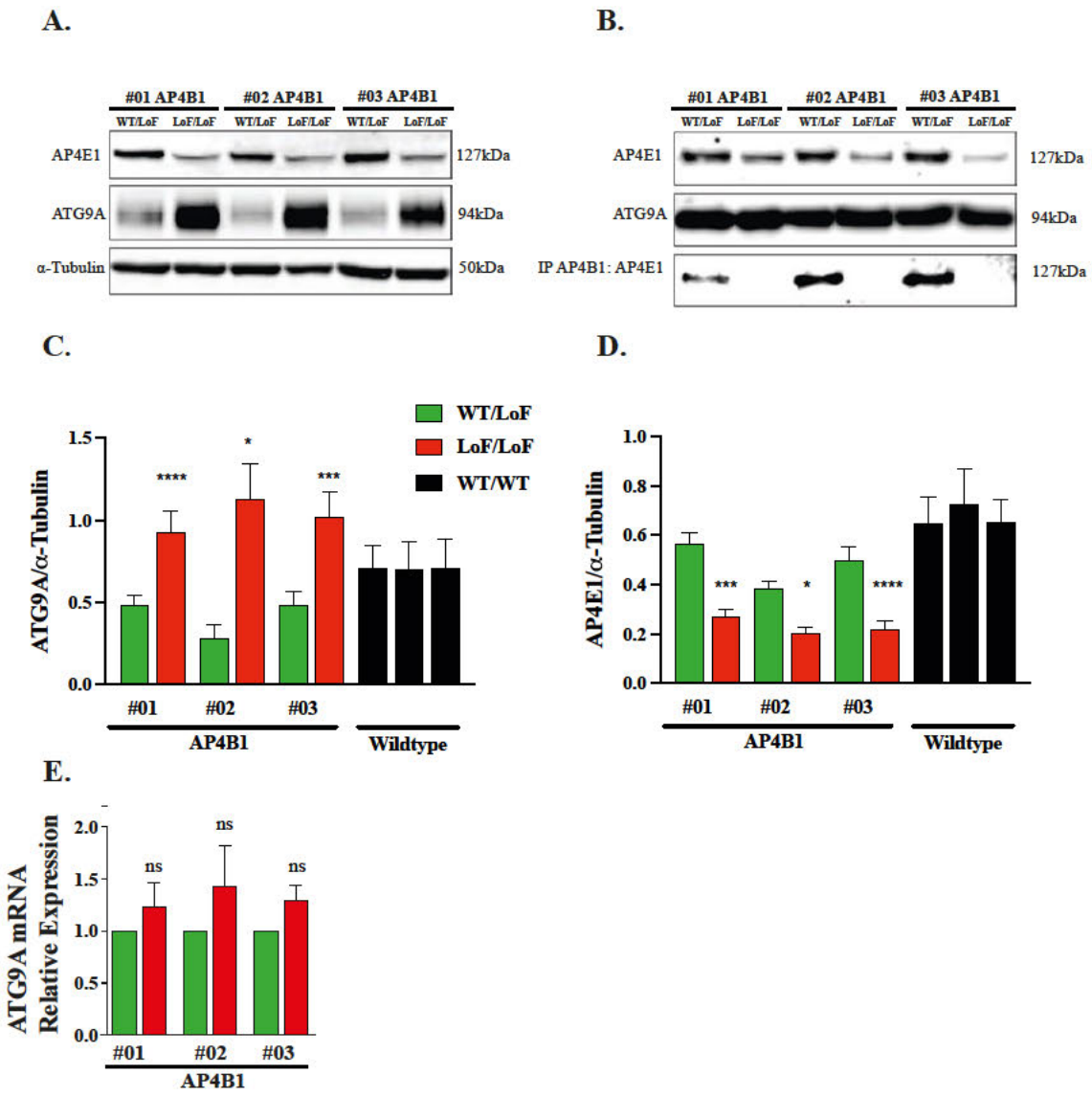

Figure 12 ATG9A and AP4E1 levels in AP-4-deficient human fibroblasts

A. Western blot of whole cell lysates of patient-derived AP-4-deficient fibroblasts with increased levels of ATG9A **(C.)**, in comparison to parental controls. **D.** AP4E1 levels, that were used as a surrogate marker for the AP-4-complex, are decreased in AP-4-deficient fibroblasts. **B.** Co-immunoprecipitation of the AP4B1- and AP4E1-subunit is seen in heterozygous parental controls, but not in AP-4-deficient fibroblasts. **E.** Relative ATG9A mRNA expression does not show significant differences between AP-4-deficient fibroblasts and controls. IP, immunoprecipitation; kDA, kilo Dalton; LoF, loss of function; WT, wildtype.

3.3 Lentiviral Re-Expression Of AP4B1 In AP-4-Deficient Fibroblasts Rescues Elevated ATG9A Levels And ATG9A Accumulation

AP-4-deficient fibroblasts show an altered cellular phenotype, that can clearly be distinguished from the heterozygous parental control and wildtype cells. To test whether re-expression of the AP4B1-subunit could rescue this phenotype, a V5-tagged lentiviral vector carrying human *AP4B1* was used to infect AP4B1-deficient cells as well as parental controls. Lentiviral re-expression of AP4B1 resulted in a robust increase of relative AP4B1 mRNA levels in AP-4-deficient fibroblasts and also in heterozygous controls (Figure 13B). Western blotting showed that AP4B1 was successfully re-expressed in AP-4-deficient cells, that were treated with the lentivirus (Figure 13C). Western blotting also showed a significant reduction of the increased ATG9A levels while heterozygous parental controls exhibited no significant change in ATG9A levels (Figure 13D).

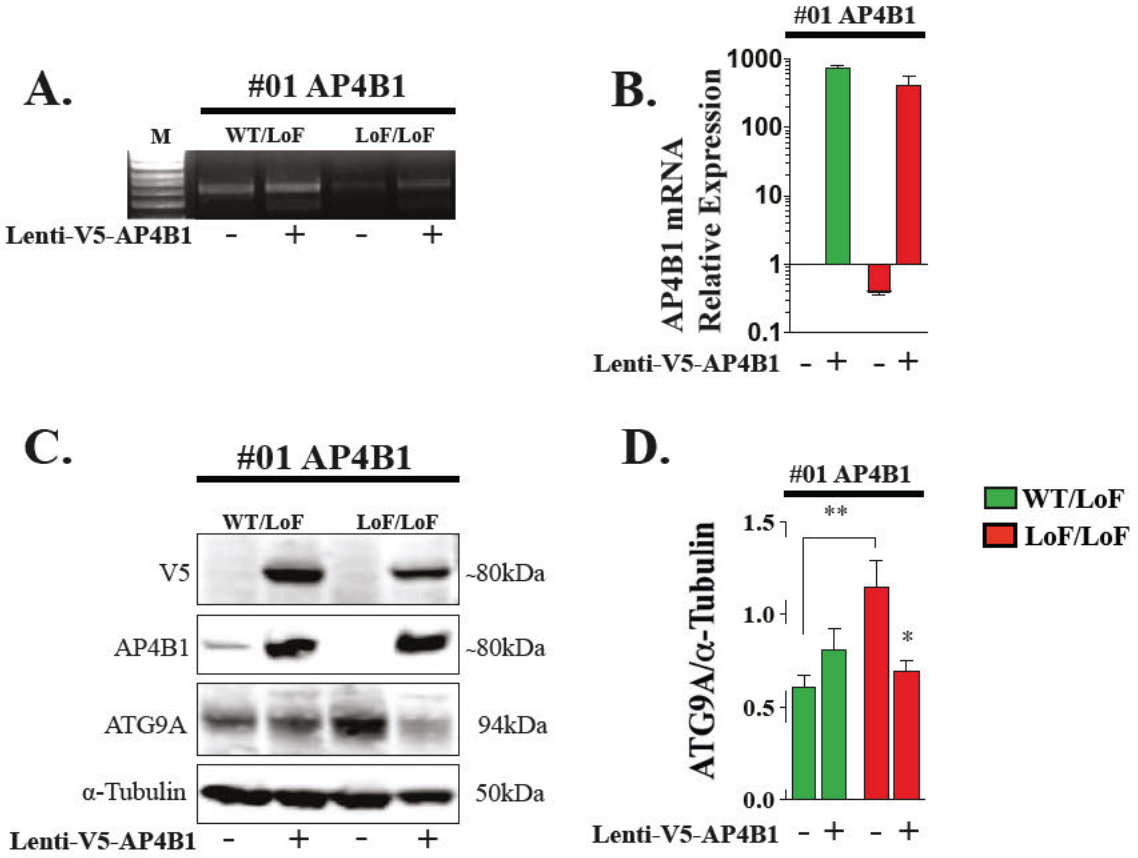

Figure 13 Lentiviral re-expression of AP4B1 lowers ATG9A levels

A. Example of agarose electrophoresis gel showing PCR products of line #01 treated with Lenti-V5-AP4B1. M, DNA marker. **B.** Relative AP4B1 mRNA expression in AP-4-deficient fibroblasts is similar to those of parental controls. **C.** Western blotting demonstrates AP4B1 re-expression in AP-4-deficient fibroblasts after lentiviral treatment. **E.** Quantitation of ATG9A levels before and after lentiviral treatment show a significant decrease to levels comparable to those of parental controls in AP-4-deficient fibroblasts. LoF, loss of function; WT, wildtype.

Immunocytochemistry revealed a redistribution of ATG9A signal to the cell periphery which was measured by looking at the ATG9A signal overlapping with the TGN signal in relation to the total ATG9A signal of a cell using in automated pipeline as described above (Figure 14 A&B).

Re-expression of AP4B1 in AP4B1-deficient fibroblasts rescues the cellular phenotype of increased ATG9A levels and ATG9A accumulation in the TGN. This further supports the notion that AP4B1 is needed for a stable AP-4-complex and that the AP-4-complex is indeed responsible for distributing ATG9A to the cell periphery.

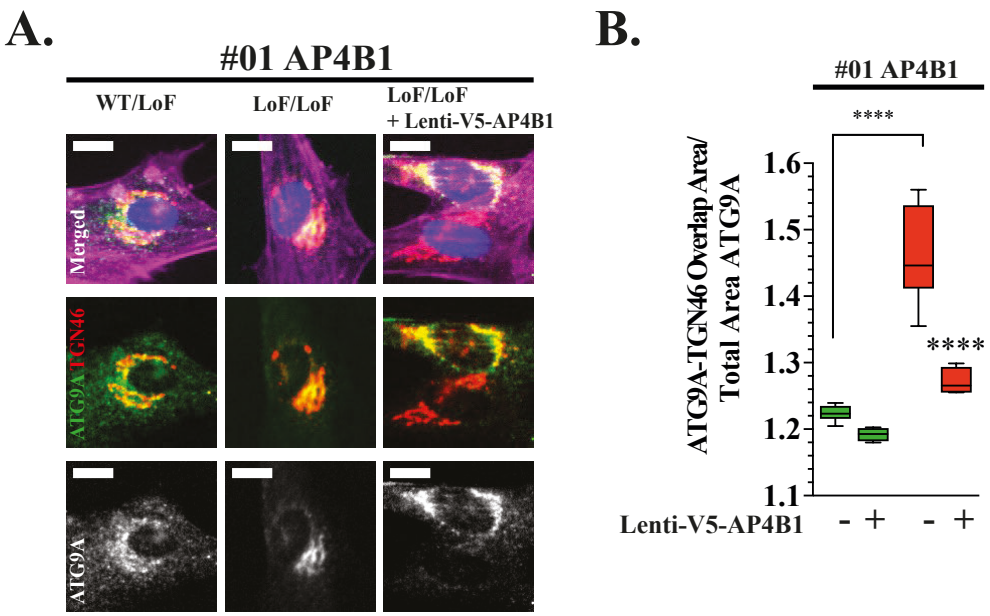

Figure 14 Redistribution of ATG9A to the cell periphery after lentiviral re-expression of AP4B1

A. Immunocytochemistry of AP-4-deficient fibroblast line #01 before and after lentiviral re-expression of AP4B1 shows a redistribution of ATG9A to the cell periphery (third row, *white*). ATG9A signal (second row, *green*) and TGN46 (second row, *red*) show a strong overlap before lentiviral treatment, which was less pronounced after lentiviral treatment. Actin (first row, *purple*) was used to stain the whole cell body and DAPI (first row, *blue*) as a nuclear marker. Scale bar 5µm. **B.** Re-expression of AP4B1 reduces the ratio of ATG9A-TGN46 overlap area to total ATG9A area to the level of parental controls in AP-4-deficient fibroblast line #01. LoF, loss of function; WT, wildtype.

3.4 Autophagic Flux Is Present In AP-4-Deficient Fibroblasts

Since ATG9A is known to be involved in autophagosome formation (C. M. Guardia et al., 2020) and CNS-specific *Atg9A*-knockout mice (Yamaguchi et al., 2018) show impairment of autophagy with a phenotype resembling that of *Ap4e1*-knockout mice (D. Ivankovic et al., 2020), the question arose whether AP-4-deficient human fibroblasts exhibit impaired autophagosome formation or autophagic flux. The LC3II/I ratio and SQSTM1/p62 levels (Chapter 2.4) were used to assess formation and degradation of autophagosomes. Looking at total LC3II levels as well as LC3II/I ratio at baseline, no significant differences between AP-4-deficient fibroblasts and parental controls were

seen (Figure 15A, B&C). SQSTM1/p62 levels were also unchanged in AP-4-deficient fibroblasts, when compared to parental controls. Wild type controls showed LC3II and SQSTM1 levels in a similar range. These findings suggest that autophagic flux in AP-4-deficient fibroblasts is present under nutrient-rich conditions.

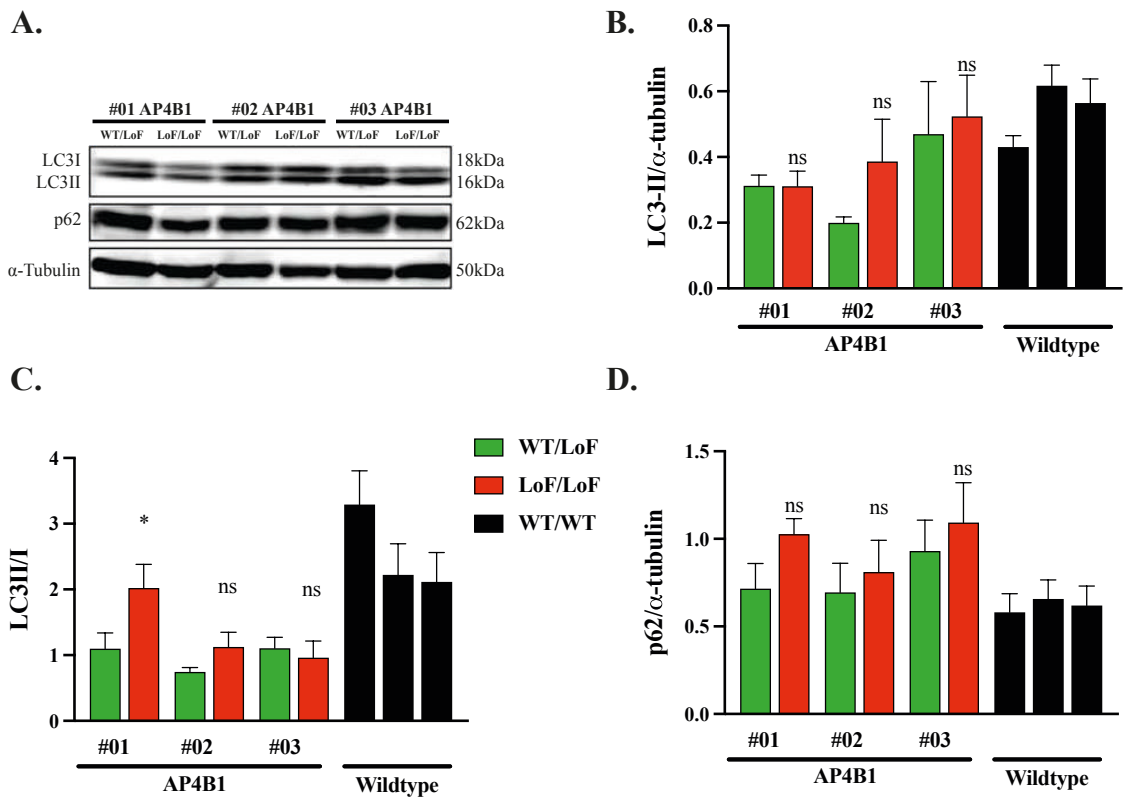

Figure 15 Unaltered baseline autophagy markers in AP-4-deficient fibroblasts

A. Western blot of whole cell lysates of AP-4-deficient fibroblasts shows LC3I and II and SQSTM1/p62 signal and α-tubulin as loading control. **B.** LC3II levels are not significantly higher in whole cell lysates of AP-4-deficient fibroblasts compared to parental controls. Wild type cells show similar levels with slight interindividual differences. **C.** Whole cell lysates of AP-4-deficient fibroblasts show unaltered LC3II/I ratio compared to parental controls under growth conditions. Wildtype controls show a ratio in the same range. **D.** SQSTM1/p62 levels are unchanged in AP-4-deficient fibroblasts under growth conditions as compared to parental and wild type controls. LoF, loss of function; WT, wildtype.

To assess the starvation response of AP-4-deficient fibroblasts, well-established protocols were employed to detect alterations in autophagic flux and autophagosome degradation (Klionsky et al., 2016; Mizushima & Yoshimori, 2007; Sahani et al., 2014). Fibroblasts were starved for 4h and treated with Bafilomycin A1 to inhibit lysosome-autophagosome fusion, blocking autophagosome degradation, or DMSO, which is the solvent of Bafilomycin A1. Unstarved fibroblasts were given the same treatment as control conditions. After a starvation period of 4h, a significant increase of the LCII/I ratio was seen in western blots of whole cell lysates of AP-4-deficient fibroblasts as well as controls compared to unstarved samples (Figure 16A&B). This suggests an intact starvation response with functioning autophagosome formation. With Bafilomycin A1 treatment for 4h, LC3II/I ratio increased significantly under nutrient-rich conditions and was even higher under starvation conditions in AP-4-deficient fibroblasts and controls (Figure 16A&B). This demonstrates that treatment with Bafilomycin A1 successfully inhibited lysosome-autophagosome fusion and that initiation of autophagy as well as autophagic flux upstream of the autolysosomal degradation process is unaltered in AP-4-deficient fibroblasts. Unexpectedly, SQSTM1/p62 levels did not change significantly after 4h in AP-4-deficient cells as well as controls as measured by western blotting (Figure 16A&C). Nonetheless, a trend towards higher levels was seen for starvation alone or in combination with Bafilomycin A1. These results could either be explained by insufficient sensitivity of the method, by the replenishing of SQSTM1/p62 levels after a short period of starvation as described previously by Sahani et al. (Sahani et al., 2014) or by a minor role of SQSTM1/p62 in unselective autophagy of fibroblasts.

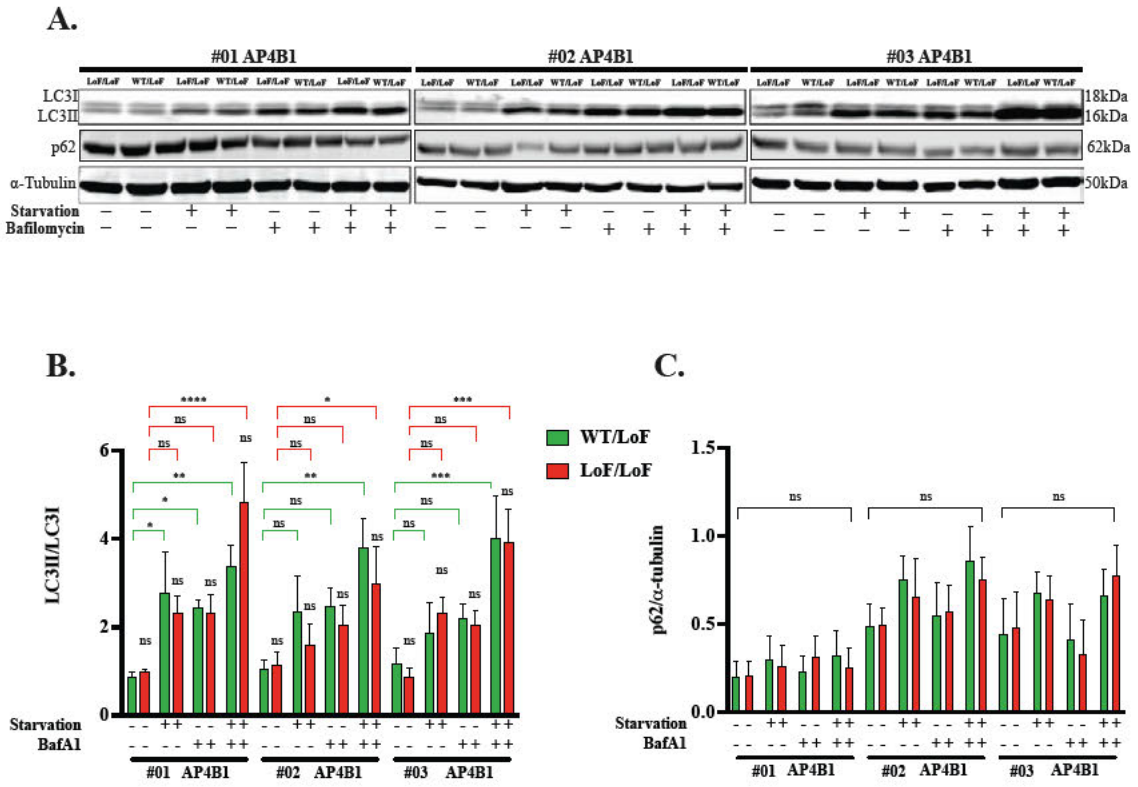

Figure 16 Intact starvation response in AP-4-deficient fibroblasts

A. Western blotting of whole cell lysates from AP-4-deficient fibroblasts and parental controls showing LC3I and II and p62 signal with (+) or without (-) 4h starvation or Bafilomycin treatment and α-Tubulin as loading control. **B.** LC3II/I ratio increases significantly in patient-derived fibroblasts and parental control lines when combining starvation and Bafilomycin treatment. Starvation or Bafilomycin treatment alone does increase LC3II/I ratio, but not significantly in all lines. There are no significant differences between patient-derived fibroblasts and parental lines (asterisks without brackets). **C.** Starvation or blockage of lysosome-autophagosome fusion or the combination of both does not significantly change SQSTM1/p62 levels in patient or control fibroblast lines and no significant differences are seen between these lines. LoF, loss of function; WT, wildtype.

To further examine autophagic flux, immunocytochemistry was used to stain fibroblasts for LC3 as well as SQSTM1/p62 to determine changes in number of LC3 and SQSTM1/p62 puncta as well as size. The number of LC3 positive vesicles, a surrogate marker of autophagosomes, increased significantly after 4h starvation and even more after Bafilomycin A1 treatment for 4h. The increase of vesicle number was highest when starvation and Bafilomycin A1 treatment were combined confirming the western blotting results (Figure 17A&B). However, no consistent differences were seen between AP-4-deficient fibroblasts and controls. Regarding average vesicle size, AP-4-deficient lines #01 and #03 showed significantly larger LC3-positive vesicles when starved or treated with Bafilomycin compared to their parental heterozygous controls while line #02 showed an opposite trend (Figure 17A&D). In contrast to western blotting, SQSTM1/p62 puncta per cell did increase significantly after Bafilomycin A1 treatment in both AP-4-deficient and parental lines suggesting a successful inhibition of autophagosome degradation and a functioning autophagosome formation in AP-4-deficient cells (Figure 17A&C). Starvation alone did not increase the number of SQSTM1/p62 puncta for all lines and interestingly, combined starvation and Bafilomycin A1 treatment resulted in a smaller increase of SQSTM1/p62 puncta per cell as compared to Bafilomycin A1 treatment alone. This could suggest that starvation increases degradation of SQSTM1/p62 in autophagosomes, which cannot fully be prevented by Bafilomycin A1. Similar to LC3-positive vesicles, the size of SQSTM1/p62 was higher in patient line #01 and #03 and smaller in #02 compared to parental controls (Figure 17A&E). For both LC3-positive vesicle size and SQSTM1/p62 puncta size, an increase was seen for all lines, when cells were starved or treated with Bafilomycin A1, respectively. The increase of vesicle size under starvation or Bafilomycin A1 treatment can at least partly be explained by methodical limitations since the image analysis software will count overlapping vesicles as one resulting in seemingly increased vesicle size. In contrast to a previous study (Davies et al., 2018), LC3-positive vesicles were not unequivocally enlarged in AP-4-deficient lines. Interindividual differences need to be taken into account when looking at LC3-positive vesicle size, because the difference between patient and control lines remains constant throughout conditions. In summary, this suggests that AP-4-deficient cell lines have an intact starvation response and autophagic flux similar to parental controls, although they might exhibit smaller or bigger LC3-positive vesicles.

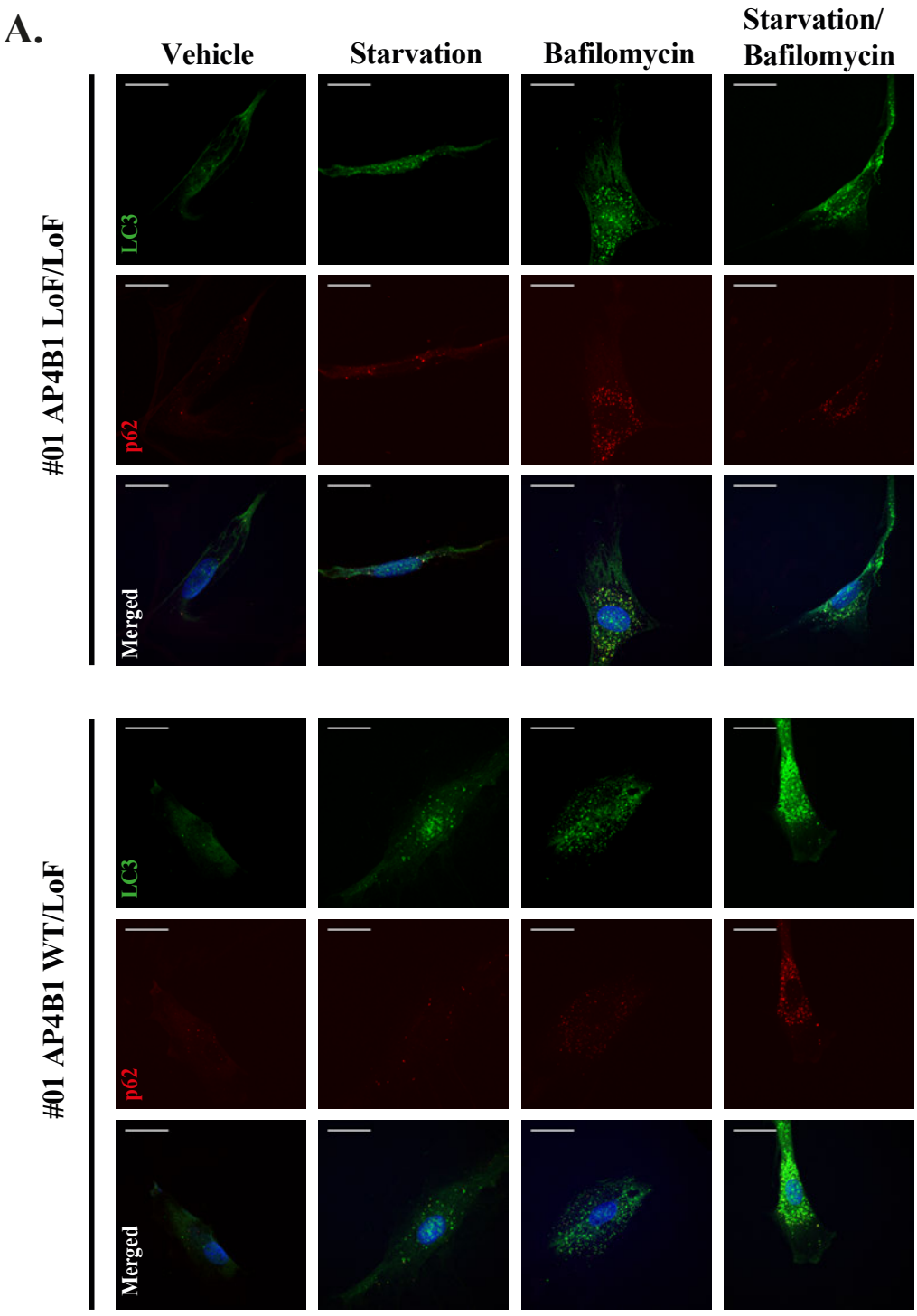
A.
Vehicle
Starvation
Bafilomycin
Starvation/
Bafilomycin
#01 AP4B1 LoF/LoF
LC3
p62
Merged
#01 AP4B1 WT/LoF
LC3
p62
Merged

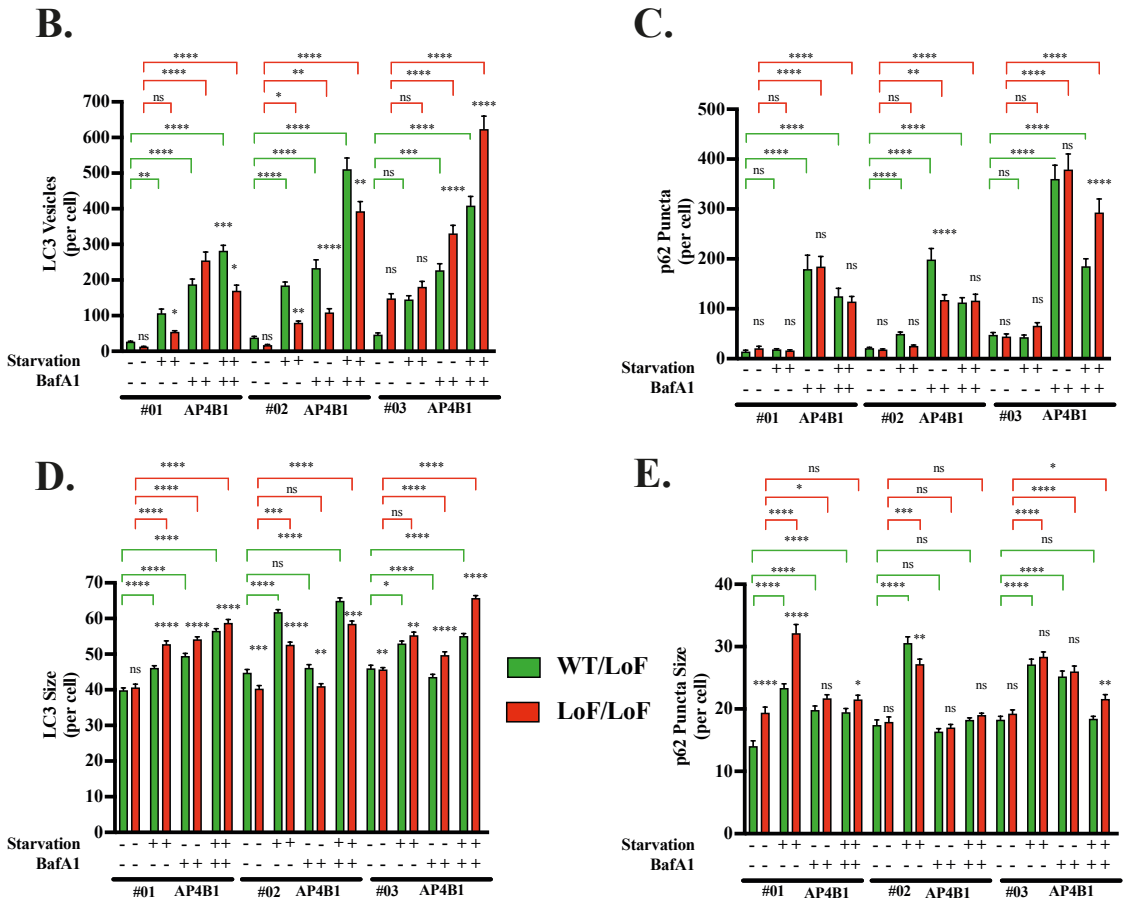

Figure 17 LC3-positive vesicles and SQSTM1/p62 puncta under starvation conditions

A. Immunocytochemistry shows LC3-positive vesicles (*green*) and SQSTM1/p62 puncta (*red*) and DAPI as nuclear marker (*blue*) of AP-4-deficient fibroblasts and heterozygous parental controls (line #01) under nutrient rich (*vehicle*) and starvation conditions, Bafilomycin A1 treatment and combination of starvation and Bafilomycin A1 treatment. Scale bar 20µm. **B.&D.** Number and average size of LC3-positive vesicles as measured by an unbiased CellProfiler pipeline is increased under starvation conditions and Bafilomycin A1 treatment suggesting intact autophagic flux in AP-4-deficient fibroblasts. **C.** Bafilomycin A1 treatment significantly increases number SQSTM1/p62 puncta indicative of a successful blockage of lysosome-autophagosome fusion. Starvation alone has no effect on puncta number **E.** SQSTM1/p62 puncta size increases the most under starvation conditions and less with additional Bafilomycin A1 treatment. Differences between patient and control lines are indicated as asterisks without brackets. LoF, loss of function; WT, wildtype.

AP-4-deficient cells show preserved autophagy induction and autophagic flux under starvation conditions after 4h. To exclude, that the starvation period was too short or that subtle changes in LC3II/I ratio or SQSTM1/p62 levels were not detected, a time course experiment was conducted using AP-4-deficient line #02 and the parental control line. Timepoints ranging from 1h to 8h were investigated. ATG9A levels and AP4E1 levels were also monitored. As an additional condition besides starvation and Bafilomycin A1 treatment, Torin 1, a potent mTORC1 inhibitor and therefore inductor of autophagy, was used to test the response of AP-4-deficient fibroblasts to autophagy induction. Phosphorylated ribosomal protein S6 (pS6) was used to monitor mTORC activity and confirm successful Torin 1 treatment.

In keeping with the previous findings, the LC3II/I ratio increased in all conditions compared to a nutrient rich environment, but no significant differences were seen between AP-4-deficient and control lines (Figure 18A). SQSTM1/p62 levels did not replenish after 4h or 8h of starvation as described in MEFs and HepG2 cells by Sahani et al. (Sahani et al., 2014). No clear trend could be identified in SQSTM1/p62 dynamics in contrast to immunocytochemistry (Figure 18B). Decreased levels of phosphorylated ribosomal protein S6 indicated successful inhibition of mTORC and autophagy activation, when cells where starved or treated with Torin 1 (Figure 18C). As expected, Bafilomycin A1 treatment alone did not significantly change pS6 levels as it does not induce autophagy.

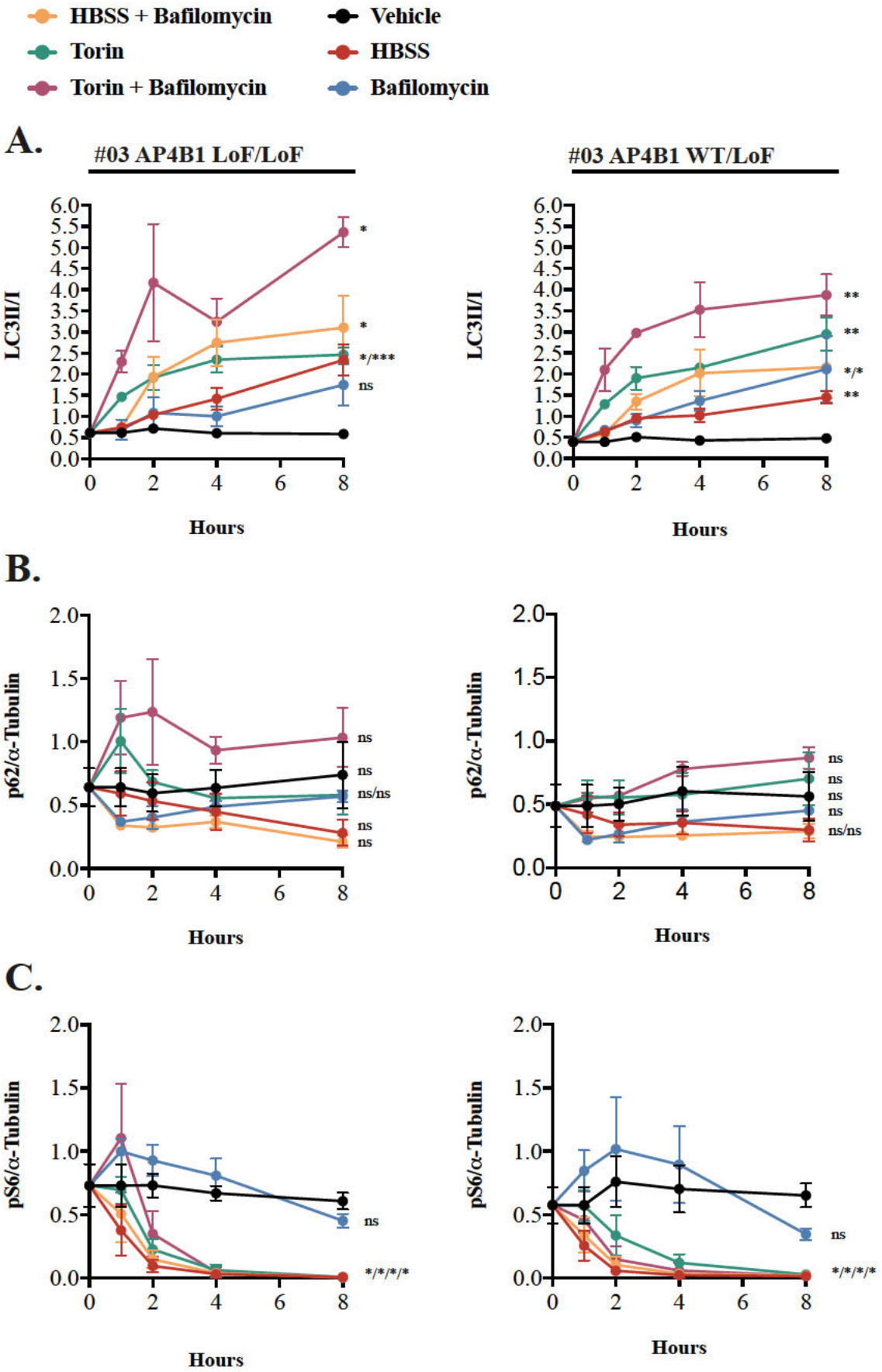
HBSS + Bafilomycin
Torin
Torin + Bafilomycin
Vehicle
HBSS
Bafilomycin
A.
#03 AP4B1 LoF/LoF
#03 AP4B1 WT/LoF
LC3II/I
Hours
B.
p62/α-Tubulin
C.
pS6/α-Tubulin
ns
*
*/***
/
**
//*/*

Figure 18 Dynamics of autophagy markers under starvation conditions

A. LC3II/I ratio increases over time under starvation conditions and pharmacological autophagy induction or blockage of lysosome-autophagosome fusion suggestive of intact autophagosome formation. **B.** SQSTM1/p62 levels do not change significantly. **C.** Starvation conditions or autophagy induction via Torin 1 decrease pS6 levels indicative of mTORC inhibition and unimpaired upregulation of autophagy. LoF, loss of function; WT, wildtype. Asterisks indicate significance between hour 0 and 8 of each condition. Comparison of AP-4-deficient fibroblasts and parental controls was not significant (asterisks not displayed).

During the time course of 8h, ATG9A levels were significantly higher in AP-4-deficient fibroblasts in all conditions as seen before but did not change significantly over time (Figure 19A). AP4E1 levels were significantly higher in parental control lines in all conditions and did not change over time (Figure 19B).

Together, neither western blotting nor immunostaining using autophagy markers could detect impairments in autophagic flux and starvation response of AP-4-deficient fibroblasts and upregulation of ATG9A either seems to be sufficient for autophagosome formation or ATG9A is not obligatory for autophagosome formation in human fibroblasts.

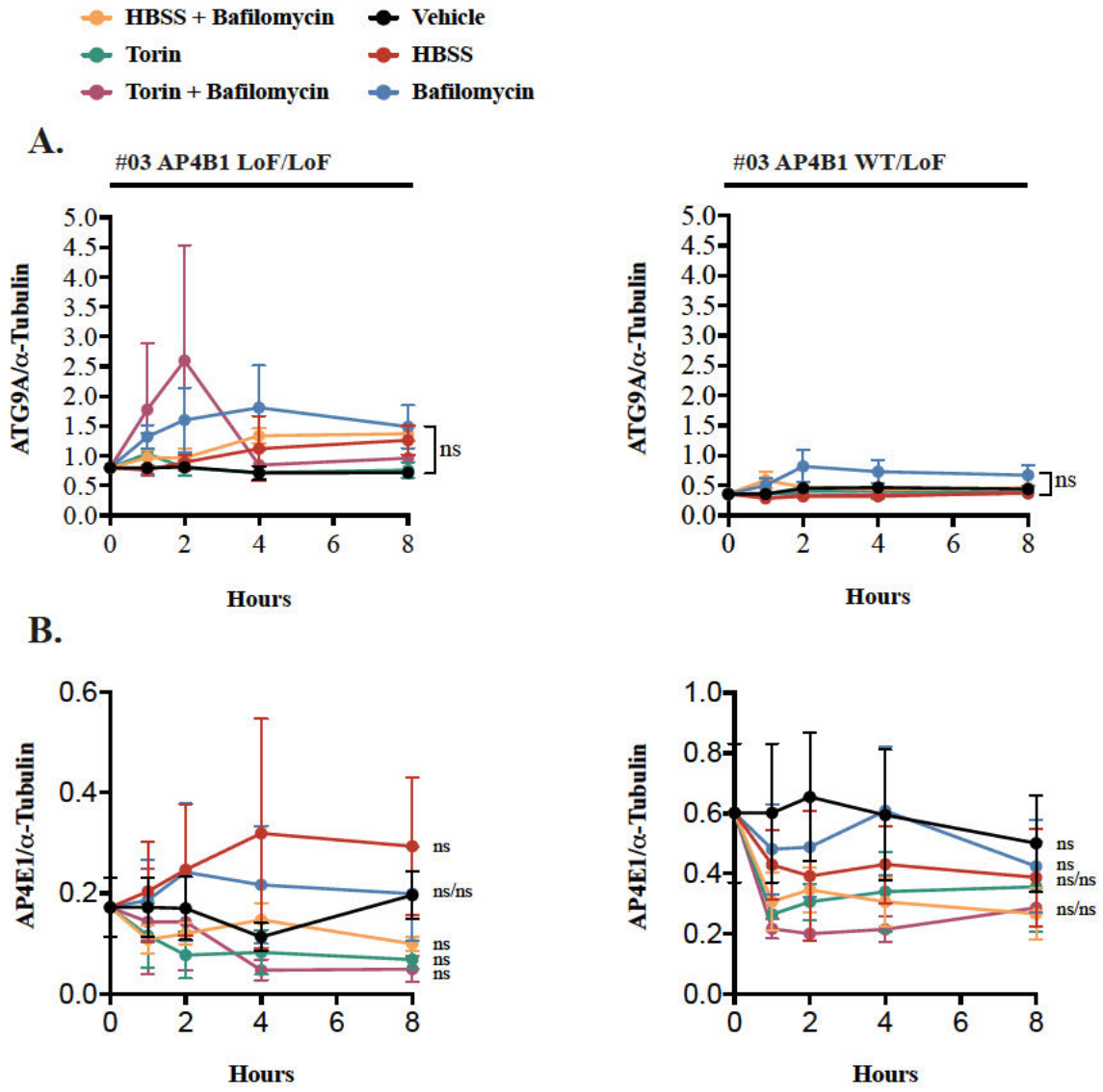

Figure 19 Dynamics of ATG9A levels and AP4E1 levels under starvation conditions

A. ATG9A levels of AP-4-deficient fibroblasts show no significant changes during 8h of starvation, autophagy blockage or induction. Asterisks indicate significance between hour 0 and 8 of each condition. ATG9A levels of AP-4-deficient fibroblasts were significantly higher compared to parental controls at all timepoints (asterisks not displayed). **B.** AP4E1 levels do not change significantly over time and show no clear trend in AP-4-deficient fibroblasts and parental controls. Asterisks indicate significance between hour 0 and 8 of each condition. AP4E1 levels of AP-4-deficient fibroblasts were significantly lower than those of parental controls (asterisks not displayed). LoF, loss of function; WT, wildtype.

3.5 Mitochondrial Mass And Membrane Potential Is Unaltered In AP-4-Deficient Fibroblasts

Impaired mitophagy is known to contribute to a number of diseases ranging from Alzheimer's disease (Chakravorty, Jetto, & Manjithaya, 2019) to inherited metabolic disorders (Luciani et al., 2020). Since unselective autophagy was intact in AP-4-deficient fibroblasts, it was of interest whether selective autophagy of mitochondria, mitophagy, was impaired. Detection of alterations in mitochondrial mass and membrane potential could point towards such impairment.

Two microscopy-based approaches, JC1 dye and a combination of tetramethylrhodamine, ethyl ester (TMRE) and MitoTracker Deep Red (MTDR), were employed to examine mitochondrial membrane potential ($\Delta\Psi_m$) and mitochondrial mass (Figure 20A). The JC1 600nm/530nm signal ratio as a measure of mitochondrial polarization status showed no difference between AP-4-deficient fibroblasts and heterozygous controls (Figure 20D). TMRE intensity, which corresponds to the number of active mitochondria did not differ between AP-4-deficient fibroblasts and heterozygous controls (Figure 20B). MTDR accumulates in active mitochondria and can be used as a measure of mitochondrial mass. Similarly, no significant difference in mitochondrial mass could be detected (Figure 20C). These results suggest that mitochondrial mass and membrane potential are unaltered in AP-4-deficient fibroblasts and that mitophagy is unimpaired under nutrient-rich conditions.

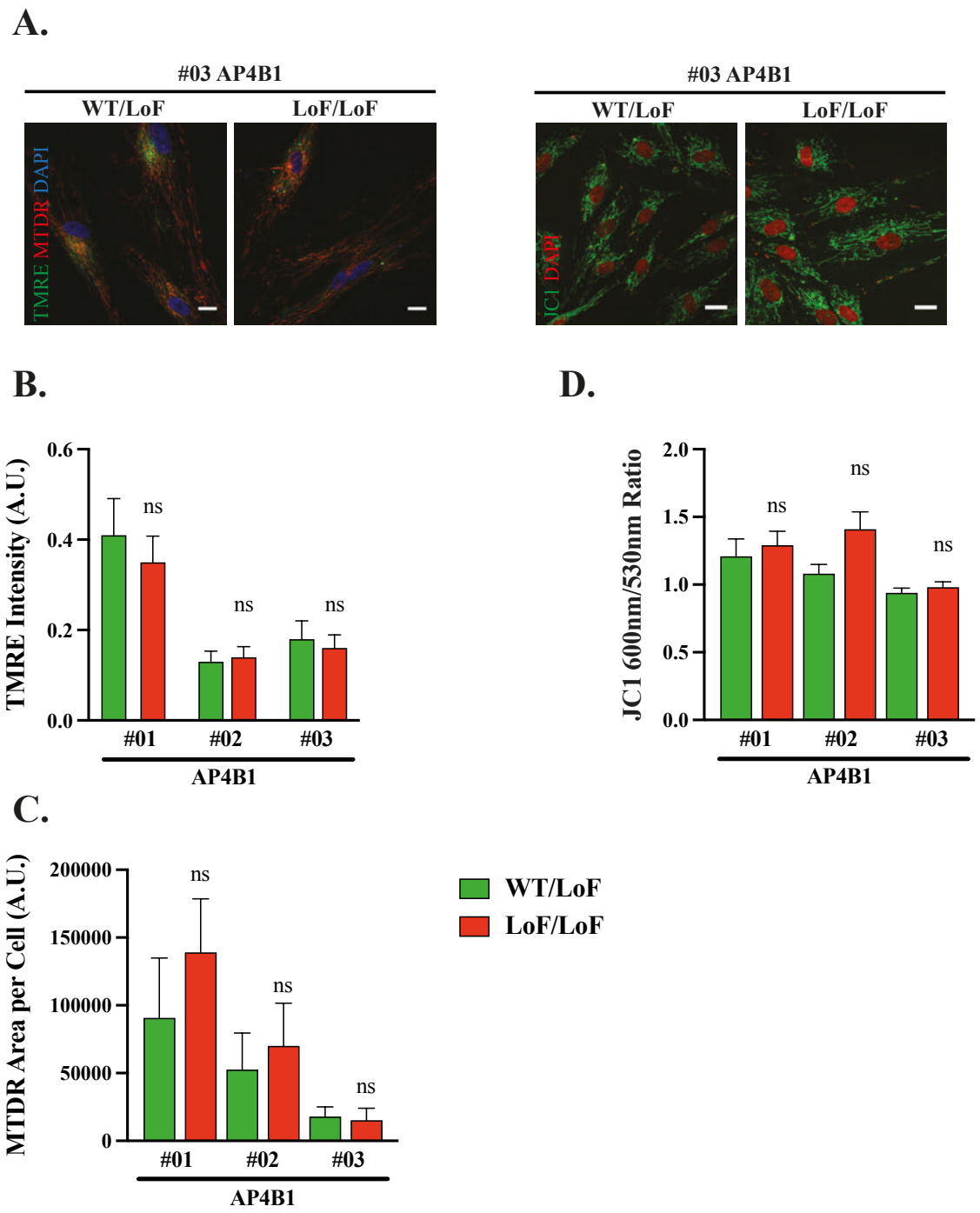

Figure 20 Mitochondrial mass and membrane potential in AP-4-deficient fibroblasts

A. Live immunofluorescence images of AP-4-deficient fibroblasts and parental controls of line #03 stained for TMRE (*green*), MTDR (*red*) and DAPI (*blue*) as a nuclear marker on the left. The right panel shows JC1 signal (600nm/530nm both *green*) and DAPI (*blue*) as a nuclear marker. Scale bar 10µm. **B.&C.** Quantitation of TMRE intensity and MTDR area per cell shows no significant differences between AP-4-deficient fibroblasts and parental controls. A.U., arbitrary units. **D.** AP-4-deficient fibroblasts and parental controls show similar JC1 600nm/530nm ratio. LoF, loss of function; WT, wildtype.

3.6 iPSC-Derived Cortical Neurons *(With Julian Teinert)*

Human iPSC-derived neurons have proven to be powerful models of neurodegenerative disease providing new insights into pathophysiology and serving as platforms for drug development (C.-Y. Chang et al., 2020; Seibler et al., 2018). The ATG9A mislocalization phenotype together with the elevated ATG9A levels in AP-4-deficient fibroblasts are robust phenotypic markers, which, if also present in iPSC-derived neurons, could be utilized in a high-throughput drug screens. iPSC-derived cortical neurons were differentiated from the same three AP4B1-deficient fibroblast lines and their heterozygous parental controls.

3.7 AP-4-Deficient iPSC-Derived Cortical Neurons Have Increased ATG9A Levels

AP-4-deficient fibroblasts showed significantly increased ATG9A levels as well as lowered levels of the AP4E1 subunit and this was examined in iPSC-derived cortical neurons as well. Whole cell lysates of all three AP-4-deficient iPSC-derived cortical neuron lines showed significantly increased levels of ATG9A compared to heterozygous parental controls (Figure 21A&B). Levels of the AP4E1-subunit were significantly reduced in AP-4-deficient iPSC-derived cortical neurons, again pointing towards an unstable AP-4-complex (Figure 21A&C). Together, AP-4-deficient iPSC-derived cortical neurons show a similarly robust increase in ATG9A levels and lowered AP4E1 levels suggesting that increased levels of ATG9A is a common compensatory mechanism.

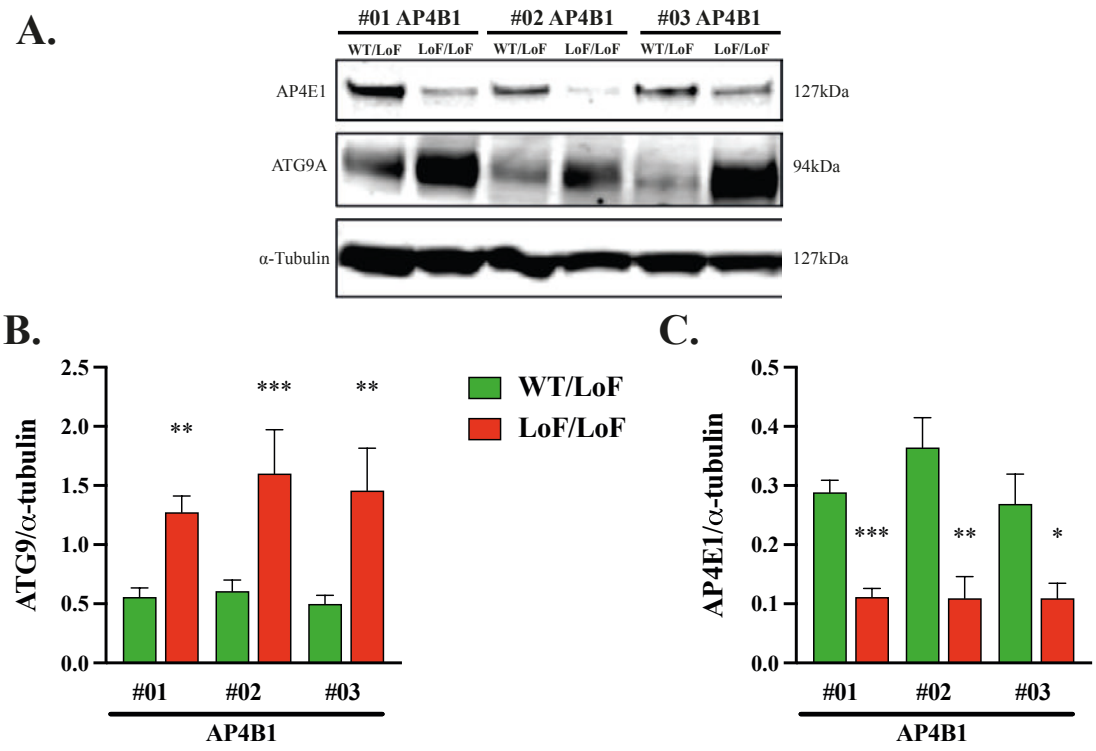

Figure 21 ATG9A and AP4E1 levels of AP-4-deficient iPSC-derived cortical neurons

A. Western blotting of whole cell lysates from AP-4-deficient iPSC-derived cortical neurons and parental controls showing ATG9A and AP4E1 signal and α-Tubulin as loading control. **B.** Quantitation of ATG9A levels in AP-4-deficient iPSC-derived cortical neurons and parental controls reveals increased levels in AP-4-deficient cells **C.** Quantitation of lower AP4E1 levels in AP-4-deficient iPSC-derived cortical neurons indicative of an unstable AP-4-complex. LoF, loss of function; WT, wildtype.

3.8 ATG9A Is Mislocalized In AP-4-Deficient iPSC-Derived Cortical Neurons

ATG9A accumulates in the TGN of AP-4-deficient fibroblasts and has the potential to serve as a phenotypic marker in a high content screening of iPSC-derived neurons. The ImageXpress Micro (IXM) Confocal High-Content Imaging System (Molecular Devices) served as an image and analysis platform for over $9x10^4$ cells per condition. iPSC-derived AP-4-deficient cortical neurons and their heterozygous parental control lines were stained for ATG9A and ß-Tubulin III as a neuronal cell marker. An automated pipeline was used to detect the ATG9A signal, which shows a higher intensity and a confinement to the juxtanuclear region in AP-4-deficient neurons while heterozygous control cells show a much weaker ATG9A signal that is more evenly distributed throughout the cell.

ß-Tubulin III was used to identify the neuronal soma and the ratio of the high intensity ATG9A area in relation to the whole cell area was calculated (Chapter 2.11). AP-4-deficient iPSC-derived cortical neurons exhibited a significantly higher ratio, i.e. more neurons with high intensity ATG9A signal, a surrogate for accumulating ATG9A (Figure 22C, D&E). The cells were fixed and stained 7 days after replating (day *in vitro* 14), but interestingly, iPSC-derived AP-4-deficient cortical neurons, that were fixed and stained 24h after plating (day *in vitro* 8, IncuCyte experiment), exhibited the same ATG9A missorting phenotype even at this early stage (Figure 22A&B). This was seen throughout all lines and confirmed mislocalized ATG9A as a robust phenotypic marker.

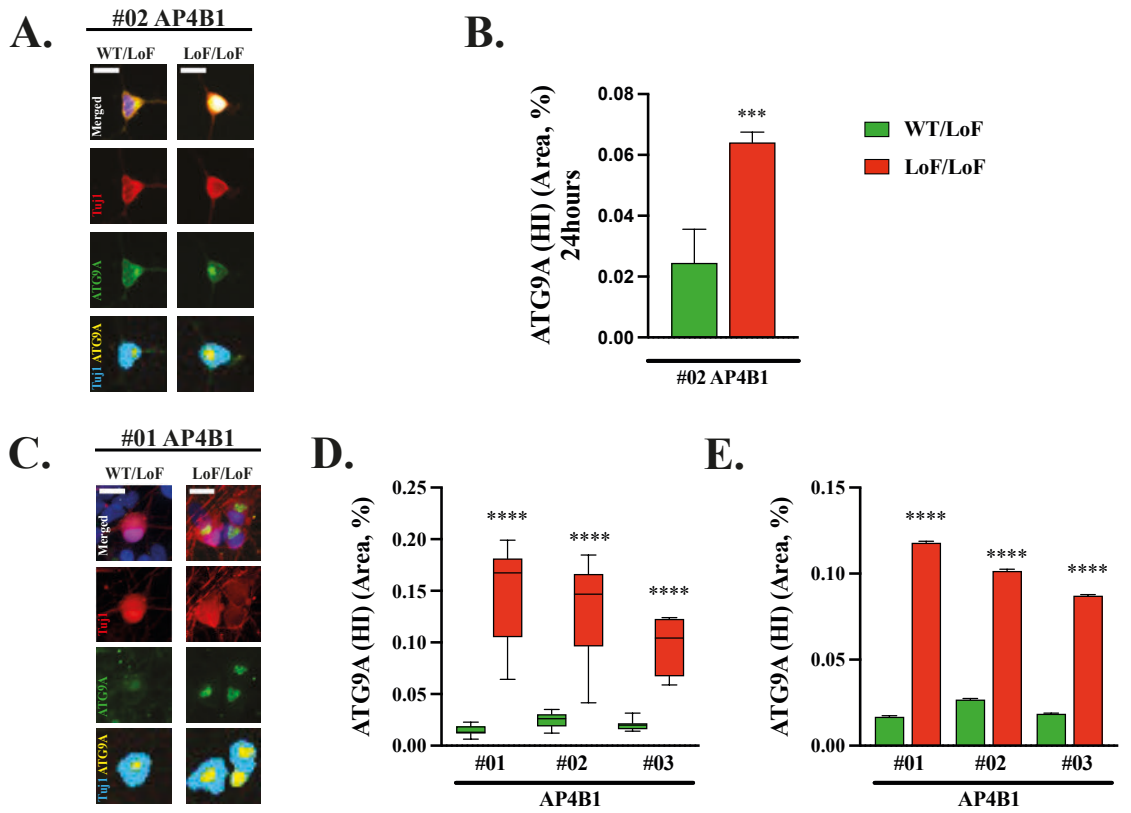

Figure 22 ATG9A is mislocalized in AP-4-deficient iPSC-derived cortical neurons

A. Immunofluorescence images of AP-4-deficient iPSC-derived cortical neurons of line #01 at 24h after plating showing a high intensity ATG9A signal (second row, *green*) confined to the juxtanuclear region. Neuron-specific class III beta-tubulin (Tuj1, third row, *red*) was used as neuronal marker. The fourth row shows the overlay of the IXM analysis software with whole cell area (Tuj1, *blue*) and high intensity ATG9A signal (*yellow*). Scale bar 20 µm. **B.** Quantitation of ATG9A high intensity area on a per cell basis as percent of the whole cell area defined by Tuj1 signal showing a bigger area for all AP-4-deficient iPSC-derived cortical neurons 24h after plating. HI, high intensity. **C.** Immunofluorescence images of AP-4-deficient iPSC-derived cortical neurons at DIV7. **D.** Quantitation of ATG9A high intensity area as percent of the whole cell area defined by Tuj1 signal. AP-4-deficient iPSC-derived cortical neurons show a significantly larger high intensity ATG9A area. Data are shown on a per differentiation basis summarizing three independent differentiations for every cell line. HI, high intensity. **E.** Quantitation of ATG9A high intensity area on a per cell basis as percent of the whole cell area at DIV7. HI, high intensity; LoF, loss of function; WT, wildtype.

The anti-TGN46-antibody as well as the anti-GM130-antibody, both used as TGN markers, did not work reliably enough to be employed in the automated image analysis. Nonetheless, images of AP-4-deficient iPSC-derived cortical neurons, in which the GM130 staining was successful, show a clear overlap of ATG9A signal and GM130 signal reminiscent of the findings in fibroblasts (Figure 23). This suggests, that ATG9A accumulates in the TGN in AP-4-deficient iPSC-derived cortical neurons in a similar fashion to AP-4-deficient fibroblasts.

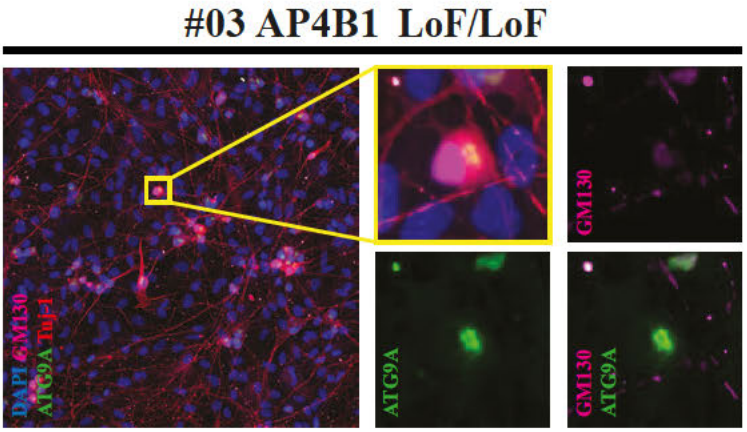

Figure 23 GM130 And ATG9A Signal In AP-4-Deficient iPSC-Derived Cortical Neurons

Immunofluorescence images of AP-4-deficient iPSC-derived cortical neurons of line #03 showing a single neuron (middle column, first row) with clear overlap of ATG9A signal (middle column, second row, *green*) and GM130 signal (right column, first row, *pink*), a TGN marker. LoF, loss of function.

3.9 AP-4-Deficient iPSC-Derived Cortical Neurons Show Altered Autophagy Markers At Baseline

ATG9A is mislocalized in AP-4-deficient fibroblasts. However, they do not exhibit any detectable alteration in autophagic flux but recent studies suggest that ATG9A might play a role in spatially controlled autophagy, for instance autophagosome formation in the axonal compartment (De Pace et al., 2018; D. Ivankovic et al., 2020). To assess this question, the LC3II/I ratio and SQSTM1/p62 levels were measured at baseline.

Interestingly, even under nutrient-rich conditions, AP-4-deficient iPSC-derived cortical neurons show a significantly decreased LCII/I ratio (Figure 24A&B). SQSTM1/p62 levels did not differ significantly from parental controls (Figure 24A&C). This could be the result of insufficient autophagosome formation, speculatively because of a lack of ATG9A in the axonal compartment. A chronic overactivation of autophagy with increased autolysosome degradation seems unlikely but must be considered. Further investigations including autophagic flux under starvation conditions as well as investigation of axon-specific autophagy are needed to establish impaired autophagy as marker of neuronal AP-4-deficiency.

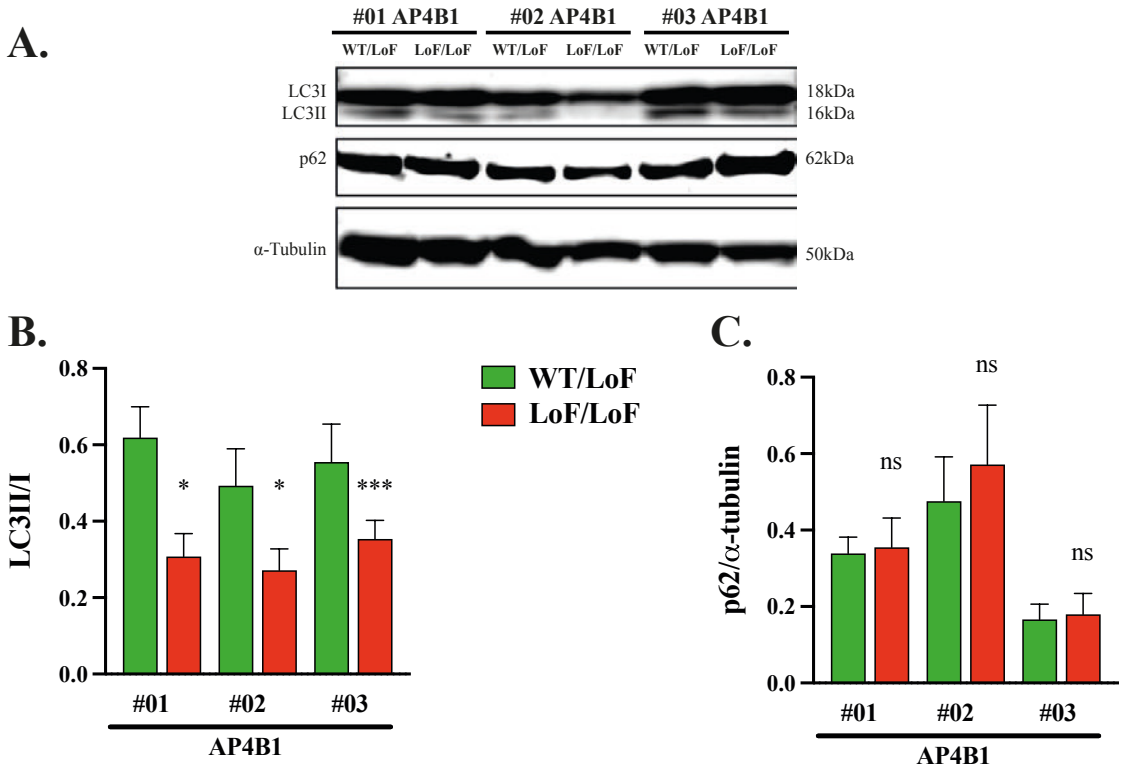

Figure 24 Autophagy markers in AP-4-deficient iPSC-derived cortical neurons

A. Western blotting of whole cell lysates from AP-4-deficient iPSC-derived cortical neurons and parental controls showing LC3I and II, p62 signal and α-Tubulin as loading control. **B.** Quantitation showing that AP-4-deficient iPSC-derived cortical neurons have a lower LC3II/I ratio under nutrient rich conditions suggestive of altered autophagy. **C.** SQSTM1/p62 levels are unchanged in AP-4-deficient iPSC-derived cortical neurons under nutrient rich conditions. LoF, loss of function; WT, wildtype.

3.10 AP-4-Deficient iPSC-Derived Cortical Neurons Have Impaired Neurite Outgrowth And Branchpoints

In a CNS-specific *Atg9a*-knockout mouse model, Yamaguchi et al. demonstrated impaired neurite outgrowth in primary neuron culture, which was independent of autophagy (Yamaguchi et al., 2018). This points towards additional roles of ATG9A in neuronal development, for instance in membrane recruitment for axonal growth.

To investigate, whether outgrowth and branching of neurites is altered in human AP-4-deficient iPSC-derived cortical neurons, potentially serving as another phenotypic marker, cells were imaged in an incubator for 24h after plating using the IncuCyte S3 Live-Cell Analysis System (Essen Bioscience). Automated analysis of AP-4-deficient iPSC-derived cortical neurons showed a shorter neurite length per cell body at any time point (Figure 25A, B&C) as wells as less branch points per cell body (Figure 25A, D&E). Imaging started 4h after plating to allow attachment and even at this early stage, neurites were significantly shorter and less branched in AP-4-deficient neurons compared to heterozygous controls. Even directly after plating, iPSC-derived AP-4-deficient neurons show decreased neurite outgrowth and branching. Together, these findings suggest that AP-4 is crucial for normal neurite outgrowth and branching.

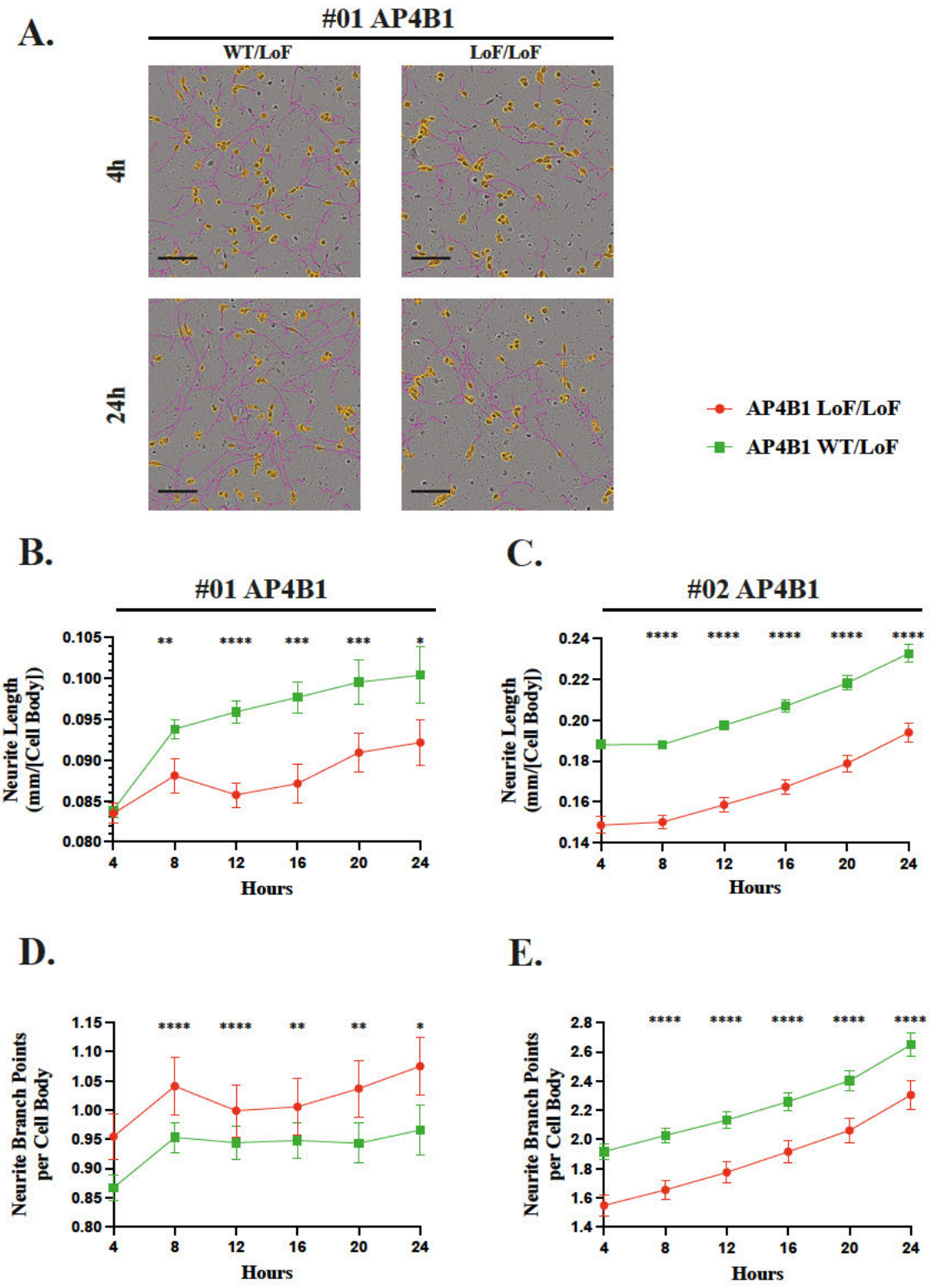
A.
#01 AP4B1
WT/LoF
LoF/LoF
4h
24h
AP4B1 LoF/LoF
AP4B1 WT/LoF
B.
#01 AP4B1
Neurite Length (mm/[Cell Body])
Hours
C.
#02 AP4B1
Neurite Length (mm/[Cell Body])
Hours
D.
Neurite Branch Points per Cell Body
Hours
E.
Neurite Branch Points per Cell Body
Hours

Figure 25 Neurite outgrowth and branching in AP-4-deficient iPSC-derived cortical neurons

A. Brightfield microscopy images of live iPSC-derived cortical neurons of line #01 with overlay of the IncuCyte analysis software marking neuronal soma (*yellow*) and neurites (*purple*) after 4h and 24h under growth conditions. Scale bar 100µm; h, hours. **B.-C.** Quantitation of neurite length in mm per cell body identified by the IncuCyte image analysis software (**A.**, *yellow*) showing significantly shorter neurite length in AP-4-deficient iPSC-derived cortical neurons. Data shown contains two independent differentiations of all lines. **D.-E.** Quantitation of neurite branch points per cell body identified by the IncuCyte image analysis software (**A.**, *yellow*) showing significantly less neurite branch points in AP-4-deficient iPSC-derived cortical neurons. LoF, loss of function; WT, wildtype.

4 Discussion

The aim of this study was to develop a cellular model of AP-4-related HSP using patient-derived fibroblasts and iPSC-derived cortical neurons from patients with bi-allelic variants in the *AP4B1* gene and their heterozygous sex-matched parents. The second aim of this study was to establish robust, AP-4-related cellular phenotypes in fibroblasts and iPSC-derived cortical neurons for the use in a high-content screen.

The heterotetrameric AP-4-complex plays a crucial role in vesicle coating and sorting of transmembrane cargo (Burgos et al., 2010; Davies et al., 2018; Mattera et al., 2015; Mattera et al., 2017) and deficiency of any of the four subunits leads to a complicated form of childhood-onset HSP, characterized by progressive spasticity, cognitive impairment, motor and speech developmental delay. Two groups independently identified ATG9A, an autophagy-related protein, as a cargo of AP-4 (Davies et al., 2018; Mattera et al., 2017). Findings from other groups show, that ATG9A is missorted to the TGN in AP-4-knockout HeLa, SH-SY5Y, MEFs, leukemia-derived HAP1 cells and patient-derived fibroblasts (Davies et al., 2018; Mattera et al., 2017) independent of the AP-4-subunit, that is deficient. Hippocampal neurons from *Ap4e1*-knockout mice show a similar ATG9A missorting phenotype (De Pace et al., 2018; D. Ivankovic et al., 2020). Since ATG9A is crucial for membrane recruitment and elongation of autophagosomes (C. M. Guardia et al., 2020; Matoba et al., 2020; Noda et al., 2000), its loss from the cell periphery, especially from axons of the long corticospinal tracts, might lead to a compartment-specific “autophagopathy”. This fits into the picture of a “dying back” axonopathy, i.e. a progressive degeneration of the axons of the long corticospinal tracts, that defines HSPs pathologically. A *post-mortem* study of a patient with *AP4M1* mutations confirmed axonal swellings and damage as a pathological theme in AP-4-related HSP (Verkerk et al., 2009). *Ap4e1*-knockout mice show axonal swellings in Purkinje cells, hippocampal and spinal cord neurons (De Pace et al., 2018) providing evidence for an axonopathy. Similarly, *Ap4s1*-knockout zebrafish show reduced length of spinal motor neurons (D'Amore et al., 2020). Intriguingly, a CNS-specific conditional knockout of *Atg9a* in mice results in a phenotype reminiscent of AP-4-associated HSP including axonal degeneration (Yamaguchi et al., 2018). Of note, an autophagy-independent function of ATG9A in neurite outgrowth has been described in these mice.

Despite the recent advances in the understanding of AP-4 and its cargo ATG9A, no clear definition exists of the underlying pathomechanism causing the clinical phenotype of AP-4-related HSP and treatment options are still limited to symptomatic. Disease models using patient-derived iPSC-derived neurons have been proven to be powerful tools to study neurological disease on a patient-individual level, that animal models fail to achieve. (C. Y. Chang et al., 2015; Chen et al., 2014; Kondo et al., 2013; Seibler et al., 2018). Parallel advances in imaging and image analysis on a high-throughput basis have enabled for the screening of thousands of compounds in patient-derived cellular models and aided in the discovery of new therapeutic approaches (Fang et al., 2019; Rehbach et al., 2019).

Here, the development of the first iPSC-derived cortical neuron model of AP-4-associated HSP of patients with variants in the *AP4B1* gene provides novel insights into AP-4-related cellular phenotypes and creates a powerful platform to further study AP-4-associated HSP. It describes for the first time the ATG9A missorting phenotype in a patient-derived neuronal model and through identifying impairment of neurite outgrowth and neuronal autophagy expands the range of phenotypic markers. Its implementation in a high-content screening will support the search for novel therapeutic targets and studying this model has the potential to expand the existing knowledge of not only AP-4-deficiency, but the role of the AP-4-complex and its cargo proteins in neurons in general and particularly in autophagy and neuronal growth.

4.1 AP-4-Related Phenotypes In Patient-Derived Fibroblasts

Patient-derived fibroblasts represent a relatively cost-efficient option to study human disease and have been successfully used in previous studies of HSP to reveal disease-associated phenotypes (Breza et al., 2021; J. Chang, Lee, & Blackstone, 2014). Our study found a robust colocalization of ATG9A with TGN markers and confirmed the depletion of ATG9A from the cell periphery described previously for different cell types (Davies et al., 2018; Mattera et al., 2017). Recent studies have shown, that this missorting phenotype is present in all fibroblasts of patients with AP-4-associated HSP regardless of the affected subunit (Behne et al., 2020) making it a useful biomarker to support a clinical suspicion especially when novel genetic variants of unclear significance are identified. Elevated ATG9A levels in AP-4-deficient fibroblasts might represent a compensatory

mechanism enabling at least some ATG9A to reach the cell periphery and are a common finding in different cell types (Davies et al., 2018; Davor Ivankovic et al., 2020). In keeping with this, overexpression of SERINC3, a recently identified cargo of AP-4, leads to its distribution in an AP-4-independent manner suggesting that high amounts of protein, being "swept out" of the TGN reach their intracellular destination even in AP-4-deficient cells (Davies et al., 2018). Lentiviral re-expression of the missing AP4B1-subunit rescues the ATG9A mislocalization phenotype lending further evidence to the fact that ATG9A depends on AP-4 for sorting and transport. All AP-4-subunits are needed for a functioning complex and loss of AP4B1 leads to an unstable complex demonstrated by co-immunoprecipitation and the decreased levels of the other subunits (e.g. AP4E1). This phenomenon has been described previously (Borner et al., 2012; Hirst et al., 2013) and is further corroborated by the fact that organisms have none or all four genes encoding for the AP-4-subunits (Hirst et al., 2014). The lentiviral re-expression of AP4B1 also led to a reduction of ATG9A levels to those of parental controls suggesting a negative feedback mechanism, which is activated when ATG9A reaches the cell periphery.

Since ATG9A is a core autophagy protein, it seems likely that AP-4-deficient cells show alterations in autophagic flux. At baseline, no clear-cut changes in protein levels of the autophagy markers LC3 and SQSTM1/p62 were detected. Surprisingly, this continued during the investigation of the starvation response of AP-4-deficient fibroblasts. Protein levels of LC3 as well as immunostaining and automated analysis of LC3-positive vesicles revealed an intact starvation response. All AP-4-deficient fibroblast lines showed an increase of LC3II/I ratio suggestive of increased autophagosome formation and this was mirrored in number and size increases of LC3-positive vesicles as a surrogate for autophagosomes. Differences between patient and control lines were present especially in LC3-positive vesicle number and size but constant throughout different conditions. This suggests interindividual differences, since the response to starvation conditions, autophagy induction or inhibition was similar in all lines. SQSTM1/p62 is an autophagy substrate and elevated levels are expected in cells with impaired autophagy. Like LC3, SQSTM1/p62 levels in AP-4-deficient fibroblasts were unchanged at baseline. Under starvation conditions western blotting was not sensitive enough to detect significant changes and only immunostaining revealed an increase of puncta number upon Bafilomycin A1 treatment. Interestingly, this increase was less pronounced when

starvation was added suggesting that not all degradational activity is blocked by Bafilomycin A1. Together, AP-4-deficient fibroblasts show no autophagy impairment detectable by well-established protocols raising the question to what extent ATG9A is necessary in fibroblast autophagy and if the increased levels might compensate for its loss from the periphery. A knockout of ATG9A and subsequent investigation of autophagic flux could be used to further examine this. In contrast to these findings, the Borner and Robinson labs together found elevated LC3II levels and a decreased LC3II/I ratio in *Ap4e1*- and *Ap4b1*-knockout HeLa cells as well as an increase in LC3-positive vesicle size (Davies et al., 2018). Elevated LC3II levels were also described in *Ap4b1*-knockout mice cerebellar lysates (S. Matsuda et al., 2008). Both groups argue that AP-4-deficiency causes aberrant autophagy. ATG9A links the AP-4-complex to autophagy and the defective distribution could potentially cause a cell-type-specific impairment of autophagy. Although HeLa cells, Purkinje neurons and fibroblasts all depend on a polarized cell organization, the demands of distributing ATG9A into axons in neurons, i.e. compartmental autophagy, might be higher than those in fibroblasts and cannot be compensated by increased ATG9A. A cell-type-specific effect is also plausible in the light of the fact that patients with AP-4-associated HSP have neurological symptoms, but no affection of connective tissue or other organs. Intriguingly, patients with loss of the S3-subunit of adaptor-protein-complex-1 (AP1S3) show an autoinflammatory skin disorder with impaired keratinocyte autophagy (Mahil et al., 2016). Additionally, autophagy-independent functions of ATG9A must be considered. Besides unselective autophagy, the investigation of mitochondrial mass and membrane potential showed no differences between patient-derived fibroblasts and controls suggesting a functioning turnover of mitochondria through selective mitophagy.

In summary, this study confirmed the instability of the AP-4-complex and the ATG9A-related phenotypes including missorting and overexpression as robust phenotypic markers but failed to recapitulate findings of impaired autophagy.

4.2 An iPSC-Derived Cortical Neuron Model Of AP-4-associated HSP

The experiments carried out in patient-derived fibroblasts provided robust phenotypic markers, that would prove useful in a high-content screening and were then to be confirmed in iPSC-derived cortical neurons. It was possible to demonstrate the same ATG9A missorting phenotype and increased ATG9A levels in iPSC-derived cortical neurons. This phenotype was found as early as 24h after plating suggesting that sorting of ATG9A begins early during neurodevelopment. Although autophagic flux is unimpaired in AP-4-deficient fibroblasts at least under starvation conditions of up to 8h, a specialized function of ATG9A in neuronal autophagy is possible. Intriguingly, the LC3II/I ratio was significantly lower in AP-4-deficient iPSC-derived cortical neurons compared to parental controls contrasting the findings in fibroblasts. A lack of ATG9A from the axonal compartment could lead to a decrease in autophagosome formation and reduced LC3II/I ratio. However, because autophagosomes get constantly degraded, a higher turnover of autophagosomes could also decrease LC3II/I ratio. Contrasting these findings, a study showcased LC3-positive vesicles containing missorted AMPA receptors in axons of *Ap4b1*-knockout mice and an increased LC3II/I ratio (S. Matsuda et al., 2008). This might resemble a later disease stage, where missorted cargo proteins of AP-4 accumulate in axons and dendrites and chronically increased levels of ATG9A may enable a fraction of ATG9A to reach the axonal or dendritic compartment to form autophagosomes, which in turn cannot be sufficiently degraded due to the accumulating missorted AP-4-cargo blocking axonal autophagosome transport. It would therefore be interesting to investigate LC3II/I ratio and ATG9A distribution to the neurites as well as autophagosome mobility in more mature iPSC-derived cortical neurons. Further investigations in AP-4-deficient iPSC-derived cortical neurons including inhibitors of lysosome-autophagosome fusion (Bafilomycin A1), immunocytochemistry and starvation experiments are needed to reveal the cause of altered LC3II/I ratio and to establish altered autophagic flux as an additional phenotypic marker.

The decreased neuronal outgrowth and branching added to the range of phenotypic markers in AP-4-deficient iPSC-derived cortical neurons. A recent study including 156 patients with AP-4-associated HSP found that 90% of patients show a thinning of the corpus callosum and ventriculomegaly in 65% presumably due to white matter loss (Ebrahimi-Fakhari et al., 2020). It is interesting to speculate, that the findings in iPSC-

derived cortical neurons recapitulate *in vitro* the impaired neurite outgrowth affecting axonal or neurite development in patients with AP-4-associated HSP leading to these imaging phenotypes. Further studies are needed however, to determine whether axonal, dendritic or neurite outgrowth in general is impaired in AP-4-deficient neurons. Also, the role of ATG9A and autophagy in neurite outgrowth needs to be further elucidated, but findings in CNS-specific *Atg9a*-knockout mice suggest an autophagy-independent function in neurite outgrowth and brain development (Yamaguchi et al., 2018). The recent development of an *Ap4s1*-knockout zebrafish model lends further evidence showing reduced motor neuron axonal length (D'Amore et al., 2020). It is interesting to speculate, that imaging findings and early-onset of symptoms in AP-4-associated HSP can be attributed to an impairment of neurite growth and/or branching, while the loss of acquired skills, such as walking, in around 50% of patients (Ebrahimi-Fakhari et al., 2020) is attributed to a progressive neurodegeneration due to swellings damaging the long axons. In keeping with this, a *post-mortem* study of a patient with AP-4-associated HSP describes "irregular thickening of axons" (Verkerk et al., 2009). However, it is not clear if the swellings themselves cause axonal damage or if they just represent a sign of accumulating immature autophagosomes or other structures, which lie at the heart of the axonal damage. Another possibility to be considered is a toxic effect of accumulating ATG9A in the TGN, that disturbs the distribution of other cargo proteins from the TGN. Other cargo proteins of AP-4 include AMPARs, that are missorted to dendrites in *Ap4b1*-knockout mice and missorted amyloid precursor protein (APP) in HeLa cells (S. Matsuda et al., 2008). However, a recent study could not replicate the APP missorting in patient-derived fibroblasts (Behne et al., 2020). Another AP-4-cargo, RUSC2 binds ATG9A-containing vesicles to kinesin-1 for intracellular transport (C. M. Guardia et al., 2021) and may aggravate the missorting of ATG9A, since it is AP-4-dependently sorted as well (Davies et al., 2018). On top of this, loss of RUSC2 causes impairments of autophagy in HeLa cells (Davies et al., 2018) and RUSC2 loss-of-function mutations in humans lead to a neurological disease with phenotypic overlap to AP-4-associated HSP (Alwadei et al., 2016).

Looking at the current knowledge, it is not possible to pin down a certain element of AP-4-sorting, that is responsible for the entire phenotype seen in AP-4-deficient patients. Instead, a combination of defective sorting and transport of AP-4-cargo and the resulting

loss of proteins from their intended intracellular destination results in a complex impairment of neuronal development and homeostasis. This experimental work provides the first insights into AP-4-dependent phenotypes in iPSC-derived cortical neurons of patients with AP-4-associated HSP. It shows that ATG9A is missorted in AP-4-deficient cortical neurons and that this likely leads to altered autophagy. It shows that increased levels of ATG9A and impaired neurite outgrowth and branching are robust phenotypic markers and provides a powerful platform for a high-content screen.

4.3 Limitations Of This Study And Future Directions

This works aim was to identify robust AP-4-dependent phenotypic markers in an *in vitro* patient-derived fibroblast and iPSC-derived cortical neuron model of AP-4-associated HSP. Inherent to *in vitro* disease models is the inability to recapitulate the processes of a complex organism thus providing only a glimpse into the mechanisms underlying the disease. When looking at cellular protein trafficking through immunoblotting or immunocytochemistry, a single or even multiple timepoints can be analyzed but without recreating the environment, that a fibroblast or neuronal cell would encounter in the human body. The same goes for monitoring of autophagy. Further, like AP-4-associated HSP showing progressive symptoms as the patient ages, some cellular phenotypes might not be detectable after the timespan, that was investigated in this work. This study used AP4B1-deficient cells and assumed that loss of any of the four subunits leads to the same phenotype. For the ATG9A-related phenotypes, this assumption holds true for different cell types including patient-derived fibroblasts (Behne et al., 2020; Davies et al., 2018; Mattera et al., 2017). In fact, the affected AP-4-subunit cannot be determined by looking at the clinical phenotype either (Ebrahimi-Fakhari et al., 2020). It is unclear though, whether iPSC-derived cortical neuron models of patients with variants in different AP-4-subunits will exhibit the same cellular phenotypes described here. These questions are already undergoing investigation, e.g. with the recently developed iPSC-derived cortical neuron model of patients with variants in the AP4M1-subunit (Eberhardt et al., 2021). Excitatory iPSC-derived cortical neurons were used in this study, but it is important to investigate the effects of AP-4-deficiency on other neuronal cell types since they are not affected to the same extent and some AP-4-cargoes such as GRID2 are only expressed in

certain types of neurons (Verkerk et al., 2009). This work strongly focused on ATG9A-related phenotypes because of the growing research suggesting its crucial role in AP-4-deficiency. Nonetheless, it is not clear to what extent ATG9A missorting contributes to the disease and which roles other AP-4-cargoes, some of which might not be known yet, play in AP-4-associated HSP.

Further research aiming to find therapeutic targets and treatment options for AP-4-associated HSP will focus on three main targets.

1. The identification of robust AP-4-associated cellular phenotypes in this and previous works makes a high-content screening feasible and has the potential to reveal new druggable pathways and therapeutic targets. Finding these targets will also aid in the understanding of the pathomechanism.
2. Further basic research is needed to improve our understanding of AP-4 and its cargoes. Promising topics include compartment-specific autophagy, the role of ATG9A in neurite outgrowth and other cargo proteins of AP-4.
3. The emerging field of gene therapy holds a big promise for treating monogenic diseases and recent successes (Esrick et al., 2021; Mendell et al., 2020; Pasi et al., 2020) and the development of better ways of delivery may enable clinicians to alter the course of AP-4-associated HSP or even reverse some of its effects on the nervous system.

5 Summary

Adaptor-protein-4-deficiency (AP-4-deficiency) is an autosomal-recessive childhood-onset form of complicated hereditary spastic paraplegia (HSP) caused by bi-allelic loss-of-function mutations in one of the four subunits of the AP-4-complex. These four conditions are named SPG47 (*AP4B1*, OMIM #614066), SPG50 (*AP4M1*, OMIM #612936), SPG51 (*AP4E1*, OMIM #613744) and SPG52 (*AP4S1*, OMIM #614067), respectively and all present with global developmental delay, progressive spasticity and seizures. Imaging features include a thinning of the corpus callosum, ventriculomegaly and white matter changes. AP-4 is a highly conserved heterotetrameric complex, which is responsible for polarized sorting of transmembrane cargo including the autophagy-related protein 9 A (ATG9A). Loss of any of the four subunits leads to an instable complex and defective sorting of AP-4-cargo. ATG9A is implicated in autophagosome formation and neurite outgrowth. It is missorted in AP-4-deficient cells and CNS-specific knockout of *Atg9a* in mice results in a phenotype reminiscent of AP-4-deficiency. However, the AP-4-related cellular phenotypes including ATG9A missorting have not been investigated in human neurons.

Thus, the aim of this study is to provide the first human induced pluripotent stem cell-derived (iPSC) cortical neuron model of AP-4-deficiency to explore AP-4-related phenotypes in preparation for a high-content screening. Under the hypothesis that AP-4-deficiency leads to ATG9A missorting, elevated ATG9A levels, impaired autophagy and neurite outgrowth in human iPSC-derived cortical neurons, *in vitro* biochemical and imaging assays including automated high-content imaging and analysis were applied. First, these phenotypes were investigated in fibroblasts from three patients with compound heterozygous mutations in the *AP4B1* gene and their sex-matched parental controls. The same cell lines were used to generate iPSCs and differentiate them into human excitatory cortical neurons.

This work shows that ATG9A is accumulating in the trans-Golgi-network in AP-4-deficient human fibroblasts and that ATG9A levels are increased compared to parental controls and wild type cells suggesting a compensatory mechanism. Protein levels of the AP4E1-subunit were used as a surrogate marker for the AP-4-complex and were decreased in AP-4-deficient fibroblasts with co-immunoprecipitation confirming the instability of the complex. Lentiviral re-expression of the AP4B1-subunit rescues this

corroborating the fact that a stable AP-4-complex is needed for ATG9A trafficking. Surprisingly, autophagic flux was present in AP-4-deficient fibroblasts under nutrient-rich and starvation conditions. These phenotypic markers were evaluated in iPSC-derived cortical neurons and here, a robust accumulation of ATG9A in the juxtanuclear area was seen together with elevated ATG9A protein levels. Strikingly, assessment of autophagy markers under nutrient-rich conditions showed alterations in AP-4-deficient iPSC-derived cortical neurons indicating dysfunctional autophagosome formation. These findings point towards a neuron-specific impairment of autophagy and need further investigation. Adding to the range of AP-4-related phenotypes, neurite outgrowth and branching are impaired in AP-4-deficient iPSC-derived cortical neurons as early as 24h after plating and together with recent studies point towards a distinct role of ATG9A in neurodevelopment independent of autophagy.

Together, this work provides the first patient-derived neuron model of AP-4-deficiency and shows that ATG9A is sorted in an AP-4-dependent manner. It establishes ATG9A-related phenotypes and impaired neurite outgrowth as robust markers for a high-content screening. This disease model holds the promise of providing a platform to further study AP-4-deficiency and to search for novel therapeutic targets.

6 Zusammenfassung

Die Adaptor-Protein-4-Defizienz (AP-4-Defizienz) ist eine autosomal-rezessiv vererbte, komplizierte Form hereditären spastischen Paraplegien (HSPs), welche durch biallelische Mutationen in einer der vier Untereinheiten des AP-4-Gens verursacht wird. Die vier resultierenden Erkrankungen werden SPG47 (AP4B1, OMIM #614066), SPG50 (AP4M1, OMIM #612936), SPG51 (AP4E1, OMIM #613744) und SPG52 (AP4S1, OMIM #614067) genannt und präsentieren sich mit globaler Entwicklungsverzögerung im frühen Säuglingsalter, progressiver Spastik sowie Krampfanfällen. Radiologische Zeichen beinhalten ein verschmälertes Corpus callosum, Ventrikulomegalie und Veränderungen der weißen Substanz. AP-4 ist ein hoch konservierter, heterotetramerer Proteinkomplex, welcher für die polarisierte Verteilung von Transmembranproteinen einschließlich des „autophagy-related protein 9 A“ (ATG9A) zuständig ist. Eine „loss-of-function“ Mutation in einer der vier Untereinheiten führt zur Instabilität des gesamten Komplexes und zur Beeinträchtigung des AP-4-abhängigen Proteintransportes. ATG9A ist notwendig für die Bildung von Autophagosomen und das Neuritenwachstum. In AP-4-defizienten Zellen ist der ATG9A-Transport beeinträchtigt und ein ZNS-spezifischer Knockout von ATG9A erzeugt in Mäusen einen Phenotyp, der große Überschneidungen mit dem der AP-4-Defizienz aufweist. Bisher sind diese AP-4-abhängigen zellulären Phenotypen nicht in humanen Neuronen untersucht worden.

Daher ist die Entwicklung des ersten humanen aus induzierten pluripotenten Stammzellen (iPSC) abgeleiteten kortikalen Neuronenmodells der AP-4-Defizienz und die Identifikation AP-4-abhängiger Phenotypen für die Anwendung in einem Hochdurchsatzscreening das Ziel dieser Arbeit. Unter der Hypothese, dass AP-4-Defizienz in humanen iPSC-abgeleiteten kortikalen Neuronen zu ATG9A Fehltransport, erhöhtem ATG9A Protein, beeinträchtigter Autophagie und vermindertem Neuritenwachstum führt, wurden biochemische und automatisierte, Mikroskopie-basierte *in vitro* Assays entwickelt. Zunächst wurden primäre humane Fibroblasten von Patienten mit compound-heterozygoten Mutationen im AB4B1-Gen und geschlechtsangepasste, elterliche Kontrollzellen auf die genannten Phenotypen hin untersucht. Dieselben Zelllinien wurden anschließend für die Generierung von iPSCs und die Differenzierung in exzitatorische kortikale Neurone verwendet.

Diese Arbeit zeigt, dass ATG9A in AP-4-defizienten Fibroblasten im Bereich des Trans-Golgi-Netzwerkes akkumuliert und das ATG9A Proteinlevel erhöht sind, was auf eine kompensatorische Hochregulierung hindeutet. Die Proteinlevel der AP4E1-Untereinheit wurden als Surrogatparameter für einen stabilen AP-4-Komplex genutzt und waren in AP-4-defizienten Fibroblasten vermindert. In der Co-Immunpräzipitation konnte eine Instabilität des AP-4-Komplexes bestätigt werden. Die lentivirale Reexpression der AB4B1-Untereinheit führte zu einer Wiederherstellung des Wildtyp-Phänotyps und zeigt damit, dass ein stabiler AP-4-Komplex für die korrekte Verteilung von ATG9A notwendig ist. Trotz der bekannten Beteiligung von ATG9A an der Bildung von Autophagosomen, zeigte sich eine intakte Autophagosomenbildung und Degradation in AP-4-defizienten Fibroblasten. Die beschriebenen phänotypischen Marker wurden in iPSC-abgeleiteten kortikalen Neuronen evaluiert und auch hier konnten eine juxtanukleäre Akkumulation von ATG9A sowie erhöhte ATG9A Proteinlevel demonstriert werden. Im Gegensatz zu den Fibroblasten, zeigten AP-4-defiziente iPSC-abgeleitete kortikale Neurone bereits unter nährstoffreichen Bedingungen eine Konstellation von Autophagiemarkern, die auf eine gestörte Autophagosomenbildung und damit auf eine Neuronen-spezifische Störung von Autophagie hindeuten und der weiteren Untersuchung bedürfen. Zusätzlich fand sich bei AP-4-defizienten kortikalen Neuronen bereits in den ersten 24 Stunden im Inkubator eine Störung des Neuritenwachstums und der -verzweigung, welche in Zusammenschau mit kürzlich erschienenen Arbeiten auf eine zusätzliche Autophagie-unabhängige Funktion von ATG9A hinweisen.

Diese Arbeit stellt zusammenfassend die Entwicklung des ersten Patienten-abgeleiteten Neuronenmodells der AP-4-Defizienz dar und zeigt das ATG9A in einer AP-4-abhänigen Weise in der Zelle verteilt wird. Weiterhin etabliert diese Arbeit ATG9A-abhängige zelluläre Phänotypen und gestörtes Neuritenwachstum als robuste phänotypische Marker für ein High-Content Screening. Dieses zelluläre Krankheitsmodell trägt das Potential als Plattform für weitere Studien der AP-4-Defizienz zu dienen und damit neue therapeutische Möglichkeiten aufzudecken.

7 References

Abdollahpour, H., Alawi, M., Kortum, F., Beckstette, M., Seemanova, E., Komarek, V., . . . Kutsche, K. (2015). **An AP4B1 frameshift mutation in siblings with intellectual disability and spastic tetraplegia further delineates the AP-4 deficiency syndrome**. *Eur J Hum Genet, 23*(2), 256-259. doi:10.1038/ejhg.2014.73

Abou Jamra, R., Philippe, O., Raas-Rothschild, A., Eck, S. H., Graf, E., Buchert, R., . . . Colleaux, L. (2011). **Adaptor protein complex 4 deficiency causes severe autosomal-recessive intellectual disability, progressive spastic paraplegia, shy character, and short stature**. *Am J Hum Genet, 88*(6), 788-795. doi:10.1016/j.ajhg.2011.04.019

Accogli, A., Hamdan, F. F., Poulin, C., Nassif, C., Rouleau, G. A., Michaud, J. L., & Srour, M. (2018). **A novel homozygous AP4B1 mutation in two brothers with AP-4 deficiency syndrome and ocular anomalies**. *Am J Med Genet A, 176*(4), 985-991. doi:10.1002/ajmg.a.38628

Aguilar, R. C., Boehm, M., Gorshkova, I., Crouch, R. J., Tomita, K., Saito, T., . . . Bonifacino, J. S. (2001). **Signal-binding Specificity of the μ4 Subunit of the Adaptor Protein Complex AP-4***. *Journal of Biological Chemistry, 276*(16), 13145-13152. doi:https://doi.org/10.1074/jbc.M010591200

Alwadei, A. H., Benini, R., Mahmoud, A., Alasmari, A., Kamsteeg, E. J., & Alfadhel, M. (2016). **Loss-of-function mutation in RUSC2 causes intellectual disability and secondary microcephaly**. *Dev Med Child Neurol, 58*(12), 1317-1322. doi:10.1111/dmcn.13250

Ashrafi, G., & Schwarz, T. L. (2013). **The pathways of mitophagy for quality control and clearance of mitochondria**. *Cell Death & Differentiation, 20*(1), 31-42. doi:10.1038/cdd.2012.81

Bayer, M., Fischer, J., Kremerskothen, J., Ossendorf, E., Matanis, T., Konczal, M., . . . Barnekow, A. (2005). **Identification and characterization of Iporin as a novel interaction partner for rab1**. *BMC Cell Biology, 6*(1), 15. doi:10.1186/1471-2121-6-15

Behne, R., Teinert, J., Wimmer, M., D'Amore, A., Davies, A. K., Scarrott, J. M., . . . Ebrahimi-Fakhari, D. (2020). **Adaptor protein complex 4 deficiency: a paradigm of childhood-onset hereditary spastic paraplegia caused by defective protein trafficking**. *Hum Mol Genet, 29*(2), 320-334. doi:10.1093/hmg/ddz310

Bettencourt, C., Salpietro, V., Efthymiou, S., Chelban, V., Hughes, D., Pittman, A. M., . . . Xiromerisiou, G. (2017). **Genotype-phenotype correlations and expansion of the molecular spectrum of AP4M1-related hereditary spastic paraplegia**. *Orphanet J Rare Dis, 12*(1), 172. doi:10.1186/s13023-017-0721-2

Bjørkøy, G., Lamark, T., Pankiv, S., Øvervatn, A., Brech, A., & Johansen, T. (2009). **Monitoring autophagic degradation of p62/SQSTM1**. *Methods Enzymol, 452*, 181-197. doi:10.1016/s0076-6879(08)03612-4

Blackstone, C. (2012). **Cellular pathways of hereditary spastic paraplegia**. *Annu Rev Neurosci, 35*, 25-47. doi:10.1146/annurev-neuro-062111-150400

Blackstone, C. (2018). **Hereditary spastic paraplegia**. *Handb Clin Neurol, 148*, 633-652. doi:10.1016/B978-0-444-64076-5.00041-7

Boehm, M., Aguilar, R. C., & Bonifacino, J. S. (2001). **Functional and physical interactions of the adaptor protein complex AP-4 with ADP-ribosylation factors (ARFs)**. *The EMBO journal, 20*(22), 6265-6276. doi:10.1093/emboj/20.22.6265

Boehm, M., & Bonifacino, J. S. (2001). **Adaptins: the final recount**. *Mol Biol Cell, 12*(10), 2907-2920. doi:10.1091/mbc.12.10.2907

Bonifacino, J. S. (2014). **Adaptor proteins involved in polarized sorting**. *J Cell Biol, 204*(1), 7-17. doi:10.1083/jcb.201310021

Borner, G. H. H., Antrobus, R., Hirst, J., Bhumbra, G. S., Kozik, P., Jackson, L. P., . . . Robinson, M. S. (2012). **Multivariate proteomic profiling identifies novel accessory proteins of coated vesicles**. *J Cell Biol, 197*(1), 141-160. doi:10.1083/jcb.201111049

Breza, M., Hirst, J., Chelban, V., Banneau, G., Tissier, L., Kol, B., . . . Stevanin, G. (2021). **Expanding the Spectrum of AP5Z1-Related Hereditary Spastic Paraplegia (HSP-SPG48): A Multicenter Study on a Rare Disease**. *Mov Disord, 36*(4), 1034-1038. doi:10.1002/mds.28487

Burgos, P. V., Mardones, G. A., Rojas, A. L., daSilva, L. L., Prabhu, Y., Hurley, J. H., & Bonifacino, J. S. (2010). **Sorting of the Alzheimer's disease amyloid precursor protein mediated by the AP-4 complex**. *Dev Cell, 18*(3), 425-436. doi:10.1016/j.devcel.2010.01.015

Byrne, S., Jansen, L., JM, U. K.-I., Siddiqui, A., Lidov, H. G., Bodi, I., . . . Jungbluth, H. (2016). **EPG5-related Vici syndrome: a paradigm of neurodevelopmental disorders with defective autophagy**. *Brain, 139*(Pt 3), 765-781. doi:10.1093/brain/awv393

Carpenter, A. E., Jones, T. R., Lamprecht, M. R., Clarke, C., Kang, I. H., Friman, O., . . . Sabatini, D. M. (2006). **CellProfiler: image analysis software for identifying and quantifying cell phenotypes**. *Genome Biol, 7*(10), R100. doi:10.1186/gb-2006-7-10-r100

Chakravorty, A., Jetto, C. T., & Manjithaya, R. (2019). **Dysfunctional Mitochondria and Mitophagy as Drivers of Alzheimer's Disease Pathogenesis**. *Front Aging Neurosci, 11*, 311. doi:10.3389/fnagi.2019.00311

Chang, C.-Y., Ting, H.-C., Liu, C.-A., Su, H.-L., Chiou, T.-W., Lin, S.-Z., . . . Ho, T.-J. (2020). **Induced Pluripotent Stem Cell (iPSC)-Based Neurodegenerative Disease Models for Phenotype Recapitulation and Drug Screening**. *Molecules (Basel, Switzerland), 25*(8), 2000. doi:10.3390/molecules25082000

Chang, C. Y., Chen, S. M., Lu, H. E., Lai, S. M., Lai, P. S., Shen, P. W., . . . Su, H. L. (2015). **N-butylidenephthalide attenuates Alzheimer's disease-like cytopathy in Down syndrome induced pluripotent stem cell-derived neurons**. *Sci Rep, 5*, 8744. doi:10.1038/srep08744

Chang, J., Lee, S., & Blackstone, C. (2014). **Spastic paraplegia proteins spastizin and spatacsin mediate autophagic lysosome reformation**. *J Clin Invest, 124*(12), 5249-5262. doi:10.1172/JCI77598

Chen, C., Jiang, P., Xue, H., Peterson, S. E., Tran, H. T., McCann, A. E., . . . Deng, W. (2014). **Role of astroglia in Down's syndrome revealed by patient-derived human-induced pluripotent stem cells**. *Nat Commun, 5*, 4430. doi:10.1038/ncomms5430

Claude-Taupin, A., Jia, J., Bhujabal, Z., Garfa-Traoré, M., Kumar, S., da Silva, G. P. D., . . . Deretic, V. (2021). **ATG9A protects the plasma membrane from programmed and incidental permeabilization**. *Nature Cell Biology, 23*(8), 846-858. doi:10.1038/s41556-021-00706-w

Claudiani, P., Riano, E., Errico, A., Andolfi, G., & Rugarli, E. I. (2005). **Spastin subcellular localization is regulated through usage of different translation start sites and active export from the nucleus**. *Exp Cell Res, 309*(2), 358-369. doi:10.1016/j.yexcr.2005.06.009

Condo, I., Ventura, N., Malisan, F., Tomassini, B., & Testi, R. (2006). **A pool of extramitochondrial frataxin that promotes cell survival**. *J Biol Chem, 281*(24), 16750-16756. doi:10.1074/jbc.M511960200

D'Amore, A., Tessa, A., Naef, V., Bassi, M. T., Citterio, A., Romaniello, R., . . . Santorelli, F. M. (2020). **Loss of ap4s1 in zebrafish leads to neurodevelopmental defects resembling spastic paraplegia 52**. *Ann Clin Transl Neurol, 7*(4), 584-589. doi:10.1002/acn3.51018

Davies, A. K., Itzhak, D. N., Edgar, J. R., Archuleta, T. L., Hirst, J., Jackson, L. P., . . . Borner, G. H. H. (2018). **AP-4 vesicles contribute to spatial control of autophagy via RUSC-dependent peripheral delivery of ATG9A**. *Nat Commun, 9*(1), 3958. doi:10.1038/s41467-018-06172-7

De Pace, R., Skirzewski, M., Damme, M., Mattera, R., Mercurio, J., Foster, A. M., . . . Bonifacino, J. S. (2018). **Altered distribution of ATG9A and accumulation of axonal aggregates in neurons from a mouse model of AP-4 deficiency syndrome**. *PLoS Genet, 14*(4), e1007363. doi:10.1371/journal.pgen.1007363

Dell'Angelica, E. C., & Bonifacino, J. S. (2019). **Coatopathies: Genetic Disorders of Protein Coats**. *Annual review of cell and developmental biology, 35*, 131-168. doi:10.1146/annurev-cellbio-100818-125234

Dell'Angelica, E. C., Mullins, C., & Bonifacino, J. S. (1999). **AP-4, a novel protein complex related to clathrin adaptors**. *J Biol Chem, 274*(11), 7278-7285. doi:10.1074/jbc.274.11.7278

Drouin-Ouellet, J., Lau, S., Brattas, P. L., Rylander Ottosson, D., Pircs, K., Grassi, D. A., . . . Parmar, M. (2017). **REST suppression mediates neural conversion of adult human fibroblasts via microRNA-dependent and -independent pathways**. *EMBO Mol Med, 9*(8), 1117-1131. doi:10.15252/emmm.201607471

Eastman, S. W., Yassaee, M., & Bieniasz, P. D. (2009). **A role for ubiquitin ligases and Spartin/SPG20 in lipid droplet turnover**. *J Cell Biol, 184*(6), 881-894. doi:10.1083/jcb.200808041

Eberhardt, K., Jumo, H., D'Amore, A., Alecu, J. E., Ziegler, M., Afshar Saber, W., . . . Ebrahimi-Fakhari, D. (2021). **Generation and characterization of six human induced pluripotent stem cell lines (iPSC) from three families with AP4M1-associated hereditary spastic paraplegia (SPG50)**. *Stem Cell Res, 53*, 102335. doi:10.1016/j.scr.2021.102335

Ebrahimi-Fakhari, D., Alecu, J. E., Ziegler, M., Geisel, G., Jordan, C., D'Amore, A., . . . Yang, E. (2021). **Systematic Analysis of Brain MRI Findings in Adaptor Protein Complex 4-Associated Hereditary Spastic Paraplegia**. *Neurology, 97*(19), e1942-e1954. doi:10.1212/wnl.0000000000012836

Ebrahimi-Fakhari, D., Behne, R., Davies, A. K., & Hirst, J. (1993). AP-4-Associated Hereditary Spastic Paraplegia. In M. P. Adam, H. H. Ardinger, R. A. Pagon, S. E. Wallace, L. J. H. Bean, K. Stephens, & A. Amemiya (Eds.), *GeneReviews((R))*. Seattle (WA): University of Washington, Seattle
University of Washington, Seattle. GeneReviews is a registered trademark of the University of Washington, Seattle. All rights reserved.

Ebrahimi-Fakhari, D., Cantuti-Castelvetri, I., Fan, Z., Rockenstein, E., Masliah, E., Hyman, B. T., . . . Unni, V. K. (2011). **Distinct roles in vivo for the ubiquitin-proteasome system and the autophagy-lysosomal pathway in the degradation of alpha-synuclein**. *J Neurosci, 31*(41), 14508-14520. doi:10.1523/JNEUROSCI.1560-11.2011

Ebrahimi-Fakhari, D., Cheng, C., Dies, K., Diplock, A., Pier, D. B., Ryan, C. S., . . . Bennett, J. T. (2018). **Clinical and genetic characterization of AP4B1-associated SPG47**. *Am J Med Genet A, 176*(2), 311-318. doi:10.1002/ajmg.a.38561

Ebrahimi-Fakhari, D., Cheng, C., Dies, K., Diplock, A., Pier, D. B., Ryan, C. S., . . . CureSpg. (2018). **Clinical and genetic characterization of AP4B1-associated SPG47**. *Am J Med Genet A, 176*(2), 311-318. doi:10.1002/ajmg.a.38561

Ebrahimi-Fakhari, D., Saffari, A., & Pearl, P. L. (2021). **Childhood-onset hereditary spastic paraplegia and its treatable mimics**. *Mol Genet Metab*. doi:10.1016/j.ymgme.2021.06.006

Ebrahimi-Fakhari, D., Saffari, A., Wahlster, L., DiNardo, A., Turner, D., Lewis, T. L., Jr., . . . Sahin, M. (2016). **Impaired Mitochondrial Dynamics And Mitophagy In Neuronal Models Of Tuberous Sclerosis Complex**. *Cell Rep, 17*(8), 2162. doi:10.1016/j.celrep.2016.10.051

Ebrahimi-Fakhari, D., Saffari, A., Wahlster, L., Lu, J., Byrne, S., Hoffmann, G. F., . . . Sahin, M. (2016). **Congenital disorders of autophagy: an emerging novel class of inborn errors of neuro-metabolism**. *Brain, 139*(Pt 2), 317-337. doi:10.1093/brain/awv371

Ebrahimi-Fakhari, D., Teinert, J., Behne, R., Wimmer, M., D'Amore, A., Eberhardt, K., . . . Sahin, M. (2020). **Defining the clinical, molecular and imaging spectrum of adaptor protein complex 4-associated hereditary spastic paraplegia**. *Brain, 143*(10), 2929-2944. doi:10.1093/brain/awz307

Elkouzi, A., Vedam-Mai, V., Eisinger, R. S., & Okun, M. S. (2019). **Emerging therapies in Parkinson disease - repurposed drugs and new approaches**. *Nat Rev Neurol, 15*(4), 204-223. doi:10.1038/s41582-019-0155-7

Erichsen, A. K., Koht, J., Stray-Pedersen, A., Abdelnoor, M., & Tallaksen, C. M. (2009). **Prevalence of hereditary ataxia and spastic paraplegia in southeast Norway: a population-based study**. *Brain, 132*(Pt 6), 1577-1588. doi:10.1093/brain/awp056

Esrick, E. B., Lehmann, L. E., Biffi, A., Achebe, M., Brendel, C., Ciuculescu, M. F., . . . Williams, D. A. (2021). **Post-Transcriptional Genetic Silencing of BCL11A to Treat Sickle Cell Disease**. *N Engl J Med, 384*(3), 205-215. doi:10.1056/NEJMoa2029392

Fang, M. Y., Markmiller, S., Vu, A. Q., Javaherian, A., Dowdle, W. E., Jolivet, P., . . . Yeo, G. W. (2019). **Small-Molecule Modulation of TDP-43 Recruitment to Stress Granules Prevents Persistent TDP-43 Accumulation in ALS/FTD**. *Neuron, 103*(5), 802-819 e811. doi:10.1016/j.neuron.2019.05.048

Ferreirinha, F., Quattrini, A., Pirozzi, M., Valsecchi, V., Dina, G., Broccoli, V., . . . Rugarli, E. I. (2004). **Axonal degeneration in paraplegin-deficient mice is associated with abnormal mitochondria and impairment of axonal transport**. *J Clin Invest, 113*(2), 231-242. doi:10.1172/jci20138

Fink, J. K. (2013). **Hereditary spastic paraplegia: clinico-pathologic features and emerging molecular mechanisms**. *Acta Neuropathol, 126*(3), 307-328. doi:10.1007/s00401-013-1115-8

Fusaki, N., Ban, H., Nishiyama, A., Saeki, K., & Hasegawa, M. (2009). **Efficient induction of transgene-free human pluripotent stem cells using a vector based on Sendai virus, an RNA virus that does not integrate into the host genome**. *Proc Jpn Acad Ser B Phys Biol Sci, 85*(8), 348-362. doi:10.2183/pjab.85.348

Ganley, I. G., Lam du, H., Wang, J., Ding, X., Chen, S., & Jiang, X. (2009). **ULK1.ATG13.FIP200 complex mediates mTOR signaling and is essential for autophagy**. *J Biol Chem, 284*(18), 12297-12305. doi:10.1074/jbc.M900573200

Geng, J., Nair, U., Yasumura-Yorimitsu, K., & Klionsky, D. J. (2010). **Post-Golgi Sec proteins are required for autophagy in Saccharomyces cerevisiae**. *Mol Biol Cell, 21*(13), 2257-2269. doi:10.1091/mbc.e09-11-0969

Goodwin, J. M., Dowdle, W. E., DeJesus, R., Wang, Z., Bergman, P., Kobylarz, M., . . . Murphy, L. O. (2017). **Autophagy-Independent Lysosomal Targeting Regulated by ULK1/2-FIP200 and ATG9**. *Cell Rep, 20*(10), 2341-2356. doi:10.1016/j.celrep.2017.08.034

Guardia, C. M., De Pace, R., Mattera, R., & Bonifacino, J. S. (2018). **Neuronal functions of adaptor complexes involved in protein sorting**. *Current opinion in neurobiology, 51*, 103-110. doi:10.1016/j.conb.2018.02.021

Guardia, C. M., Jain, A., Mattera, R., Friefeld, A., Li, Y., & Bonifacino, J. S. (2021). **RUSC2 and WDR47 oppositely regulate kinesin-1-dependent distribution of ATG9A to the cell periphery**. *Mol Biol Cell*, mbcE21060295. doi:10.1091/mbc.E21-06-0295

Guardia, C. M., Tan, X. F., Lian, T., Rana, M. S., Zhou, W., Christenson, E. T., . . . Banerjee, A. (2020). **Structure of Human ATG9A, the Only Transmembrane Protein of the Core Autophagy Machinery**. *Cell Rep, 31*(13), 107837. doi:10.1016/j.celrep.2020.107837

Hardies, K., May, P., Djemie, T., Tarta-Arsene, O., Deconinck, T., Craiu, D., . . . Hirst, J. (2015). **Recessive loss-of-function mutations in AP4S1 cause mild fever-sensitive seizures, developmental delay and spastic paraplegia through loss of AP-4 complex assembly**. *Hum Mol Genet, 24*(8), 2218-2227. doi:10.1093/hmg/ddu740

Harding, A. E. (1983). **Classification of the hereditary ataxias and paraplegias**. *Lancet, 1*(8334), 1151-1155. doi:10.1016/s0140-6736(83)92879-9

Hayashi-Nishino, M., Fujita, N., Noda, T., Yamaguchi, A., Yoshimori, T., & Yamamoto, A. (2009). **A subdomain of the endoplasmic reticulum forms a cradle for autophagosome formation**. *Nat Cell Biol, 11*(12), 1433-1437. doi:10.1038/ncb1991

Hedera, P. (1993). Hereditary Spastic Paraplegia Overview. In M. P. Adam, H. H. Ardinger, R. A. Pagon, S. E. Wallace, L. J. H. Bean, G. Mirzaa, & A. Amemiya (Eds.), *GeneReviews((R))*. Seattle (WA).

Hirst, J., Barlow, L. D., Francisco, G. C., Sahlender, D. A., Seaman, M. N., Dacks, J. B., & Robinson, M. S. (2011). **The fifth adaptor protein complex**. *PLoS Biol, 9*(10), e1001170. doi:10.1371/journal.pbio.1001170

Hirst, J., Bright, N. A., Rous, B., & Robinson, M. S. (1999). **Characterization of a fourth adaptor-related protein complex**. *Mol Biol Cell, 10*(8), 2787-2802. doi:10.1091/mbc.10.8.2787

Hirst, J., Irving, C., & Borner, G. H. (2013). **Adaptor protein complexes AP-4 and AP-5: new players in endosomal trafficking and progressive spastic paraplegia**. *Traffic, 14*(2), 153-164. doi:10.1111/tra.12028

Hirst, J., Schlacht, A., Norcott, J. P., Traynor, D., Bloomfield, G., Antrobus, R., . . . Robinson, M. S. (2014). **Characterization of TSET, an ancient and widespread membrane trafficking complex**. *Elife, 3*, e02866. doi:10.7554/eLife.02866

Ichimura, Y., Kirisako, T., Takao, T., Satomi, Y., Shimonishi, Y., Ishihara, N., . . . Ohsumi, Y. (2000). **A ubiquitin-like system mediates protein lipidation**. *Nature, 408*(6811), 488-492. doi:10.1038/35044114

Ivankovic, D., Drew, J., Lesept, F., White, I. J., Lopez Domenech, G., Tooze, S. A., & Kittler, J. T. (2020). **Axonal autophagosome maturation defect through failure of ATG9A sorting underpins pathology in AP-4 deficiency syndrome**. *Autophagy, 16*(3), 391-407. doi:10.1080/15548627.2019.1615302

Ivankovic, D., Drew, J., Lesept, F., White, I. J., López Doménech, G., Tooze, S. A., & Kittler, J. T. (2020). **Axonal autophagosome maturation defect through failure of ATG9A sorting underpins pathology in AP-4 deficiency syndrome**. *Autophagy, 16*(3), 391-407. doi:10.1080/15548627.2019.1615302

Janvier, K., & Bonifacino, J. S. (2005). **Role of the endocytic machinery in the sorting of lysosome-associated membrane proteins**. *Mol Biol Cell, 16*(9), 4231-4242. doi:10.1091/mbc.e05-03-0213

Jouet, M., Rosenthal, A., Armstrong, G., MacFarlane, J., Stevenson, R., Paterson, J., . . . Kenwrick, S. (1994). **X-linked spastic paraplegia (SPG1), MASA syndrome and X-linked hydrocephalus result from mutations in the L1 gene**. *Nat Genet, 7*(3), 402-407. doi:10.1038/ng0794-402

Kabeya, Y., Mizushima, N., Ueno, T., Yamamoto, A., Kirisako, T., Noda, T., . . . Yoshimori, T. (2000). **LC3, a mammalian homologue of yeast Apg8p, is localized in autophagosome membranes after processing**. *EMBO J, 19*(21), 5720-5728. doi:10.1093/emboj/19.21.5720

Kim, J., Kundu, M., Viollet, B., & Guan, K. L. (2011). **AMPK and mTOR regulate autophagy through direct phosphorylation of Ulk1**. *Nat Cell Biol, 13*(2), 132-141. doi:10.1038/ncb2152

Klionsky, D. J. (2016). **Developing a set of guidelines for your research field: a practical approach**. *Mol Biol Cell, 27*(5), 733-738. doi:10.1091/mbc.E15-09-0618

Klionsky, D. J., Abdelmohsen, K., Abe, A., Abedin, M. J., Abeliovich, H., Acevedo Arozena, A., . . . Zughaier, S. M. (2016). **Guidelines for the use and interpretation of assays for monitoring autophagy (3rd edition)**. *Autophagy, 12*(1), 1-222. doi:10.1080/15548627.2015.1100356

Kondo, T., Asai, M., Tsukita, K., Kutoku, Y., Ohsawa, Y., Sunada, Y., . . . Inoue, H. (2013). **Modeling Alzheimer's disease with iPSCs reveals stress phenotypes associated with intracellular Abeta and differential drug responsiveness**. *Cell Stem Cell, 12*(4), 487-496. doi:10.1016/j.stem.2013.01.009

Kong, X. F., Bousfiha, A., Rouissi, A., Itan, Y., Abhyankar, A., Bryant, V., . . . Boisson-Dupuis, S. (2013). **A novel homozygous p.R1105X mutation of the AP4E1 gene in twins with hereditary spastic paraplegia and mycobacterial disease**. *PLoS One, 8*(3), e58286. doi:10.1371/journal.pone.0058286

Langouët, M., Siquier-Pernet, K., Sanquer, S., Bole-Feysot, C., Nitschke, P., Boddaert, N., . . . Colleaux, L. (2015). **Contiguous mutation syndrome in the era of high-throughput sequencing**. *Mol Genet Genomic Med, 3*(3), 215-220. doi:10.1002/mgg3.134

Lipton, J. O., & Sahin, M. (2014). **The neurology of mTOR**. *Neuron, 84*(2), 275-291. doi:10.1016/j.neuron.2014.09.034

Liu, W. J., Ye, L., Huang, W. F., Guo, L. J., Xu, Z. G., Wu, H. L., . . . Liu, H. F. (2016). **p62 links the autophagy pathway and the ubiqutin–proteasome system upon ubiquitinated protein degradation**. *Cellular & Molecular Biology Letters, 21*(1), 29. doi:10.1186/s11658-016-0031-z

Lo Giudice, T., Lombardi, F., Santorelli, F. M., Kawarai, T., & Orlacchio, A. (2014). **Hereditary spastic paraplegia: Clinical-genetic characteristics and evolving molecular mechanisms**. *Experimental Neurology, 261*, 518-539. doi:https://doi.org/10.1016/j.expneurol.2014.06.011

Lorrain, M. (1898). *Contribution à l'étude de la paraplégie spasmodique familiale: travail de la clinique des maladies du système nerveux à la Salpêtrière*: G. Steinheil.

Lossos, A., Stevanin, G., Meiner, V., Argov, Z., Bouslam, N., Newman, J. P., . . . Brice, A. (2006). **Hereditary Spastic Paraplegia With Thin Corpus Callosum: Reduction of the SPG11 Interval and Evidence for Further Genetic Heterogeneity**. *Archives of Neurology, 63*(5), 756-760. doi:10.1001/archneur.63.5.756

Luciani, A., Schumann, A., Berquez, M., Chen, Z., Nieri, D., Failli, M., . . . Devuyst, O. (2020). **Impaired mitophagy links mitochondrial disease to epithelial stress in methylmalonyl-CoA mutase deficiency**. *Nat Commun, 11*(1), 970. doi:10.1038/s41467-020-14729-8

Lugli, E., Troiano, L., Ferraresi, R., Roat, E., Prada, N., Nasi, M., . . . Cossarizza, A. (2005). **Characterization of cells with different mitochondrial membrane potential during apoptosis**. *Cytometry A, 68*(1), 28-35. doi:10.1002/cyto.a.20188

Lüningschrör, P., & Sendtner, M. (2018). **Autophagy in the presynaptic compartment**. *Curr Opin Neurobiol, 51*, 80-85. doi:10.1016/j.conb.2018.02.023

MacDonald, J. I. S., Dietrich, A., Gamble, S., Hryciw, T., Grant, R. I., & Meakin, S. O. (2012). **Nesca, a novel neuronal adapter protein, links the molecular motor kinesin with the pre-synaptic membrane protein, syntaxin-1, in hippocampal neurons**. *Journal of Neurochemistry, 121*(6), 861-880. doi:https://doi.org/10.1111/j.1471-4159.2012.07729.x

Maday, S., & Holzbaur, E. L. (2014). **Autophagosome biogenesis in primary neurons follows an ordered and spatially regulated pathway**. *Dev Cell, 30*(1), 71-85. doi:10.1016/j.devcel.2014.06.001

Maday, S., Wallace, K. E., & Holzbaur, E. L. (2012). **Autophagosomes initiate distally and mature during transport toward the cell soma in primary neurons**. *J Cell Biol, 196*(4), 407-417. doi:10.1083/jcb.201106120

Maeda, S., Yamamoto, H., Kinch, L. N., Garza, C. M., Takahashi, S., Otomo, C., . . . Otomo, T. (2020). **Structure, lipid scrambling activity and role in autophagosome formation of ATG9A**. *Nature Structural & Molecular Biology, 27*(12), 1194-1201. doi:10.1038/s41594-020-00520-2

Mahil, S. K., Twelves, S., Farkas, K., Setta-Kaffetzi, N., Burden, A. D., Gach, J. E., . . . Capon, F. (2016). **AP1S3 Mutations Cause Skin Autoinflammation by Disrupting Keratinocyte Autophagy and Up-Regulating IL-36 Production**. *J Invest Dermatol, 136*(11), 2251-2259. doi:10.1016/j.jid.2016.06.618

Maier, A., Klopocki, E., Horn, D., Tzschach, A., Holm, T., Meyer, R., & Meyer, T. (2014). **De novo partial deletion in GRID2 presenting with complicated spastic paraplegia**. *Muscle & Nerve, 49*(2), 289-292. doi:https://doi.org/10.1002/mus.24096

Mari, M., Griffith, J., Rieter, E., Krishnappa, L., Klionsky, D. J., & Reggiori, F. (2010). **An Atg9-containing compartment that functions in the early steps of autophagosome biogenesis**. *J Cell Biol, 190*(6), 1005-1022. doi:10.1083/jcb.200912089

Mariani, M., Karki, R., Spennato, M., Pandya, D., He, S., Andreoli, M., . . . Ferlini, C. (2015). **Class III beta-tubulin in normal and cancer tissues**. *Gene, 563*(2), 109-114. doi:10.1016/j.gene.2015.03.061

Matoba, K., Kotani, T., Tsutsumi, A., Tsuji, T., Mori, T., Noshiro, D., . . . Noda, N. N. (2020). **Atg9 is a lipid scramblase that mediates autophagosomal membrane expansion**. *Nat Struct Mol Biol, 27*(12), 1185-1193. doi:10.1038/s41594-020-00518-w

Matsuda, K., Miura, E., Miyazaki, T., Kakegawa, W., Emi, K., Narumi, S., . . . Yuzaki, M. (2010). **Cbln1 is a ligand for an orphan glutamate receptor delta2, a bidirectional synapse organizer**. *Science, 328*(5976), 363-368. doi:10.1126/science.1185152

Matsuda, S., Miura, E., Matsuda, K., Kakegawa, W., Kohda, K., Watanabe, M., & Yuzaki, M. (2008). **Accumulation of AMPA receptors in autophagosomes in neuronal axons lacking adaptor protein AP-4**. *Neuron, 57*(5), 730-745. doi:10.1016/j.neuron.2008.02.012

Mattera, R., Guardia, C. M., Sidhu, S. S., & Bonifacino, J. S. (2015). **Bivalent Motif-Ear Interactions Mediate the Association of the Accessory Protein Tepsin with the AP-4 Adaptor Complex**. *J Biol Chem, 290*(52), 30736-30749. doi:10.1074/jbc.M115.683409

Mattera, R., Park, S. Y., De Pace, R., Guardia, C. M., & Bonifacino, J. S. (2017). **AP-4 mediates export of ATG9A from the trans-Golgi network to promote autophagosome formation**. *Proc Natl Acad Sci U S A, 114*(50), E10697-e10706. doi:10.1073/pnas.1717327114

Mauvezin, C., & Neufeld, T. P. (2015). **Bafilomycin A1 disrupts autophagic flux by inhibiting both V-ATPase-dependent acidification and Ca-P60A/SERCA-dependent autophagosome-lysosome fusion**. *Autophagy, 11*(8), 1437-1438. doi:10.1080/15548627.2015.1066957

Mendell, J. R., Sahenk, Z., Lehman, K., Nease, C., Lowes, L. P., Miller, N. F., . . . Rodino-Klapac, L. R. (2020). **Assessment of Systemic Delivery of rAAVrh74.MHCK7.micro-dystrophin in Children With Duchenne Muscular Dystrophy: A Nonrandomized Controlled Trial**. *JAMA Neurol, 77*(9), 1122-1131. doi:10.1001/jamaneurol.2020.1484

Mitsunari, T., Nakatsu, F., Shioda, N., Love, P. E., Grinberg, A., Bonifacino, J. S., & Ohno, H. (2005). **Clathrin adaptor AP-2 is essential for early embryonal development**. *Molecular and cellular biology, 25*(21), 9318-9323. doi:10.1128/MCB.25.21.9318-9323.2005

Mizushima, N., & Yoshimori, T. (2007). **How to interpret LC3 immunoblotting**. *Autophagy, 3*(6), 542-545. doi:10.4161/auto.4600

Moreno-De-Luca, A., Helmers, S. L., Mao, H., Burns, T. G., Melton, A. M., Schmidt, K. R., . . . Martin, C. L. (2011). **Adaptor protein complex-4 (AP-4) deficiency causes a novel autosomal recessive cerebral palsy syndrome with microcephaly and intellectual disability**. *J Med Genet, 48*(2), 141-144. doi:10.1136/jmg.2010.082263

Noda, T., Kim, J., Huang, W. P., Baba, M., Tokunaga, C., Ohsumi, Y., & Klionsky, D. J. (2000). **Apg9p/Cvt7p is an integral membrane protein required for transport vesicle formation in the Cvt and autophagy pathways**. *J Cell Biol, 148*(3), 465-480. doi:10.1083/jcb.148.3.465

Orsi, A., Razi, M., Dooley, H. C., Robinson, D., Weston, A. E., Collinson, L. M., & Tooze, S. A. (2012). **Dynamic and transient interactions of Atg9 with autophagosomes, but not membrane integration, are required for autophagy**. *Mol Biol Cell, 23*(10), 1860-1873. doi:10.1091/mbc.E11-09-0746

Pankiv, S., Clausen, T. H., Lamark, T., Brech, A., Bruun, J. A., Outzen, H., . . . Johansen, T. (2007). **p62/SQSTM1 binds directly to Atg8/LC3 to facilitate degradation of ubiquitinated protein aggregates by autophagy**. *J Biol Chem, 282*(33), 24131-24145. doi:10.1074/jbc.M702824200

Papinski, D., Schuschnig, M., Reiter, W., Wilhelm, L., Barnes, C. A., Maiolica, A., . . . Kraft, C. (2014). **Early steps in autophagy depend on direct phosphorylation of Atg9 by the Atg1 kinase**. *Mol Cell, 53*(3), 471-483. doi:10.1016/j.molcel.2013.12.011

Park, S. H., Zhu, P. P., Parker, R. L., & Blackstone, C. (2010). **Hereditary spastic paraplegia proteins REEP1, spastin, and atlastin-1 coordinate microtubule interactions with the tubular ER network**. *J Clin Invest, 120*(4), 1097-1110. doi:10.1172/jci40979

Pasi, K. J., Rangarajan, S., Mitchell, N., Lester, W., Symington, E., Madan, B., . . . Wong, W. Y. (2020). **Multiyear Follow-up of AAV5-hFVIII-SQ Gene Therapy for Hemophilia A**. *N Engl J Med, 382*(1), 29-40. doi:10.1056/NEJMoa1908490

Pende, M., Um, S. H., Mieulet, V., Sticker, M., Goss, V. L., Mestan, J., . . . Thomas, G. (2004). **S6K1(-/-)/S6K2(-/-) mice exhibit perinatal lethality and rapamycin-sensitive 5'-terminal oligopyrimidine mRNA translation and reveal a mitogen-activated protein kinase-dependent S6 kinase pathway**. *Molecular and cellular biology, 24*(8), 3112-3124. doi:10.1128/MCB.24.8.3112-3124.2004

Ravikumar, B., Moreau, K., Jahreiss, L., Puri, C., & Rubinsztein, D. C. (2010). **Plasma membrane contributes to the formation of pre-autophagosomal structures**. *Nat Cell Biol, 12*(8), 747-757. doi:10.1038/ncb2078

Rehbach, K., Kesavan, J., Hauser, S., Ritzenhofen, S., Jungverdorben, J., Schule, R., . . . Brustle, O. (2019). **Multiparametric rapid screening of neuronal process pathology for drug target identification in HSP patient-specific neurons**. *Sci Rep, 9*(1), 9615. doi:10.1038/s41598-019-45246-4

Robinson, M. S. (2015). **Forty Years of Clathrin-coated Vesicles**. *Traffic, 16*(12), 1210-1238. doi:10.1111/tra.12335

Roubertie, A., Hieu, N., Roux, C. J., Leboucq, N., Manes, G., Charif, M., . . . Lenaers, G. (2018). **AP4 deficiency: A novel form of neurodegeneration with brain iron accumulation?** *Neurol Genet, 4*(1), e217. doi:10.1212/nxg.0000000000000217

Ruano, L., Melo, C., Silva, M. C., & Coutinho, P. (2014). **The global epidemiology of hereditary ataxia and spastic paraplegia: a systematic review of prevalence studies**. *Neuroepidemiology, 42*(3), 174-183. doi:10.1159/000358801

Sahani, M. H., Itakura, E., & Mizushima, N. (2014). **Expression of the autophagy substrate SQSTM1/p62 is restored during prolonged starvation depending on transcriptional upregulation and autophagy-derived amino acids**. *Autophagy, 10*(3), 431-441. doi:10.4161/auto.27344

Saitoh, T., Fujita, N., Hayashi, T., Takahara, K., Satoh, T., Lee, H., . . . Akira, S. (2009). **Atg9a controls dsDNA-driven dynamic translocation of STING and the innate immune response**. *Proceedings of the National Academy of Sciences, 106*(49), 20842-20846. doi:10.1073/pnas.0911267106

Salpietro, V., Dixon, C. L., Guo, H., Bello, O. D., Vandrovcova, J., Efthymiou, S., . . . Group, S. S. (2019). **AMPA receptor GluA2 subunit defects are a cause of neurodevelopmental disorders**. *Nature Communications, 10*(1), 3094. doi:10.1038/s41467-019-10910-w

Sanger, A., Hirst, J., Davies, A. K., & Robinson, M. S. (2019). **Adaptor protein complexes and disease at a glance**. *J Cell Sci, 132*(20). doi:10.1242/jcs.222992

Scanlon, J. M., & Reynolds, I. J. (1998). **Effects of oxidants and glutamate receptor activation on mitochondrial membrane potential in rat forebrain neurons**. *J Neurochem, 71*(6), 2392-2400. Retrieved from https://www.ncbi.nlm.nih.gov/pubmed/9832137

Schenk, D., Barbour, R., Dunn, W., Gordon, G., Grajeda, H., Guido, T., . . . Seubert, P. (1999). **Immunization with amyloid-beta attenuates Alzheimer-disease-like pathology in the PDAPP mouse**. *Nature, 400*(6740), 173-177. doi:10.1038/22124

Schüle, R., Wiethoff, S., Martus, P., Karle, K. N., Otto, S., Klebe, S., . . . Schöls, L. (2016). **Hereditary spastic paraplegia: Clinicogenetic lessons from 608 patients**. *Ann Neurol, 79*(4), 646-658. doi:10.1002/ana.24611

Seibler, P., Burbulla, L. F., Dulovic, M., Zittel, S., Heine, J., Schmidt, T., . . . Klein, C. (2018). **Iron overload is accompanied by mitochondrial and lysosomal dysfunction in WDR45 mutant cells**. *Brain, 141*(10), 3052-3064. doi:10.1093/brain/awy230

Simmen, T., Höning, S., Icking, A., Tikkanen, R., & Hunziker, W. (2002). **AP-4 binds basolateral signals and participates in basolateral sorting in epithelial MDCK cells**. *Nat Cell Biol, 4*(2), 154-159. doi:10.1038/ncb745

Stephens, D. J., & Banting, G. (1998). **Specificity of interaction between adaptor-complex medium chains and the tyrosine-based sorting motifs of TGN38 and lgp120**. *The Biochemical journal, 335 (Pt 3)*(Pt 3), 567-572. doi:10.1042/bj3350567

Strümpell, A. (1880). **Beiträge zur Pathologie des Rückenmarks**. *Archiv für Psychiatrie und Nervenkrankheiten, 10*(3), 676-717. doi:10.1007/BF02224539

Strümpell, A. (1886). **Ueber eine bestimmte Form der primären combinirten Systemerkrankung des Rückenmarks**. *Archiv für Psychiatrie und Nervenkrankheiten, 17*(1), 217-238. doi:10.1007/BF02172796

Strümpell, A. (1893). **Ueber die hereditäre spastische Spinalparalyse**. *Deutsche Zeitschrift für Nervenheilkunde, 4*(3), 173-188. doi:10.1007/BF01665286

Takahashi, K., & Yamanaka, S. (2006). **Induction of pluripotent stem cells from mouse embryonic and adult fibroblast cultures by defined factors**. *Cell, 126*(4), 663-676. doi:10.1016/j.cell.2006.07.024

Takayama, C., Nakagawa, S., Watanabe, M., Mishina, M., & Inoue, Y. (1995). **Light- and electron-microscopic localization of the glutamate receptor channel delta 2 subunit in the mouse Purkinje cell**. *Neurosci Lett, 188*(2), 89-92. doi:10.1016/0304-3940(95)11403-j

Takayama, C., Nakagawa, S., Watanabe, M., Mishina, M., & Inoue, Y. (1996). **Developmental changes in expression and distribution of the glutamate receptor channel delta 2 subunit according to the Purkinje cell maturation**. *Brain Res Dev Brain Res, 92*(2), 147-155. doi:10.1016/0165-3806(95)00212-x

Tamura, H., Shibata, M., Koike, M., Sasaki, M., & Uchiyama, Y. (2010). **Atg9A protein, an autophagy-related membrane protein, is localized in the neurons of mouse brains**. *J Histochem Cytochem, 58*(5), 443-453. doi:10.1369/jhc.2010.955690

Tanida, I., Minematsu-Ikeguchi, N., Ueno, T., & Kominami, E. (2005). **Lysosomal turnover, but not a cellular level, of endogenous LC3 is a marker for autophagy**. *Autophagy, 1*(2), 84-91. doi:10.4161/auto.1.2.1697

Teinert, J., Behne, R., D'Amore, A., Wimmer, M., Dwyer, S., Chen, T., . . . Ebrahimi-Fakhari, D. (2019). **Generation and characterization of six human induced pluripotent stem cell lines (iPSC) from three families with AP4B1-associated hereditary spastic paraplegia (SPG47)**. *Stem Cell Res, 40*, 101575. doi:10.1016/j.scr.2019.101575

Teinert, J., Behne, R., Wimmer, M., & Ebrahimi-Fakhari, D. (2019). **Novel Insights Into The Clinical And Molecular Spectrum Of Congenital Disorders of Autophagy**. *J Inherit Metab Dis*. doi:10.1002/jimd.12084

Teinert, J., Behne, R., Wimmer, M., & Ebrahimi-Fakhari, D. (2020). **Novel insights into the clinical and molecular spectrum of congenital disorders of autophagy**. *J Inherit Metab Dis, 43*(1), 51-62. doi:10.1002/jimd.12084

Tessa, A., Battini, R., Rubegni, A., Storti, E., Marini, C., Galatolo, D., . . . Santorelli, F. M. (2016). **Identification of mutations in AP4S1/SPG52 through next generation sequencing in three families**. *Eur J Neurol, 23*(10), 1580-1587. doi:10.1111/ene.13085

Tesson, C., Koht, J., & Stevanin, G. (2015). **Delving into the complexity of hereditary spastic paraplegias: how unexpected phenotypes and inheritance modes are revolutionizing their nosology**. *Hum Genet, 134*(6), 511-538. doi:10.1007/s00439-015-1536-7

Thoreen, C. C., Kang, S. A., Chang, J. W., Liu, Q., Zhang, J., Gao, Y., . . . Gray, N. S. (2009). **An ATP-competitive mammalian target of rapamycin inhibitor reveals rapamycin-resistant functions of mTORC1**. *J Biol Chem, 284*(12), 8023-8032. doi:10.1074/jbc.M900301200

Traub, L. M., & Bonifacino, J. S. (2013). **Cargo recognition in clathrin-mediated endocytosis**. *Cold Spring Harb Perspect Biol, 5*(11), a016790. doi:10.1101/cshperspect.a016790

Tsukada, M., & Ohsumi, Y. (1993). **Isolation and characterization of autophagy-defective mutants of Saccharomyces cerevisiae**. *FEBS Letters, 333*(1-2), 169-174. doi:https://doi.org/10.1016/0014-5793(93)80398-E

Tüysüz, B., Bilguvar, K., Koçer, N., Yalçınkaya, C., Çağlayan, O., Gül, E., . . . Günel, M. (2014). **Autosomal recessive spastic tetraplegia caused by AP4M1 and AP4B1 gene mutation: expansion of the facial and neuroimaging features**. *Am J Med Genet A, 164a*(7), 1677-1685. doi:10.1002/ajmg.a.36514

Utine, G. E., Haliloğlu, G., Salanci, B., Çetinkaya, A., Kiper, P., Alanay, Y., . . . Alikaşifoğlu, M. (2013). **A homozygous deletion in GRID2 causes a human phenotype with cerebellar ataxia and atrophy**. *J Child Neurol, 28*(7), 926-932. doi:10.1177/0883073813484967

Verkerk, A. J., Schot, R., Dumee, B., Schellekens, K., Swagemakers, S., Bertoli-Avella, A. M., . . . Mancini, G. M. (2009). **Mutation in the AP4M1 gene provides a model for neuroaxonal injury in cerebral palsy**. *Am J Hum Genet, 85*(1), 40-52. doi:10.1016/j.ajhg.2009.06.004

Verny, C., Guegen, N., Desquiret, V., Chevrollier, A., Prundean, A., Dubas, F., . . . Procaccio, V. (2011). **Hereditary spastic paraplegia-like disorder due to a mitochondrial ATP6 gene point mutation**. *Mitochondrion, 11*(1), 70-75. doi:https://doi.org/10.1016/j.mito.2010.07.006

Vill, K., Müller-Felber, W., Alhaddad, B., Strom, T. M., Teusch, V., Weigand, H., . . . Haack, T. B. (2017). **A homozygous splice variant in AP4S1 mimicking neurodegeneration with brain iron accumulation**. *Mov Disord, 32*(5), 797-799. doi:10.1002/mds.26922

Want, A., Gillespie, S. R., Wang, Z., Gordon, R., Iomini, C., Ritch, R., . . . Bernstein, A. M. (2016). **Autophagy and Mitochondrial Dysfunction in Tenon Fibroblasts from Exfoliation Glaucoma Patients**. *PLoS One, 11*(7), e0157404. doi:10.1371/journal.pone.0157404

Wong, P. M., Puente, C., Ganley, I. G., & Jiang, X. (2013). **The ULK1 complex: sensing nutrient signals for autophagy activation**. *Autophagy, 9*(2), 124-137. doi:10.4161/auto.23323

Wullschleger, S., Loewith, R., & Hall, M. N. (2006). **TOR signaling in growth and metabolism**. *Cell, 124*(3), 471-484. doi:10.1016/j.cell.2006.01.016

Yamaguchi, J., Suzuki, C., Nanao, T., Kakuta, S., Ozawa, K., Tanida, I., . . . Uchiyama, Y. (2018). **Atg9a deficiency causes axon-specific lesions including neuronal circuit dysgenesis**. *Autophagy, 14*(5), 764-777. doi:10.1080/15548627.2017.1314897

Yap, C. C., Murate, M., Kishigami, S., Muto, Y., Kishida, H., Hashikawa, T., & Yano, R. (2003). **Adaptor protein complex-4 (AP-4) is expressed in the central nervous system neurons and interacts with glutamate receptor δ2**. *Molecular and Cellular Neuroscience, 24*(2), 283-295. doi:https://doi.org/10.1016/S1044-7431(03)00164-7

Young, A. R., Chan, E. Y., Hu, X. W., Kochl, R., Crawshaw, S. G., High, S., . . . Tooze, S. A. (2006). **Starvation and ULK1-dependent cycling of mammalian Atg9 between the TGN and endosomes**. *J Cell Sci, 119*(Pt 18), 3888-3900. doi:10.1242/jcs.03172

Zhang, Y., Pak, C., Han, Y., Ahlenius, H., Zhang, Z., Chanda, S., . . . Sudhof, T. C. (2013). **Rapid single-step induction of functional neurons from human pluripotent stem cells**. *Neuron, 78*(5), 785-798. doi:10.1016/j.neuron.2013.05.029

Zizioli, D., Meyer, C., Guhde, G., Saftig, P., von Figura, K., & Schu, P. (1999). **Early embryonic death of mice deficient in gamma-adaptin**. *J Biol Chem, 274*(9), 5385-5390. doi:10.1074/jbc.274.9.5385

8 Acknowledgement

I would like to thank my first supervisor Prof. Dr. med. Jens Volkmann without whom this work would not have been possible. I am grateful for his mentorship and for his agreement on letting me join the Sahin lab at Boston Children's Hospital while supporting me continuously and giving great advice, be it for organizing the project or applying for grants and scholarships.

I want to thank my second supervisor Prof. Dr. med. Helge Hebestreit, who sparked my interested in rare diseases with his outstanding elective on this topic, which eventually led to my wish to conduct research in this field. His advice before, during and after my time in the lab has greatly helped me navigate through many challenges.

I want to thank my third supervisor Prof. Dr. Philip Tovote for giving valuable insights from a basic science perspective, for always demanding a critical view and helping me ask the right questions.

I want to thank the Graduate School Of Life Sciences Würzburg and the Medical Faculty and all its members for making this work possible.

I would like to thank Prof. Mustafa Sahin, MD, PhD, who gave me the opportunity to come to his lab and experience the exciting field of experimental research firsthand. His ability to create a friendly, but highly competitive and productive environment has deeply impressed and motivated me. I feel privileged to have been part of his lab.

I especially want to thank my mentor Dr. med. Darius Ebrahimi-Fakhari, MD, PhD, who has been my greatest source of inspiration and motivation during my time at the lab and who taught me with great patience how to conduct research altogether. From my first experiments under his guidance to the first own ideas and questions, he always gave useful advice and helped me with every step. For him, it seems to me, working on better treatments for patients in the clinic and the lab is not merely "work" but a lifelong dedication. I vividly remember many occasions where, after a long night in the clinic, he still had a cheerful comment or a new idea, that was pushing things in the right direction and I want to take this as an example for my own work.

I am thankful to Dr.med. Lara Wahlster, MD, for being so welcoming and warmhearted everytime we met.

I am grateful for the time at the Sahin lab and for all its members, who integrated me without hesitation and gave me a feeling of belonging to the team. My special thanks goes to Alessia Di Nardo, PhD, who patiently watched my first steps and to Julian Teinert, Sean Dwyer and Isadora Lenoël for their lasting friendships.

I am grateful for the continuous advice on all topics from Stefan Kölker, who also had the initial idea, that started this journey. I want to thank my family Paul, Andrea and Dietrich Behne for their support and understanding. I want to thank Lotte for her patience and for always having an open ear no matter the time. I am thankful that Kolja and Clara followed with interest and kept in touch without hesitation.

9 List Of Publications

Original articles related to this work

Data shown in figures 11 – 25 has been published in modified form in the following article:

Behne R*, Teinert J*, Wimmer M, D'Amore A, Davies AK, Scarrott JM, Eberhardt K, Brechmann B, Chen IP, Buttermore ED, Barrett L, Dwyer S, Chen T, Hirst J, Wiesener A, Segal D, Martinuzzi A, Duarte ST, Bennett JT, Bourinaris T, Houlden H, Roubertie A, Santorelli FM, Robinson M, Azzouz M, Lipton JO, Borner GHH, Sahin M, Ebrahimi-Fakhari D.
Adaptor protein complex 4 deficiency: a paradigm of childhood-onset hereditary spastic paraplegia caused by defective protein trafficking. Hum Mol Genet. 2020 Jan 15;29(2):320-334. doi: 10.1093/hmg/ddz310. PMID: 31915823; PMCID: PMC7001721.

*co-first authorship

Original articles

Ebrahimi-Fakhari D, Teinert J, **Behne R**, Wimmer M, D'Amore A, Eberhardt K, Brechmann B, Ziegler M, Jensen DM, Nagabhyrava P, Geisel G, Carmody E, Shamshad U, Dies KA, Yuskaitis CJ, Salussolia CL, Ebrahimi-Fakhari D, Pearson TS, Saffari A, Ziegler A, Kölker S, Volkmann J, Wiesener A, Bearden DR, Lakhani S, Segal D, Udwadia-Hegde A, Martinuzzi A, Hirst J, Perlman S, Takiyama Y, Xiromerisiou G, Vill K, Walker WO, Shukla A, Dubey Gupta R, Dahl N, Aksoy A, Verhelst H, Delgado MR, Kremlikova Pourova R, Sadek AA, Elkhateeb NM, Blumkin L, Brea-Fernández AJ, Dacruz-Álvarez D, Smol T, Ghoumid J, Miguel D, Heine C, Schlump JU, Langen H, Baets J, Bulk S, Darvish H, Bakhtiari S, Kruer MC, Lim-Melia E, Aydinli N, Alanay Y, El-Rashidy O, Nampoothiri S, Patel C, Beetz C, Bauer P, Yoon G, Guillot M, Miller SP, Bourinaris T, Houlden H, Robelin L, Anheim M, Alamri AS, Mahmoud AAH, Inaloo S, Habibzadeh P, Faghihi MA, Jansen AC, Brock S, Roubertie A, Darras BT, Agrawal PB, Santorelli FM, Gleeson J, Zaki MS, Sheikh SI, Bennett JT, Sahin M.
Defining the clinical, molecular and imaging spectrum of adaptor protein complex 4-associated hereditary spastic paraplegia. Brain. 2020 Oct 1;143(10):2929-2944. doi: 10.1093/brain/awz307. PMID: 32979048; PMCID: PMC7780481.

Di Nardo A, Lenoël I, Winden KD, Rühmkorf A, Modi ME, Barrett L, Ercan-Herbst E, Venugopal P, **Behne R**, Lopes CAM, Kleiman RJ, Bettencourt-Dias M, Sahin M.
Phenotypic Screen with TSC-Deficient Neurons Reveals Heat-Shock Machinery as a Druggable Pathway for mTORC1 and Reduced Cilia. Cell Rep. 2020 Jun 23;31(12):107780. doi: 10.1016/j.celrep.2020.107780. PMID: 32579942; PMCID: PMC7381997.

Teinert J*, **Behne R***, D'Amore A, Wimmer M, Dwyer S, Chen T, Buttermore ED, Chen IP, Sahin M, Ebrahimi-Fakhari D.
Generation and characterization of six human induced pluripotent stem cell lines (iPSC) from three families with AP4B1-associated hereditary spastic paraplegia (SPG47). Stem Cell Res. 2019 Oct;40:101575. doi: 10.1016/j.scr.2019.101575. Epub 2019 Sep 11. PMID: 31525725; PMCID: PMC7269118.

*co-first authorship

Review articles

Teinert J*, **Behne R***, Wimmer M*, Ebrahimi-Fakhari D.
Novel insights into the clinical and molecular spectrum of congenital disorders of autophagy. J Inherit Metab Dis. 2020 Jan;43(1):51-62. doi: 10.1002/jimd.12084. Epub 2019 Apr 8. PMID: 30854657.

*co-first authorship

Ebrahimi-Fakhari D, **Behne R**, Davies AK, Hirst J.
AP-4-Associated Hereditary Spastic Paraplegia. 2018 Dec 13. In: Adam MP, Ardinger HH, Pagon RA, Wallace SE, Bean LJH, Mirzaa G, Amemiya A, editors. GeneReviews® [Internet]. Seattle (WA): University of Washington, Seattle; 1993–2021. PMID: 30543385.

Poster Presentations

Behne R*, Teinert J*, Wimmer M, Dwyer S, Davies AK, Hirst J, Borner GHH, Robinson M, Barrett L, Chen IP , Buttermore ED, Sahin M, Ebrahimi-Fakhari D.
Adaptor Protein Complex 4 Deficiency: A Paradigm of Complex Hereditary Spastic Paraplegia With Defective Protein Trafficking
International Congress of Parkinson's Disease and Movement Disorders 2019

*presenting authors

10 Lebenslauf

11 Affidavit

I hereby confirm that my thesis entitled “Development Of A Human iPSC-Derived Cortical Neuron Model Of Adaptor-Protein-4-Complex-Deficiency” is the result of my own work. I did not receive any help or support from commercial consultants. All sources and / or materials applied are listed and specified in the thesis.

Furthermore, I confirm that this thesis has not yet been submitted as part of another examination process neither in identical nor in similar form.

Heidelberg, 01.02.2024 Signature

Eidesstattliche Erklärung

Hiermit erkläre ich an Eides statt, die Dissertation „Entwicklung eines humanen iPSC-abgeleiteten kortikalen Neuronenmodells der Adaptor-Protein-Komplex-4-Defizienz“ eigenständig, d.h. insbesondere selbstständig und ohne Hilfe eines kommerziellen Promotionsberaters, angefertigt und keine anderen als die von mir angegebenen Quellen und Hilfsmittel verwendet zu haben.

Ich erkläre außerdem, dass die Dissertation weder in gleicher noch in ähnlicher Form bereits in einem anderen Prüfungsverfahren vorgelegen hat.

Heidelberg, 01.02.2024 Unterschrift

12 Oxford University Press License